JIANYI DU

COMBUSTION CFD SIMULATION

Thèse
présentée
à la Faculté des études supérieures
de l'Université Laval
pour l'obtention
du grade de Philosophiae Doctor (Ph.D.)

Département de génie mécanique
FACULTÉ DES SCIENCES ET DE GÉNIE
UNIVERSITÉ LAVAL
QUÉBEC

NOVEMBRE 2000

©Jianyi Du, 2000

National Library of Canada
Acquisitions and Bibliographic Services
395 Wellington Street
Ottawa ON K1A 0N4
Canada

Bibliothèque nationale du Canada
Acquisitions et services bibliographiques
395, rue Wellington
Ottawa ON K1A 0N4
Canada

Your file Votre référence

Our file Notre référence

The author has granted a non-exclusive licence allowing the National Library of Canada to reproduce, loan, distribute or sell copies of this thesis in microform, paper or electronic formats.

The author retains ownership of the copyright in this thesis. Neither the thesis nor substantial extracts from it may be printed or otherwise reproduced without the author's permission.

L'auteur a accordé une licence non exclusive permettant à la Bibliothèque nationale du Canada de reproduire, prêter, distribuer ou vendre des copies de cette thèse sous la forme de microfiche/film, de reproduction sur papier ou sur format électronique.

L'auteur conserve la propriété du droit d'auteur qui protège cette thèse. Ni la thèse ni des extraits substantiels de celle-ci ne doivent être imprimés ou autrement reproduits sans son autorisation.

0-612-56437-1

Canada

Résumé

Cette thèse présente des résultats de simulations numériques pour un écoulement réactif laminaire et turbulent. De plus la thèse inclut l'implantation d'un nouveau modèle de combustion intégré au logiciel commercial Fluent. La combustion est un phénomène très complexe, pour la décrire on doit couvrir plusieurs sujets. Dans ces travaux, les différents comportements physiques du fluide, considéré en régime permanent, sont décrits par les équations de Navier-Stokes pour transport de masse, quantité de mouvement et d'énergie. La méthode de calcul numérique permet de décrire la turbulence et la cinétique chimique avec plusieurs modèles appropriés. Une nouvelle méthode basée sur le modèle du "eddy break up" est proposée et développée pour permettre le calcul de coefficients autrement empirique afin d'obtenir de meilleurs résultats en simulation numérique.

Tous les modèles étudiés numériquement sont validés à l'aide de données expérimentales. Dans le cas de la flamme laminaire, des méthodes à une ou plusieurs étapes de réaction chimique sont comparées entre elles pour en assurer un choix judicieux. Aussi des résultats pour un maillage structuré et non structuré sont présentés. Pour la simulation avec turbulence, plusieurs modèles sont proposés avec des fonctions de probabilité adiabatique et non adiabatique. Finalement un nouveau modèle est ajouté dans le logiciel Fluent. Les résultats présentés sont tout à fait adéquats démontrant une certaine amélioration pour un écoulement turbulent surtout pour la prédiction des certaines substances formées par la combustion.

Jianyi Du Alain de Champlain

Abstract

This thesis deals with the numerical simulation of the laminar and the turbulent reacting flow including the implementation of a new combustion model in the Fluent code.

Combustion is a very complex phenomenon. It involves many subjects. In this work, the governing equations are the steady-state, Reynolds averaged Navier-Stokes equations for mass, momentum, energy and scalar transport. Many physical and chemical models involving turbulence, chemical kinetics, numerical method are employed respectively. A new method based eddy break up model is proposed and developed to calculate the varied coefficient for getting better results.

All models are studied numerically and compared with experimental data. In the laminar combustion case, one-step and multi-step methods are studied. The results for structured and unstructured grids are compared. In turbulent reaction flow, various kinds of turbulent models are proposed. Adiabatic and nonadiabatic probability density functions are used. The effect of changing coefficients is discussed. Finally, a code with a new model is inserted into Fluent. The calculated results show that this model is suitable.

Jianyi Du Alain de Champlain

Sommaire

La simulation numérique (CFD) est de plus en plus utilisée en combustion. Dans la présente thèse, des simulations numériques sont faites à partir d'un code de calcul commercial pour faire différentes comparaisons entre des données expérimentales et des modèles de la chimie et de la physique d'un phénomène de combustion. La simulation numérique d'écoulements réactifs laminaires et turbulents est faite et discutée. Les travaux incluent la modification d'un modèle de combustion existant pour améliorer la simulation en ingénierie.

La turbulence est résolue en utilisant le modèle standard $k-\varepsilon$, le modèle basée sur les contraintes de Reynolds (RSM) et le modèle basé sur la simulation des grands tourbillons (LES). Le modèle standard $k-\varepsilon$ est le plus fréquemment utilisé des trois, par contre les modèles RSM et LES commencent à prendre un rôle de plus en plus important. Des résultats avec ces trois modèles sont présentés. Plusieurs modèles de combustion sont utilisés pour des flammes de diffusion turbulentes. Les modèles avec vitesse de réaction finie et infiniment rapide sont considérés avec leurs avantages et leurs désavantages. Pour le modèle avec réaction infiniment rapide, basé sur une approche avec scalaire conservé, des fonctions de probabilités de densité sont utilisés pour des systèmes adiabatiques et non-adiabatiques. Pour le modèle avec réaction finie, les équations du taux de réaction d'Arrhénius avec une étape et plusieurs étapes de réaction sont utilisées et évaluées. Par adaptation, le maillage est optimisée pour la solution de l'écoulement. Des maillages structurés et non structurés sont employés. Les résultats calculés montrent bien qu'un maillage triangulaire peut souvent donner moins de cellules que le maillage équivalent en quadrilatère.

Le modèle de combustion sur la base d'Arrhénius par tourbillon rompu (EBU) avec interaction de la turbulence est aussi étudié en détail. Dans ce modèle, développé par Magnussen et Hjertager (1977), la formulation inclut un paramètre empirique. De part la combinaison du modèle avec vitesse de réaction finie et celui avec réaction à vitesse très rapide sur la base d'une PDF, une nouvelle formulation pour ce paramètre empirique a pu être trouvée en fonction de la fraction de mélange et de l'écart type, tel que proposé par Bilger (1996). Afin de surmonter la difficulté d'implantation de ce concept dans le code de simulation Fluent, un nouveau modèle a été proposé et développé pour obtenir de meilleurs résultats.

Tous les modèles sont étudiés numériquement et comparés à des données expérimentales. Premièrement des cas de combustion laminaire sont étudiés avec des méthodes à une étape et à plusieurs étapes de réaction; de plus des maillages structurés et non structurés sont respectivement utilisés. Avec la méthode par plusieurs étapes de réaction, la température adiabatique de flamme et la distribution des espèces chimiques sont plus près des valeurs expérimentales que la méthode à une étape de réaction. Puis un exemple de combustion avec turbulence est présenté; des fonctions de probabilité de densité adiabatique et non adiabatique sont employées pour comparer aux méthodes de vitesse de réaction finie avec l'expérimental. Différentes types de modèles de turbulence sont proposés. Il est démontré que le modèle de contrainte de Reynolds (RSM) est légèrement meilleur que le modèle standard $k - \varepsilon$. Pour le modèle avec tourbillon rompu (EBU), l'influence sur les espèces chimiques et la température est évaluée avec différentes valeurs des paramètres. Une partie de code pour le nouveau modèle de combustion est insérée dans Fluent par l'entremise de fonctions définies par l'usager. En comparant avec des données expérimentales, les résultats pour le O_2 et le H_2O sont meilleurs avec le nouveau modèle qu'avec la méthode standard.

Jianyi Du Alain de Champlain

Summary

Computational Fluid Dynamics (CFD) is used widely for the simulation of combustion phenomena. In this dissertation, based on the governing equations from physics and chemistry, numerical simulations of combustion are carried out using a commercial code to make comparisons of various physical and chemical models with experimental data. The numerical simulation of laminar and turbulent reacting flows is done and discussed. This work includes the modification of an existing combustion model to improve engineering simulation.

Turbulence is solved by using the standard $k-\varepsilon$ model, the Reynolds Stress Model '(RSM) and the large eddy simulation (LES) model. The standard $k-\varepsilon$ model is the most commonly used model, but RSM and LES models are starting to take a more prominent role. The results with these three models are presented. Several combustion models are used for turbulent diffusion flames. The fast chemistry and finite reaction rate models with their advantages and disadvantages are considered. For the former, based on the conserved scalar approach, Probability Density Functions (PDF) including adiabatic and nonadiabatic systems are used. For the latter, Arrhenius rate equations including one-step and multi-step reaction equations are used and evaluated. By using solution-adaptive refinements, the resulting mesh is optimal for the flow solution. Both structured and unstructured grids are used. The calculation results show that a triangular mesh can often be created with far fewer cells than the equivalent mesh consisting of quadrilateral elements.

The Arrhenius based eddy-break-up model (EBU), including turbulence-combustion interaction, is studied in detail. In this model, developed by Magnussen and Hjertager (1977), the formulation includes an empirical parameter. With the combination of the finite-rate reaction and PDF a new formulation for this empirical parameter could be expressed as a function of mixture fraction and standard deviation. In order to overcome the difficulty to implement the code of this concept, proposed by Bilger (1996), in Fluent a new model is proposed and developed for getting better results.

All models are studied numerically and compared with experimental data. First the laminar combustion cases are studied, one-step and multi-step methods; structured and unstructured grids are used respectively. Using multi-step, the adiabatic flame temperature and the chemical species distributions are closer to the experimental value than that of one-step method. Then, a turbulent combustion example is presented; adiabatic and nonadiabatic probability density functions are used to compare with finite-rate methods and experiments. Various kinds of turbulent models are proposed. It is shown that the Reynolds Stress Model is slightly better than the $k-\varepsilon$ model. For the EBU model, the effect on chemical species and temperature with different coefficient values is sought. A code for the new model is inserted into Fluent through user-defined functions. By comparison with the experimental data, the results of O_2 and H_2O with new model are better than that with "standard" method, and much closer to the experimental values.

Jianyi Du Alain de Champlain

Acknowledgements

I would like to express my gratitude and appreciation to Professor Alain De Champlain, my supervisor, for his invaluable guidance and encouragement during this research project as well as review of the manuscript and the translation of the abstract of the dissertation into French.

Financial support by "Programme québécois de bourse d'excellence, Ministère de l'Éducation, Gouvernement du Québec" is highly appreciated. I am sincerely grateful to Ms. Lucie R. Duranceau and M. Robert Rousseau for their efficient administration and earnest help.

Grateful thanks go to Professor Kretschmer for his proof reading of my thesis and to Dr. Pierre Gosselin from GE Canada and Dr. Samir Rida from Fluent Inc. for having accepted to examine my thesis and for their precious remarks.

Sincere appreciation is also extended to professors, technicians and graduate students of the department of mechanical engineering. Their friendship and help will be remembered.

Lastly and most importantly is the support and patience that I received from my family. In particular, thank my wife Liu Feng and my daughter Shan-Shan for their understanding and affection.

Contents

List of Tables

List of Figures

Nomenclature

A	area of an element; or dissipation combustion constant
A_1, A_2, A_3	coefficients of the equation (4.1)
A_k	pre-exponential factor (consistent units)
a	coefficient for an algebraic equation; or fractional reaction order in oxygen
a_{ij}	stoichiometric coefficients
B	dissipation combustion constant
B_1, B_2, B_3	coefficients of the equation (4.2)
C	function of activation energy
C_μ, C_1, C_2	turbulence model constants
C_d, C_g	constants for the transport equation of g
$C_{j'}$	molar concentration of each reactant or product species j' (kmol/m^3)
C_p	specific heat at constant pressure (J/kg-K)
D_{AB}	binary diffusivity for A-B system
E	empirical constant
E_k	activation energy for the reaction (J/kmol)

f	mixture fraction
g	square fluctuation of f
H_{fu}	heat of reaction
$h_{i'}^{o}$	standard-state enthalpy (heat of formation)
J	convection-diffusion flux
K_k	the equilibrium constant for the kth reaction
k	turbulent kinetic energy; or collision frequency; or ratio of specific heats
k_{eff}	the effective conductivity
$k_{b,k}$	backward rate constant for reaction k
$k_{f,k}$	forward rate constant for reaction k
L	characteristic length
L_s	mixing length
M	the molecular mass of species
M_a	Mach number
m	mass
N	number of chemical species; or air mass flow into a reactor
n	reaction order (overall)
P	pressure
$P(f)$	probability density function
Pr	Prandtl number
q	heat flux
R	universal gas constant(J/kmol-K)

$\hat{R}$	the molar rate of creation/destruction of species
R_i	radius (m)
$S_{i'}^{o}$	the standard-state entropy
S_ϕ	source term in transport equation of ϕ
s	stoichiometric mass of oxidant; or distance
T	temperature
t	time
u, v, w	velocity components in (x,y,z) directions
u_τ	friction velocity
V	volume
$\mathbf{v}$	velocity
v	stoichiometric coefficient
$\dot{w}$	reaction rate
X	mole fraction
Y	mass fraction
y^+	dimensionless distance in the normal direction to the wall
y_v	physical viscous sublayer thickness

Greek Symbols

β_k	temperature exponent (dimensionless)
Γ	diffusion coefficient
ε	rate of dissipation of kinetic energy

$\eta'_{j',k}$	rate exponent for reactant j' in reaction k
$\eta''_{j',k}$	rate exponent for product j' in reaction k
κ	Von Karman constant in the wall functions
λ	turbulent intensity
μ	viscosity
ξ	nondimensional mixture fraction
ρ	density
σ	Schmidt/Prandtl number; or Stefan/Boltzmann constants
τ_w	wall shear stress
ϕ	scalar variable; or equivalence ratio: $(\text{air/fuel})_{stoi} \div ((\text{air/fuel})_{actu}$
ϕ_{ij}	pressure-strain term
Ω_i	molar rate of production of species i
ω_i	mass rate of production of species i

Subscripts

A, B	Species in binary system
av	average value
axi	axisymmetric
fu	fuel
fu, b	fuel burnt
i	species
i, j, k	summation index
l	laminar

max	maximum
mix	mixture
t	turbulence
r	radiant
w	wall
∞	freestream quantities

Superscripts

-	mean value, or arriving at the wall
+	leaving from wall
$\rightarrow$	vector
$\cdot$	rate

Chapter 1

Introduction

Computational Fluid Dynamics (CFD) is now used widely for the simulation of turbulent reacting flows. By solving the fundamental equations governing fluid flow processes, CFD simulations provide information on important flow characteristics such as pressure loss, flow distribution and mixing rates. A CFD analysis complements traditional testing and experimentation, providing added insight and confidence in various designs. These considerations result in better designs, lower risk and faster time to the marketplace for products or processes. CFD method increases the understanding of complex combustion phenomena and reduce the amount of trial and error required in design. The predictions of flow and combustion in complex geometries require extensive computational time. The chemistry and turbulence-chemistry interaction models must contain a simplified description yet accurate enough to enable its incorporation in numerical combustion models. A series of commercial CFD softwares, such as FLUENT, PHOENICS and CFD-ACE+ have been developed to simulate turbulent reacting flows. FLUENT is a general purpose CFD solver provided by Fluent Inc., Lebanon, NH, USA. It offers many physical

models to predict accurately laminar, transitional and turbulent flows, various modes of heat transfer, chemical reaction, multiphase flows and other complex phenomena. Either structured or solution-adaptive unstructured mesh can be used. One goal of the present project is to check the accuracy of these models by comparing the results with experimental data. On the basis of those models, it is the primary objective of the thesis to develop a new model to implement in a CFD code using User-Defined Function(UDFs) for getting better combustion simulation.

1.1 Purpose of the Thesis

Computational combustion and, more generally, the modelling of physical processes which may involve fluid flow, chemical reactions with heat and mass transfer, are interrelated disciplines that require a significant level of expertise to be effectively applied to practical problems.

Chemical reactions usually involve many species and proceed through a large number of finite rate reaction steps. These reaction rates are nonlinear functions of the physical and chemical parameters. It is very difficult to obtain the reaction equations and solve the equations. Of the various kinds of reaction models, the fast chemistry reaction model is the most simple. In light of the fast chemistry assumption approach, the reaction is so fast that fuel and oxidant can not co-exist at any time in the same place. Only one conservation equation of mixture fraction is solved, the convergence is easy. But it can not be extended to situations where the finite rate chemistry is known to have appreciable effects, as for example, oxidation of CO in gas turbine engines, formation of trace species (NO and soot) and extinction conditions. In such cases the description involves a second variable to be integrated. The closure of turbulence chemistry interaction involves the solution for the transport equations of the mean value of the second variable together with its fluctuations from which the joint PDF of the mixture fraction and the second variable can be determined. The temperature and thermo-chemical variables are

averaged using this PDF and made available to the calculations through a look-up table.

Turbulent flows are characterized by fluctuating velocity fields. These fluctuations influence transport quantities such as momentum, energy, and species concentration, and cause these transport quantities to fluctuate as well. Since these fluctuations can be of small scale and high frequency, they are too computationally expensive to be simulated directly in practical engineering calculations. Instead, the instantaneous governing equations can be time-averaged, ensemble-averaged, or otherwise manipulated to remove the small scales, resulting in a modified set of equations that are computationally less expensive to solve. However, the modified equations contain additional unknown variables, and turbulence models are needed to determine these variables in terms of known quantities.

There are many turbulence models. It is an unfortunate fact that no single turbulence model is universally superior for all classes of problems. The choice of turbulence model will depend on considerations such as the physics encompassed in the flow, the established practice for a specific class of problem, the level of accuracy required, the available computational resources, and the amount of time available for the simulation. The purpose of this work is to discuss several turbulence models including the standard $k-\varepsilon$ model, Reynolds Stress Model (RSM) and Large Eddy Simulation (LES) model, which are popularly used in engineering to compare between numerical and experimental results.

The computation of turbulent flows involving chemical reactions is one of the most challenging numerical problems today. While significant advances in flow algorithms have been made recently, numerical codes involving chemical reactions still suffer from stability and convergence problems. The focus of the present project is to develop further the Eddy-Break-Up(EBU) method. The proposed combustion model is to consider the implementation of a simpler approach to consider partial equilibrium in interaction with an improved Eddy-Break up turbulence model as suggested by Bilger (1996) and to consider mixing effects that are different from

one combustor to another. The formulation was developed from an expression for the loading parameter expanded from Longwell (1956), by Kretschmer and Odgers (1972) to get an oxygen consumption efficiency and to relate that to a suitable formulation for the combustion products. This formulation will be valid for a combustor or each cell of a discretized combustor with a mixing rate fast enough to resemble the well-stirred reactor that the original formulation from Kretschmer and Odgers applied to a large degree. To account for different rates of mixing when the combustor is not well stirred, the oxygen consumption rate has to be calculated locally, i.e. at each cell volume, with a different expression. The Eddy-Break Up combustion with mixing interaction model has been demonstrated by Bilger (1976) with a theoretical basis. Using the turbulence kinetic energy and dissipation rate, then the rate of consumption of oxygen can be calculated according to Bilger's formulation or a modification to the rate equation from Kretschmer and Odgers to change the mixing rate appropriately.

The chemistry of combustion is notoriously complex involving literally hundreds of free radical reactions and dozens of chemical species even for the simplest hydrocarbons (Frenklach, 1992). For example, in the case of the two-dimensional methane-air combustor (Mazumder, 1997), the reaction source calculations using Gear's method and a single-step reaction (with five species, i.e., CH_4, O_2, CO_2, H_2O and N_2) used up 63% of the total CPU time. CPU limitations usually restrict the chemical models that can be used. For turbulent flames, it is impossible to describe turbulence and chemistry in complete detail, thus studies often focus on either the fluid mechanics using reduced chemical mechanisms or the chemistry with simple fluid models.

In order to provide better agreement between computed and experimentally observed results, multi-step approaches can be used to satisfy the requirements over wide range of operating conditions. In this thesis, the one-step, two-step and six-step reactions are used in methane-air combustion. The purpose is to reach an optimal approach between the calculating accuracy and calculating time.

In summary, the major works of the thesis include:

- Investigation of the different turbulent models,
- Survey structured grid and unstructured grid,
- Comparison between one-step and multi-step chemical reaction equations, and
- Develop the EBU model for diffusion combustion.

1.2 Outline of the Thesis

Chapter 2 gives a review of the existing methods of flow field simulation in a combustor. In this chapter combustor construction, various kinds of combustion models, numerical solution, chemical reaction models, coupling between turbulence and chemical reaction, and radiation modelling are introduced.

Combustion involves many subjects. In Chapter 3 the basic theories in combustion modeling are presented.

Chapter 4 gives an introduction to FLUENT, which is the commercial CFD code used in all the calculations for this thesis.

The purpose of Chapter 5 is to present and discuss the solution of turbulent reaction flow problems with the use of various kinds of numerical methods and turbulent models. The $k-\varepsilon$ two-equation model is the most popular. Direct numerical simulation and large eddy simulation are also widely used.

Chemical-reacting turbulent flows are highly challenging. In Chapter 6, several combustion models for turbulent diffusion flames are summarized and a simplified EBU model is presented.

In Chapter 7 the different combustion models are used to calculate laminar and turbulent reacting flows. The results are compared with experimental data.

Finally, conclusions are drawn and some suggestions for future research work on combustion model are presented.

Chapter 2

Literature Review

Gas turbines are widely used in modern industry to deliver shaft power or thrust power. The combustor is part of the gas turbine. Figures 2.1 and 2.2 show two types of gas turbine engine. The main goal of the combustor design is lower emissions with less volume. Flow field simulation in the combustor is a challenging subject to both academics and industries. It is of commercial importance to understand and to predict various phenomena in the combustor.

Gas turbine combustion systems need to be designed and developed to meet many mutually conflicting design requirements, including high combustion efficiency over a wide operating envelope and low NO_x emissions, low smoke, low lean flame stability limits and good starting characteristics; low combustion system pressure loss, low pattern factor, and sufficient cooling air to maintain low wall temperature levels and gradients commensurate with structural durability.

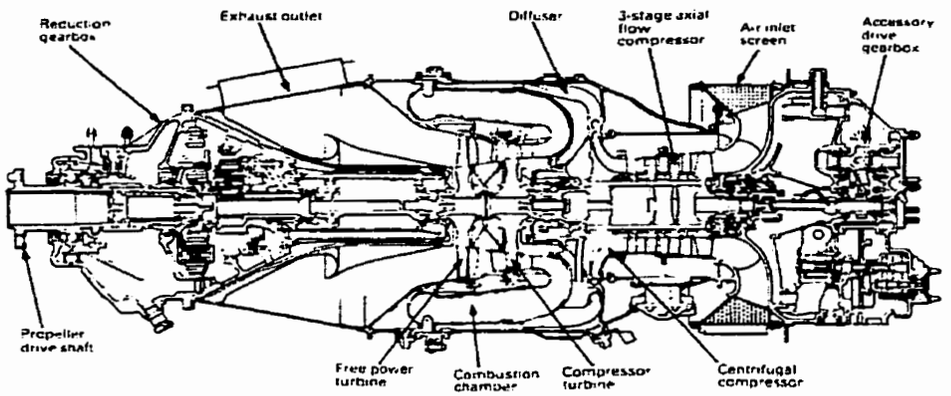

Figure 2.1 Turboprop engine [by courtesy of Pratt and Whitney Canada]

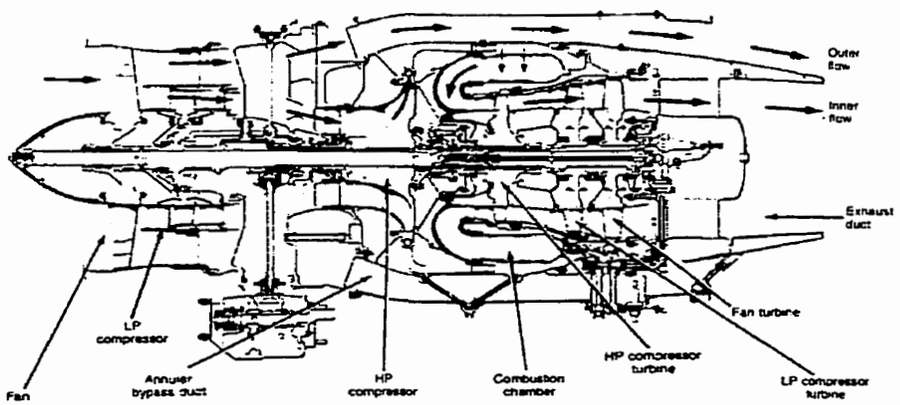

Figure 2.2 Small turbofan engine [by courtesy of Pratt and Whitney Canada]

2.1 Combustor Construction

The design of a gas turbine combustion system is a complex process involving fluid dynamics, combustion and mechanical design. For many years the combustion system was much less amenable to theoretical treatment than other components of the gas turbine, and any development program required a considerable amount of trial and error. With the very high cycle temperatures of modern gas turbines mechanical design remains difficult, and a mechanical development program is inevitable. The rapid increase of Computational Fluid Dynamics in recent years has had a major impact on the design process, greatly increasing the understanding of the complex flow and so reducing the amount of trial and error required.

A typical combustion chamber is presented in Figure 2.3. In general, there are three main regions in a combustor, they are called the re-circulation zone, the secondary zone and the dilution zone. The re-circulation zone operates normally at a rich mixture, the secondary adds air to weaken the mixture. More air is added in the dilution zone to decrease the hot gas temperature for meeting the requirement of turbine guide vanes.

The main purpose of this section is to show how the problem of design is basically one of reaching the best compromise between a number of conflicting requirements, which will vary widely with different applications. Aircraft and ground-based gas turbine combustion systems differ in some respects and are similar in others. The most common fuels for gas turbines are liquid petroleum distillates and natural gas, and attention will be focused on combustion systems suitable for these fuels. In the mid 1990s there was considerable interest in the development of systems to burn gas produced from coal. Gasification requires large amounts of steam so that it is a long-term option for modifying combined cycle plants currently burning gas.

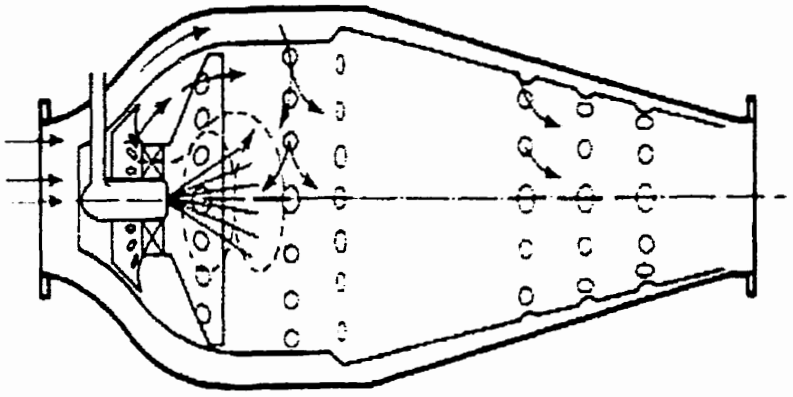

Figure 2.3 Combustion chamber with swirl vanes

In the early days of gas turbine design, major goals included high combustion efficiency and the reduction of visible smoke. A much more demanding problem has been the reduction of nitrogen oxides, and on-going research programs are essential to meet the ever more stringent pollution limits while maintaining existing levels of reliability and keeping costs affordable.

2.2 Combustion Models

Combustion models for gas turbine combustors are still not adequate to provide reasonable flow field estimates to be useful for design purposes. The combustor design process is still very empirical and requires great expertise to predict the exhaust field for pollutant concentrations or temperature distribution.

The flowfield around and within the combustor liner is quite complex in that it includes swirl, regions of re-circulation, fuel injection, atomization, fuel evaporation, mixing, turbulent combustion, soot formation/oxidation, and convective and radiative heat transfer processes.

There are various kinds of combustion model presented by investigators (Kretschmer,

1972, Rizk, 1992, 1995 and Sturgess, 1996). Mellor (1972) and Odgers (1974) made reviews. Recently Oran (1991) and Chung (1993) presented new development in combustion model. A lot of work about combustion modeling was done by Sloan (1996).

There is more work required to improve present models. The first objective is to look for a suitable reaction equation set with a reasonable number of steps. The second is to get a better turbulence interaction with the chemical reaction by improving the eddy-break up model.

2.3 Pressure-Velocity Coupling

In incompressible flow problems, another difficulty lies in the calculation of the unknown pressure field, which can be related to the fact that only pressure gradients appear in the momentum conservation equations. The pressure field is indirectly derived from the compressibility constraint, i.e., continuity equation. Because of this, if velocities and pressure are stored at the same location, when the central differencing scheme is applied to both the continuity equation and the pressure gradient terms in the momentum equations, it has been shown to produce nonphysical oscillations in the pressure field, or checkerboard pressure field.

2.3.1 Staggered Grid Method

To eliminate the checkerboard pressure problem when using the primitive variable formulation, several methods based on the different storage locations for velocities and pressure have been developed.

The staggered grid method has been used by Patankar and Spalding (1972). The method consists in storing pressure at the main grid nodes in the discretized calculation domain and staggering the velocity components relative to these nodes.

Many CFD codes use this method. It is applied to the solution of complex flow problems in curvilinear orthogonal and non-orthogonal grids (Karki and Patankar, 1988, Shyy and Vu, 1991).

2.3.2 Vorticity-Stream Function

Early work based on the vorticity-stream function formulation which satisfies the incompressibility constraint identically, avoids the necessity of computing the pressure. This formulation was adopted by Elkaim et al. (1993) using the control volume finite element method on unstructured triangular grids for the simulation of the turbulent reacting flows. However, difficulties occur in applying boundary conditions on vorticity, and extension to three dimensions is not immediate. Due to these difficulties, the primitive variable formulation is preferable. The differences between the vorticity-stream function and primitive variable formulation are discussed by Roache (1976).

2.4 Reduction of Chemical Reaction Models

Chemical reaction models describing the evolution of a mixture of chemical species, usually with corresponding energy changes, are important components of reactive-flow models (Oran, 1987). In most combustion systems, the species are not in equilibrium and the precision of the overall model prediction depends on the accuracy of the representation of the chemical kinetics, among other factors. More reliable numerical results are obtained with more detailed reaction mechanisms, usually at the level of a set of elementary reaction steps. Past interests, such as simulation of engine knock (Warnatz, 1985), production NO_x (Keller, 1988) and soot formation (Frenklach, 1987) require increasingly large reaction mechanisms, hundreds of chemical reactions and species. Wang and Frenkilach (1997) have used a reaction mechanism which consists of 527 reactions and 99 chemical species. However, the

computational capabilities for an accurate, full-scale gas dynamic/chemical-kinetic simulation of these multidimensional reactive flows are not yet available (Espino, 1987, Biswas, 1997 and Hoffmann, 1998).

Although we have to wait until sufficient computational power and efficient numerical integration techniques become available to make large-scale modeling feasible, the technological needs and scientific interests will probably always outgrow the increases in computational capabilities. The popular method is to reduce the reaction mechanism. "Reduction" does not merely mean "simplification" of the chemistry involved, but rather reduction in the complexity of the mathematical form that describes the chemical transformations of a given reaction model.

There are two kinds of chemical kinetic modeling. The first is that the same single-reaction mechanism must be used in all reactive-flow models, because different parts of this reaction set become important at different conditions. For instance, it is quite common that the rate-limiting step switches from one reaction to another with the flame height. Omission (or reduction) of certain parts of the reaction mechanism is viewed, then, as the loss of mechanism universality. Scientific progress in this view is perceived as building and expanding a comprehensive reaction set to cover the increasing number of experimental conditions. Obviously, one cannot argue against universality of nature and, hence, against universality of the reaction mechanism required to model it, because elementary processes, bond-rearrangement in chemical reactions, energy transfer in molecular collisions, etc., are the same regardless whether they occur in hydrogen, octane, or coal flames. However, current advances in experimental techniques and theoretical methods rapidly expand the present database of combustion chemistry. In principle, the kinetic database is infinitely large, and the practical reality could happen in a not-too-distant future (similarly to the presently unlimited thermodynamic database: thermodynamic properties for any chemical compound can be estimated by group additivity or quantum mechanical methods).

All conceivable chemical reactions with the associated rate parameters (available

experimentally, calculated theoretically, or simply estimated) constitute a reaction data bank. Given a specific problem, a subset of the data bank should be taken to assemble the reaction mechanism. The question is how to choose this reaction subset such that it describes faithfully the dynamic behavior of a reactive-flow system. This is, how does one reduce an extensive reaction mechanism to a minimum set of reactions required to address a given problem. Moreover, this quantitatively accurate subset can be reduced further to a different but much smaller reaction set or, in general, to a different mathematical form that substantially decreases the demand on computational capacity. The methodologies required to answer these questions constitute the now-growing field of mechanism reduction.

The idea of mechanism reduction is not new. Introduction of the pseudo-steady-state approximation for reactive intermediates led to analytical solution of nonlinear reaction systems that otherwise could not be solved at that time. Expressing the reaction events in terms of the outcome probability allowed the analysis and prediction of the behavior of chain reactions. A rigorous mathematical formulation for the problem of "lumping" in which chemical species are transformed into a few dynamically equivalent "lumped classes", was started in the 1960's (Wei 1962). It is important to realize that even the most detailed chemical reaction models used presently in combustion are lumped model in the sense that the chemical species of these models are actually lumped classes of energy-distributed species and the "elementary" rate coefficients used for the reactions of these lumped classes are certain averages over the population of these energy-distributed species.

Odgers (1974) gave some of the various combustion systems that use multi-step kinetic systems. The number of reactions varied from 6 to 24. Owing to the fact that those models exhibit large errors of prediction when applied to other experimental environments, Odgers concluded that as far as the engineer is concerned, the use of a model will depend largely upon its predictive accuracy not necessarily its approach to true representation. Maybe the simple reaction rate equations are more suitable for engineering use.

2.5 Perfect Gas

When the chemical reaction rate within the flow field is extremely slow, such that fluid particles moving within the domain do not experience any change in the chemical composition, it is referred to as a frozen flow. For flow fields where the chemical reaction rates are extremely high, the reactions take place instantaneously. Thus, reactions are completed before the fluid has a chance to move downstream. Such a flow is called equilibrium flow or, more precisely, chemical equilibrium flow. For any flow, the specific heats are function of both pressure and temperature. Therefore, the ratio of specific heats is no longer constant and becomes a function of temperature and pressure as well. The gas constant is also a variable due to changes in the molecular weight of the mixture.

In reality, chemical reactions occur as particles are moving within the domain. Therefore, in situations where the flow cannot be classified as either frozen or equilibrium, it is referred to as nonequilibrium. For nonequilibrium flows, the perfect gas equation of state still holds, except the gas constant is now a variable because the molecular weight of the mixture is changing.

An important dimensionless parameter in combustion is the Damköhler number, Da. This parameter appears in the description of many combustion problems. The Damköhler number represents the ratio of a characteristic flow or mixing time to a characteristic chemical time; thus,

$$Da \equiv \frac{\text{characteristic flow time}}{\text{characteristic chemical time}} = \frac{t_{mix}}{t_{chem}} \tag{2.1}$$

The evaluation of Da depends on the situation under study, in the same sense that the Reynolds number has many particular definitions derived from its fundamental meaning as the ratio of inertia to viscous forces. When chemical reactions

rates are fast in comparison to fluid mixing rates, then $Da \gg 1$, and a fast-chemistry regime is defined. Conversely, when reaction rates are slow in comparison to mixing rates, then $Da \ll 1$. Note that the characteristic rates are inversely proportional to their corresponding characteristic times.

A molecule possesses a force field due to the electromagnetic actions of electrons and the nuclei. When a domain composed of many molecules is considered, the force field associated with each molecule affects other molecules in that it may act as a repulsive force if molecules are very close to each other or as an attractive force if they are relatively far apart. Under normal conditions, such as atmospheric, the average distance between molecules of air is about 10 molecular diameters, resulting in weak attraction forces. Now consider a fixed region and introduce more and more molecules into this fixed region. As a result, the molecules are close. This translates into conditions where the pressure is extremely high and/or temperature is very low. Under this condition the intermolecular forces become important and the gas is defined as a real gas. On the other hand, when the intermolecular forces are negligible, the gas is defined as a perfect gas. For the majority of problems in aerodynamics, the assumption of perfect gas is a valid one and is utilized extensively. From an application point of view, the major difference between a real gas and a perfect gas is the use of the equation of state. For a perfect gas, the equation of state $p = \rho RT$ is employed, whereas for a real gas, the van der Waals equation of state expressed as

$$(p + a\rho^2)(\frac{1}{\rho} - b) = RT \tag{2.2}$$

is usually employed. Note that in the equation above a and b are gas-dependent constants. An important point to clarify at this time is the consideration of chemistry. Whether the flow under study is chemically reacting or not has nothing to do with the assumption of perfect gas or real gas. Indeed, the equation of state for a perfect gas is used extensively for chemically reacting gases. Such a chemically reacting flow is considered a mixture of perfect gases. In this regard, the following

equation of state for a species s holds

$$p_s = \rho_s R_s T \tag{2.3}$$

where p_s is the partial pressure contributed by species s; ρ_s is the partial density contributed by species s; and R_s is the gas constant for species s defined as $R_s = R/M$ where R is the universal gas constant; M is the molar mass of species; and T is the temperature. Modification to Equation (2.3) to include real gas consideration may be accomplished by introduction of a so-called compressibility factor Z, such that

$$p_s = Z\rho_s R_s T \tag{2.4}$$

where the compressibility factor Z is usually given as a function of reduced pressure and temperature. Thus, when the compressibility factor is about one, the perfect gas equation of state may be employed.

2.6 Rates of Reactions

All chemical reactions take place at a finite rate depending on the conditions of the system. Some important conditions are (1) concentrations of the chemical compounds, (2) temperature, (3) pressure, (4) presence of a catalyst or inhibitor and (5) radiative effects. The rate of reaction may be expressed in terms of the concentration of any reactant as the rate of decrease of the concentration of the reactant (the rate of consumption of the reactant). It may also be expressed in terms of product concentration as the rate of increase of the product concentration. A conventional unit for reaction rate is mol/m^{3}sec. Although someone has to keep in mind that concentration is a function of temperature and pressure without chemical reaction.

The law of mass action, which is confirmed by numerous experimental observations, states that the rate of disappearance of a chemical species is proportional to the products of the concentrations of the reacting chemical species, each concentration being raised to a power equal to the corresponding stoichiometric coefficient. Thus the reaction rate is given as

$$\hat{R} = k \prod_{i=1}^{N} [C_{A_i}]^{v_i'} \tag{2.5}$$

where k is the proportionality function called the specific reaction-rate parameter. For a given chemical reaction, k is independent of the concentration C_{A_i} and depends on the temperature.

The equation

$$k = BT^{\alpha} \exp\left(-\frac{E_a}{R_u T}\right) \tag{2.6}$$

is called the Arrhenius law. Here BT^{α} represents the collision frequency and the exponential term is the Boltzmann factor. The activation energy E_a is the energy required for the reaction to occur. The values of B, α, and E_a are based on the nature of the elementary reaction.

The net rate of production of A_i is

$$\frac{dC_{A_i}}{dt} = (v_i'' - v_i')\hat{R} = (v_i'' - v_i')k \prod_{i=1}^{N} [C_{A_i}]^{v_i'} \tag{2.7}$$

where v' is stoichiometric coefficient for reactant and v'' for product. When combustion efficiency is less than 100 %, Kretschmer and Odgers (1972) gave the reaction rate equation,

$$\frac{\dot{N}}{VP^n} = \frac{k(m+1)[5(1-y\epsilon)]^a[\phi - y\epsilon]^{n-a} e^{-c/(T_i + \epsilon\Delta T)}}{R^n y\epsilon[5(m+1) + \phi + y\epsilon]^n [T_i + \epsilon\Delta T]^{n-0.5}} \tag{2.8}$$

2.7 Coupling between Turbulence and Chemical Reaction

Although the techniques for defining the molecular diffusion of momentum, heat, and mass are reasonably well established in a reacting flow, the same statement cannot be made for our ability to describe the turbulent diffusion of these quantities. Conventional approaches have included the use of algebraic eddy-viscosity models or differential transport models. Several eddy-viscosity models have been used, in particular, the Cebeci-Smith model (Cebeci and Smith, 1974) and the Baldwin-Lomax model (Baldwin and Lomax, 1978). The differential transport models include the $k-\varepsilon$ turbulent kinetic energy model and its variants, (Jones and Launder, 1972) a modified $k-\varepsilon$ model that included a supersonic flow compressibility correction, (Fabris, Harsha and Edelman , 1981; Hanjalic et al., 1979) and a multiple dissipation length scale (k multiple ε) model with a compressibility correction (Fabris, Harsha and Edelman, 1981; Hanjalic and Launder, 1980) that addressed the existence of multiple dissipation length scales that exist in the energy cascade of a turbulent flow. In addition to these differential transport models, the algebraic Reynolds Stress Models of Rodi (1972) and Sindir (1982) have also been considered for use in modeling turbulent reacting flows. Sindir (1982) reviews all of these models. In addition, he critically compares the models against several nonreacting flow experiments prior to using the models for studying flows with reaction. He concludes that forms of the algebraic Reynolds Stress Model produced the best agreement with nonreacting data. He also found that the multiple dissipation length scale model did not offer any advantage over the basic $k-\varepsilon$ model.

All of the turbulence models described earlier have a major disadvantage when applied to reacting flowfields: they fail to account for the important coupling between the turbulence and the chemistry. Turbulent fluctuations in the fluid mechanic

variables have a direct effect on the species production rates. The coup-ling between these two fields occurs through the Arrhenius rate expression and the law of mass action. The Reynolds averaging process applied to the governing equations eliminates the direct effect of temperature and species fluctuations on species production rates. For example, a positive temperature fluctuation would cause a decrease in the size of exponential argument of the Arrhenius rate expression, with a corresponding increase in the forward kinetic rate of a particular reaction. This would, in turn, produce an increase in the time rate of change of the products of that reaction. More importantly, if the reaction was at a critical point, where perhaps a small increase in temperature would cause a reaction to enter an ignition stage, the entire species distribution of the flowfield downstream could be changed.

Two promising ways for accounting for the effects of fluid and species fluctuations on chemical reaction would be through probability density functions or direct numerical simulation. The application of probability density function approach to a reaction flow will be discussed in Chapter 6. Direct numerical simulation offers another attractive approach for modeling a turbulent reacting flow. The method has been used for several years to model laminar and turbulent flames accurately (Smooke, 1989; Jou, 1989; Poinsot, 1996). With this approach, the Navier-Stokes and species continuity equations are resolved down to the smallest scale features of the flowfield. The size of those scales goes inversely with the Reynolds number of the flowfield. Clearly, for the high Reynolds numbers, the smallest scales can become quite small, necessitating a very fine computational grid to resolve them. Also, when high-speed flow undergoes chemical reaction, additional scales are introduced by the combustion process. Herein lies the principal difficulty of applying direct simulation to a high-speed flow. The difficulty is not so much one of numerical algorithms as it is of computer power. Highly accurate numerical algorithms are required, but appropriate high-order finite-difference methods, finite-volume methods, or spectral methods have been developed that satisfy that requirement. The large number of computational grid points required to resolve the smallest scales in the flow requires large computer storage, and, therefore, meaningful calculations can be carried out

only on large memory machines. Recently, direct numerical simulation has emerged as a new methodology. It has become an essential tool to understand and model turbulent combustion. DNS numerically solves the set of equations describing turbulent flames by resolving all chemical and flow scales (Vervisch, 1998). But DNS is used only for simple problems that are not of industrial scale.

As an alternative to direct numerical simulation with its intensive memory requirements, it is possible to model rather than compute the smallest scales. In this approach, termed large-eddy simulation, the larger scales above a chosen wavelength are still computed. The smaller scales below the cutoff wavelength are modeled, however, using a subgrid scale model. Large-eddy simulation is an attractive alternative because only the larger-scale effects are computed, lessening the computer memory requirements for higher-Reynolds-number flows. Subgrid scale models must be constructed, though, that give an accurate rendering of the physics of small-scale phenomena. This is a difficult task. Work is under way to develop subgrid scale models for nonreacting flow, e.g., the early work of Schumann (1975), later work described by Speziale et al. (1987) and recent work of Misra (1997). Large-eddy simulation is an attractive technique for modeling high-speed reacting flows. Little has been done so far with this technique, but it warrants serious attention now (Meneveau, 2000).

2.8 Numerical Solution

The three principal means of discretizing the governing equations are the use of finite differences, finite elements, and finite volumes. In using finite differences, the differential operators are approximated by making a Taylor series expansion of the operators in term of differences on a grid and taking a finite subset. The finite-element method basically consists of reducing the partial differential equations to a set of ordenary differential equations or algebraic equations; one typically assumes

an expansion of the function in terms of a basis. This could include polynomial fitting. Finally, the finite-volume method involves integrating the governing equations along the faces of control volumes surrounding each node. This has the advantage of satisfying the conservation laws in the difference equation. This is particularly easy to do for continuity, momentum and energy equations which are written in divergence, or conservation-law. In integrating over a volume, the divergence theorem can be used on the second terms on the left-hand side to transform them into the fluxes of each quantity across the enclosing surface. When the volume is that of a primitive cell, this guarantees that flux leaving one cell flows into the adjacent one, conserving the flux, both locally and globally. This leads to a set of algebraic equations involving scalar terms evaluated at the center of the cell and flux terms at the cell boundaries. Thus, the PDE's describing fluid flow are approximated by large set of algebraic equations. That is true, of course, whatever discretization method is used. Birkhoff (1983) has written an excellent review article that places the numerical solutions of these equations in perspective.

The method most generally used for the solution of the nonlinear difference equations is some variant of the Newton-Raphson multivariate procedure; this is equally useful for sets of nonlinear equations. This technique generally requires the evaluation of the Jacobian of the equations.

For the steady-state case, the Navier-Stokes equations are elliptic in the spatial variables. If the problem is one-dimensional and there is no radiation, the Jacobian is tridiagonal, and the solution method is easy (Richtmyer, 1967). The nonlinear Gauss-Seidel method can also be used, but it is not as good as Newton's method for this case. For the two-dimensional case there are five diagonals, and seven diagonals in three dimensions, but the matrix is still sparse, and special methods can be used to find the solution. The best way to solve them is by iterative techniques, rather than "exactly", because truncation errors can build up to prohibitive levels. When radiation is included in the problem, every cell connects with every other (i.e., there are no zero matrix elements), and no special solution methods are available.

Explicit methods have the theoretical advantage of yielding exact results in one pass; however, they may require exceedingly short time steps. Implicit methods are more stable and permit much larger time steps, usually more than making up for the fact that iterations are necessary for convergence to a solution. An early comparison of explicit vs. implicit methods is given (Torrance, 1968).

Early in 1977, Ku et al wrote the program UNDSAFE to solve the Navier-Stokes equations with local heating, in two dimensions. They solved the problem for rectangular enclosures. They used the SIMPLE algorithm. The governing equations and their boundary conditions are approximated with finite-difference equations by a control-volume-based method. The computing cells are chosen so that their boundaries coincide with physical boundaries. A staggered grid system devised by Meng (1994) was chosen. In this system, the pressure is evaluated at the centers of the cells while the velocity components and other scalar variables are evaluated at the cell boundaries. Thus, the momentum equations are written for cells centered at the boundaries of the basic cells. The convection-diffusion terms are discretized by an hybrid scheme.

2.9 Radiation Modeling

Radiation is an important mechanism of energy transfer to the walls of large combustion chambers. The difficulties associated with radiation modeling are the multi-dimensional nature of the phenomena, the integral-differential nature of radiative transfer equation, and the coupling between the radiative transfer equation and the energy conservation equation (Chiu 1990). Unlike the flow field, which can be solved directly by a spatial integration algorithm, for radiation, both spatial integration and angular integration have to be carried out. There are several radiation models, such as Zonal (Hottel 1967), Monte-Carlo (Howell 1968), Flux (Gosman 1973) methods. The excellent reviews of various radiation models on combustion system are given by Viskanta (1987) and Howell (1988).

2.9.1 Monte Carlo Method

The Monte Carlo method is based on a statistical approach. The exchange factors are automatically calculated as the randomly chosen energy releases are tracked through the domain for their lifetimes. This method can in principle be programmed to include an exact simulation of all important processes (Howell 1988). Applications may be found in Burns et al. (1992) and Gorner (1993), which illustrate its geometry flexibility and ability to handle difficult problems.

The drawbacks of this method are that it requires long computation time to obtain good results due to the method's statistical approach. Another difficulty is the grid size incompatibility, in which the computational element size required for statistical accuracy in the Monte Carlo solution may not be compatible with the grid size necessary for numerical solution of the energy equation, even given sufficiently fast and cheap computation capability (Howell 1988).

2.9.2 Zonal Method

The Zonal method is based on the view factor and mean beam length concepts. Essentially geometric in its approach, the domain is divided into a number of surface and volume zones about which radiation balance and total energy balance are formulated. Each zone is considered to be uniform in temperature and radiation properties. The heat release and the flow patterns are specified in advance. Geometric exchange factors (exchange areas) between each zone pair are supposed to be known a priori.

The advantage of this method is that it can approach an exact solution for the radiative fluxes as the number of zones is increased, and even for a relatively coarse zone, it can give good results.

The major difficulty of applying this method is the tedious evaluation of the direct exchange areas. Attempts to improve the zonal method were made by Larsen (1985) with an exchange factor method, by Naraghi (1988), with a continuous exchange factor method in participating media, by Saltiel (1991), with an exchange factor method in non-homogeneous media, respectively. Considering the anisotropically scattering media, Yuen (1992) developed a Generalized Zonal method. However, there is a difficulty in matching the required grid sizes for radiation and fluid flow field (Howell, 1988) and the calculation of the exchange areas remains very difficult for complex geometries (Viskanta 1987).

2.9.3 Flux Method

In the flux methods, the angular variation of the radiant intensity in space is assumed to be a certain functional form. The integro-differential radiative transfer equations then reduce to a set of partial differential equations. The various flux methods are classed as Flux Model, Spherical Harmonics method, Discrete Ordinates (S_N) method according to the different functions (or weighting coefficients) used. Because this class of methods is essentially a field method, they can easily be incorporated into existing flow and reaction solvers.

2.9.4 Discrete Transfer Method

The discrete transfer method was proposed by Shah (1979). Firstly, the surface of the enclosure is divided into subsurfaces, and the volume of the medium is divided into cells; secondly, taking each subsurface as an hemisphere, the emitted radiation is subdivided into beams, where each beam is assumed to have positive and negative propagation direction (Fluxes); finally, the beams are drawn hemispherically from each subsurface in prescribed directions (similar to Monte Carlo method, in random direction). The solution proceeds along individual rays of intensity, one at a time, instead of solving for all the intensities in the field. It can be classified as

the ray tracing method. A survey of ray tracing procedure are given by Glassner (1989). This method can be considered as a combination of the Zonal method, Flux Model and Monte Carlo technique. It retains their advantages while avoiding their shortcomings.

Because the number of beams is specified in advance, it can be more economical than the Monte Carlo solution which needs a lot of random beams to obtain good results. It is flexible and able to handle complex geometries. In application to absorption media, finer discretization can yield any desired degree of precision, and even reproduce the exact solutions. For gas flames, where the scattering is small, the method can provide excellent results as evidenced by the work of Meng et al. (1992). When scattering is considered, a simple average is used in the discrete transfer computations, unlike the S_N method which uses a more accurate numerical quadrature. This will reduce the accuracy when this method is applied to solve anisotropic scattering problem.

2.9.5 Emissivity Models

For the nongray medium, the spectral effect of the radiation has to be considered, and the radiative transfer equation should be integrated over the entire wavelength spectrum. Naturally, this will make the computation times prohibitive. Under some situations this is not necessary; for example, in natural gas or oil fired combustors only three species contribute significantly to the radiation in the infrared region. These species are the products of the combustion, i.e. carbon dioxide, water vapour and hot soot particles within the flame (Khalil, 1982).

A more useful approach to modeling the spectral properties of the gases is the wide-band models of Edwards (1976), in which the band emittance of these gases is considered as a function of total and partial pressure, path length and temperature. This method makes the band properties of the gas mixture relatively easy to calculate, but the computation time is longer than the mixture of gray gas model

of Hottel and Cohen (1958). Doherty (1988) incorporated the wide band model into the computation of the nonhomogeneous combustion products by the discrete transfer method, they showed a good agreement with the narrow band model results for both spectral and total radiative intensities.

2.9.6 Other Methods

The radiative transfer equation can be solved by other methods, as the finite element (FEM) (Fiveland, 1993) and finite volume method (FVM) (Raithby, 1990), as well as boundary element method (BEM) (Bialecki, 1991).

The advantage of using FEM is that it offers the possibility of high accuracy, and can be used with the same grid as for the flow and energy conservation equation. Furthermore, it can be applied to complex geometries. Tan (1989) used the product-integration method to solve radiation problems, significantly reducing the solution time of FEM.

The FVM can give good accuracy on coarse grid. The intensity at the integration points is determined from the solution of the radiative transfer equation using the skewed upwinding procedure. It satisfies the global conservation constraints for intensity and heat flux, hence prevents the occurrence of the "ray effect" encountered in the S_N method (Chiu, 1990).

Using BEM, the integration is over the boundary, no volume integrals are present in BEM, thus it requires fewer calculations (Bialechi, 1991). However, because the ray-tracing method is used in BEM computations, it may suffer from the disadvantages of the discrete transfer method when scattering has to be considered.

Chapter 3

Basic Theories in Combustion Modeling

Combustion is a very complex phenomenon. It involves many subjects, such as fluid mechanics, heat and mass transfer, chemical kinetics, thermodynamics and turbulence. Understanding of the fundamental concepts of these coupled processes will be useful to solve combustion problems.

Combustion models for gas turbine combustors still need improvement to provide reasonable flow field estimates to be useful for design purposes. The combustor design process is still very empirical and requires great expertise to predict the exhaust field for pollutants concentration or temperature distribution.

3.1 Fluid Mechanics

3.1.1 Conservation of Mass

To derive the equation of continuity for each species in a multicomponent mixture, we begin by making a mass balance over an arbitrary differential fluid element in a binary mixture. We apply the law of conservation of mass of species A to a volume element $\Delta x \Delta y \Delta z$ fixed in space through which a binary mixture of A and B is flowing. Within this element, A may be produced by chemical reaction at a rate $\omega_A(\text{kgm}^{-3}\text{sec}^{-1})$. The various contributions to the mass balance are:

$$\frac{\partial \rho_A}{\partial t} + \left(\frac{\partial \dot{m}_{Ax}}{\partial x} + \frac{\partial \dot{m}_{Ay}}{\partial y} + \frac{\partial \dot{m}_{Az}}{\partial z} \right) = \omega_A \tag{3.1}$$

This is the equation of continuity for component A in a binary mixture. The quantities m_{Ax}, m_{Ay}, m_{Az} are the rectangular components of the mass flux vector $\dot{\mathbf{m}}_A(\text{kgm}^{-2}\text{sec}^{-1})$. In vector notation, the equation may be rewritten as

$$\frac{\partial \rho_A}{\partial t} + (\nabla \cdot \dot{\mathbf{m}}_A) = \omega_A \tag{3.2}$$

Similarly, the equation of continuity for component B is

$$\frac{\partial \rho_B}{\partial t} + (\nabla \cdot \dot{\mathbf{m}}_B) = \omega_B \tag{3.3}$$

Addition of Equations (3.2) and (3.3) gives

$$\frac{\partial \rho}{\partial t} + (\nabla \cdot \rho \mathbf{v}) = 0 \tag{3.4}$$

which is the equation of continuity for the mixture. In arriving at Equation (3.4), we have made use of both the reaction $\dot{\mathbf{m}}_A + \dot{\mathbf{m}}_B = \rho \mathbf{v}$ and the law of conservation of mass in the form $\omega_A + \omega_B = 0$. For a fluid of constant mass density ρ, Equation

(3.4) becomes

$$\nabla \cdot \mathbf{v} = 0 \tag{3.5}$$

The development given above could have been made equally well in terms of molar units. If Ω_A is the molar rate of production of A per unit volume, then the molar analog of Equation (3.2) is

$$\frac{\partial C_A}{\partial t} + \nabla \cdot \dot{\mathbf{n}}_A = \Omega_A \tag{3.6}$$

where $\dot{\mathbf{n}}$ is molar flux and

$$\frac{\partial \rho_A}{\partial t} + \nabla \cdot \rho_A \mathbf{v} = \nabla \cdot \rho D_{AB} \nabla Y_A + \omega_A \tag{3.7}$$

finally

$$\frac{\partial C_A}{\partial t} + \nabla \cdot C_A \mathbf{v}^* = \nabla \cdot C D_{AB} \nabla X_A + \Omega_A \tag{3.8}$$

where $\mathbf{v}^*$ is molar-average velocity. If no chemical reaction occur, $\omega_A, \omega_B, \Omega_A, \Omega_B$ are all zero. If in addition $\mathbf{v}$ is zero in Eq.(3.7) or $\mathbf{v}^*$ is zero in Eq.(3.8), we get

$$\frac{\partial C_A}{\partial t} = D_{AB} \nabla^2 C_A \tag{3.9}$$

which is called Fick's second law of diffusion. This equation is generally used for diffusion in solids or stationary liquids and for equimolar counterdiffusion in gases. This equation is similar to the heat-conduction equation.

For a multicomponent system, Eq. (3.2) becomes

$$\frac{\partial Y_i \rho}{\partial t} + \nabla \cdot \rho Y_i (\mathbf{v} + \mathbf{V}_i) = \omega_i \tag{3.10}$$

$$\frac{\partial Y_i}{\partial t} + \mathbf{v} \cdot Y_i + \frac{1}{\rho} \nabla \cdot \rho Y_i \mathbf{V}_i = \frac{\omega_i}{\rho} \qquad i = 1, 2, \ldots, N \tag{3.11}$$

In a general multicomponent system, there are N equations of this kind. The addition of these equations gives the equation of continuity for the mixture. Any one of these N equations may be replaced by the equation of continuity for the mixture in any given problem. The fact that these are N-1 independent equations for Y_i corresponds to the fact that only N-1 of the Y_i are independent.

3.1.2 Conservation of Momentum

The basic assumption is that we are dealing with continuous, isotropic, and homogeneous media. We shall consider that special case of a Newtonian fluid, that is, a fluid exhibiting a linear relationship between shear stress and rate of deformation, resulting in the Navier-Stokes equation.

The momentum equation can be derived in terms of stress using three different approaches. The basis for any derivation of the momentum conservation equations is Newton' second law of motion.

$$\sum \mathbf{F} = \frac{d(m\mathbf{v})}{dt} \tag{3.12}$$

Where three approaches are used:

a) Infinitesimal Particle. Consider a fluid particle as it moves through space relative to some fixed coordinate system. Equation (3.12) describes the motion of the particle. The acceleration of that particle is then related to various particles at "fixed points" in the flow field. Thus, we relate the motion of a particle to the observation of conditions of various particles at a fixed point in space.

b) Infinitesimal Control Volume. Consider a cubical infinitesimal volume element fixed in space. Then, equate the net momentum flux out of the control volume plus the time rate of change of momentum in the control volume to the net force on the mass within the control volume.

c) Finite Control Volume. Consider a gas-permeable control volume of finite size. This control volume can have any arbitrary shape and is fixed resulting in an equation involving only volume integrals. It is argued that the conditions must be satisfied for the integrand, since the integration is arbitrary. This results in the desired differential momentum equation.

With three similar but basically different approaches, the same momentum equation in terms of stress can be obtained:

$$\rho\left[u_j\frac{\partial u_i}{\partial x_j}+\frac{\partial u_i}{\partial t}\right]=\frac{\partial \sigma_{ji}}{\partial x_j}+\rho\sum_{k=1}^{N}(Y_k f_k)_i \tag{3.13}$$

3.1.3 Conservation of Energy

Similarly, we can get the energy equation,

$$\rho C_p\left[\frac{\partial T}{\partial t}+(\mathbf{u}\cdot\nabla)T\right]-\frac{\partial p}{\partial t}-(\mathbf{u}\cdot\nabla)p-\sigma_{ij}u_{i,j}-$$

$$\nabla\cdot(\rho c_p DT\nabla Y_k)-\nabla\cdot(\rho C_p D\nabla T)=-\sum_{k=1}^{N}H_k^0\omega_k \tag{3.14}$$

where the stagnation energy E as

$$E=e+\frac{1}{2}\mathbf{u}\cdot\mathbf{u} \tag{3.15}$$

3.2 Chemical Kinetics

Chemical kinetics deal with the quantitative study of the rates of chemical reactions and of the factors upon which they depend. It deals with the interpretation of

the empirical kinetic laws in terms of reaction mechanisms. All chemical reactions, whether hydrolysis or combustion, take place at a definite rate, depending on the conditions of the system. Some important conditions are: concentrations of the chemical compounds, temperature, pressure, presence of a catalyst or inhibitor and radiative effects.

3.2.1 One-Step Chemical Reactions

A one-step chemical reaction of arbitrary complexity can be represented by the following stoichiometric equation:

$$\sum_{i=1}^{N} v_i' A_i \rightarrow \sum_{i=1}^{N} v_i'' A_i \tag{3.16}$$

where v_i' are the stoichiometric coefficients of the reactants, v_i'' the stoichiometric coefficients of the products, A the arbitrary specification of all chemical species, and N the total number of compounds involved. If a species represented by A_i does not occur as a reactant, then v_i'=0; if the species does not occur as a product, then v_i'' =0.

Successful combustion system modeling depends on a correct description and coupling of the pertinent fluid mechanic, turbulent, heat transfer and chemical processes entailed. Until recently, hydrocarbon chemistry has frequently been described by very simple expressions. However, it is becoming increasingly apparent that success in understanding a significant portion of present combustion problems depends on a detailed and correct understanding of the hydrocarbon chemistry.

The simplest mechanism and the one which is the most convenient for numerical modeling is the one-step overall kinetic mechanism. This approach considers the oxidation process to occur directly to CO_2 and H_2O:

$$C_nH_m + \left(n + \frac{m}{4}\right)O_2 \Rightarrow nCO_2 + \frac{m}{2}H_2O \tag{3.17}$$

The advantage is immediately obvious that only 4 chemical species are involved in the formulation. Since it is a linear function of the amount of fuel which is reacted, the heat release calculation is also quite simple. Unfortunately, this mechanism does not account for the characteristics of hydrocarbon oxidation. The formation of intermediate hydrocarbons and CO is not taken into account.

3.2.2 Multi-Step Chemical Reactions

By using the above one-step chemical reaction, the total heat of reaction is over-predicted. At adiabatic flame temperatures typical of hydrocarbon fuels (~2000K) substantial amounts of CO and some H_2 exist in the combustion process. Their presence lowers the total heat release and consequently the adiabatic flame temperature is below the values predicted by the one-step method.

One-step mechanism can be modified by using two- or multi-steps. For example, a two-step method (Westbrook, 1981) with hydrocarbon fuels results in:

$$C_nH_m + \left(\frac{n}{2} + \frac{m}{4}\right)O_2 \Rightarrow nCO + \frac{m}{2}H_2O \tag{3.18}$$

$$CO + \frac{1}{2}O_2 \Leftrightarrow CO_2 \tag{3.19}$$

No prediction is made as to the formation of intermediate species. This mechanism still does not account for the time delay in the initial release of a significant amount of energy.

A detailed chemical kinetic reaction mechanism (Westbrook and Pitz, 1984) is developed to describe the oxidation and pyrolysis of propane and propene. The mechanism consists of 163 elementary reactions among 41 chemical species. New rate expressions are developed for a number of reactions of propane, propene and intermediate hydrocarbon species with radicals including H, O and OH. The mechanism is tested by comparisons between computed and experimental results in shock

tubes and the turbulent flow reactor. The resulting comprehensive mechanism accurately reproduces experimental data for pressures from 1 to 15 atmospheres, combustion temperatures from 1000 to 1700 K and fuel-oxidizer equivalence ratios from very lean to pyrolysis conditions. The mechanism also predicts correctly laminar flame properties for propane and propene and detonation properties for propane.

A more detailed reaction mechanism is used by Wang and Frenkilach (1997) for studying laminar premixed flames. The reaction mechanism consists of 527 reactions and 99 chemical species. The rate coefficients were either taken from literature or estimated based upon analogous reactions. It was shown that the reaction model predicts reasonably well the concentration profiles of major and intermediate species and aromatic molecules in a number of acetylene and ethylene flames reported in the literature.

3.3 Thermodynamics

3.3.1 The Zeroth Law

There exists an intensive variable, the temperature

$$T = T(p, V, n) \tag{3.20}$$

When two bodies have the same temperature as a third body, they have the same temperature as each other, and so will be in equilibrium if placed in thermal contact.

3.3.2 The First Law

$$\oint \delta\hat{Q} = \oint \delta\hat{W} \qquad \text{(for a cycle)} \tag{3.21}$$

During any cycle a system undergoes, the cyclic integral of the heat is equal to the cyclic integral of work.

$$E = H + KE + PE \qquad \text{(open system)} \tag{3.22}$$

where H is enthalpy, KE is kinetic energy and PE potential energy.

$$KE = \frac{1}{2}m\mathbf{v}^2 \tag{3.23}$$

$$PE = mgz \tag{3.24}$$

Energy associated with internal energy, U, combined with the energy associated with flow work, pV, is represented by a property called enthalpy, H

$$H = U + pV \tag{3.25}$$

Specific enthalpy is defined by

$$h = u + pv \tag{3.26}$$

3.3.3 The Second Law

The state function called the entropy

$$S = S(p, V, n) \tag{3.27}$$

For a closed system that undergoes a change from one state of thermodynamic equilibrium 1 to another state 2, the change in entropy is given by

$$S_2 - S_1 = \int_1^2 \left(\frac{\delta\hat{Q}}{T}\right)_{rev} \tag{3.28}$$

where *rev* implies any reversible path between 1 and 2, $\delta\hat{Q}$ is the heat received from or added to the system and T is the corresponding absolute temperature.

If the same system undergoes an irreversible or real process between the same two equilibrium states 1 and 2,

$$S_2 - S_1 > \int_1^2 \left(\frac{\delta\hat{Q}}{T}\right) \tag{3.29}$$

In general,

$$dS \geq \frac{\delta\hat{Q}}{T} \tag{3.30}$$

3.4 Turbulence

As the turbulent motion is random and irregular, it has a broad range of length scales. In order to obtain theoretical solutions by solving three-dimensional, time-dependent problems, we would have to consider computer storage capacity and use some type of averaged quantities in turbulent flows. There are two different averaging procedures commonly used, conventional time averaging (also called Reynolds averaging) and mass-weighted averaging (also called Favre averaging).

3.4.1 Conventional Time Averaging and Mass-Weighted Averaging

In order to obtain governing conservation equations for turbulent flames, it is convenient to decompose instantaneous quantities into mean and fluctuating quantities. In the conventional time-averaging procedure, the mean quantity $\bar{h}$ is defined by

$$\bar{h} = \lim_{\Delta t \to \infty} \frac{1}{\Delta t} \int_{t_o}^{t_o + \Delta t} h(t) dt \tag{3.31}$$

Clearly, the time average is useful only if it is independent of t_o; then, the averaged quantities are called statistically stationary. Physical quantities for stationary mean flows can now be decomposed into two parts, related to the mean motion and the fluctuation, or eddy motion:

$$u_i(x_i, t) = \overline{u_i(x_i)} + u_i'(x_i, t) \tag{3.32}$$

$$p(x_i, t) = \overline{p(x_i)} + p'(x_i, t) \tag{3.33}$$

$$\rho(x_i, t) = \overline{\rho(x_i)} + \rho'(x_i, t) \tag{3.34}$$

$$h_t(x_i, t) = \overline{h_t(x_i)} + h_t'(x_i, t) \tag{3.35}$$

$$T(x_i, t) = \overline{T(x_i)} + T'(x_i, t) \tag{3.36}$$

where the average of fluctuating quantities, $\overline{q'}(t)$, is zero, thus

$$\overline{\rho'} = \overline{h_t'} = \overline{p'} = \overline{T'} = 0 \tag{3.37}$$

In addition if f and g are two dependent variables and if s denotes any one of the independent variables x, y, z and t, then the Reynolds averaging rule requires that

$$\overline{\overline{f}} = \overline{f} \tag{3.38}$$

$$\overline{f + g} = \overline{f} + \overline{g} \tag{3.39}$$

$$\overline{\bar{f}\bar{g}} = \bar{f}\bar{g} \qquad \overline{fg} = \bar{f}\bar{g} + \overline{f'g'} \tag{3.40}$$

$$\overline{\frac{df}{ds}} = \frac{d\bar{f}}{ds} \tag{3.41}$$

$$\overline{\int f ds} = \int \bar{f} ds \tag{3.42}$$

and the conservation equations can be expressed in terms of the average and fluctuation correlation quantities.

The continuity equation is

$$\frac{\partial \bar{\rho}}{\partial t} + \frac{\partial \bar{\rho}\bar{u}_i}{\partial x_i} + \frac{\partial \overline{\rho' u_i'}}{\partial x_i} = 0 \tag{3.43}$$

The momentum equation for an incompressible fluid is

$$\rho\left[\frac{\partial \bar{u}_i}{\partial t} + \bar{u}_j \frac{\partial \bar{u}_i}{\partial x_j}\right] = -\frac{\partial \bar{p}}{\partial x_i} + \frac{\partial}{\partial x_j}\left[\mu \frac{\partial \bar{u}_i}{\partial x_j} - \rho \overline{u_i' u_j'}\right] + \bar{f}_i \tag{3.44}$$

where

$-\rho \overline{u_i' u_j'}$ is called the apparent or Reynolds stress.

A mass-weighted mean velocity can be defined as

$$\tilde{u}_i \equiv \frac{\overline{\rho u_i}}{\bar{\rho}} \tag{3.45}$$

The velocity may then be written as

$$u_i(x_i, t) \equiv \tilde{u}_i(x_i) + u_i''(x_i, t) \tag{3.46}$$

where $u_i''(x_i,t)$ is the superimposed velocity fluctuation.

$$h(x_i,t) \equiv \tilde{h}(x_i) + h''(x_i,t) \tag{3.47}$$

$$T_i(x_i,t) \equiv \tilde{T}_i(x_i) + T_i''(x_i,t) \tag{3.48}$$

$$h_t(x_i,t) \equiv \tilde{h}_t(x_i) + h_t''(x_i,t) \tag{3.49}$$

By time-averaging,

$$\overline{\rho u_i} = \overline{\rho}\tilde{u}_i + \overline{\rho u_i''} \tag{3.50}$$

noticing

$$\overline{\rho u_i''} = \overline{\rho T''} = \overline{\rho h''} = \overline{\rho h_t''} = 0 \tag{3.51}$$

3.4.2 Navier-Stokes Equations

The equations of fluid motion in complete form which include the conservation of mass, momentum and energy are referred to as Navier-Stokes equations. The nondimensional Navier-Stokes equations in the Cartesian coordinate system in a vector form are

$$\frac{\partial Q^*}{\partial t^*} + \frac{\partial E^*}{\partial x^*} + \frac{\partial F^*}{\partial y^*} + \frac{\partial G^*}{\partial z^*} = \frac{\partial E_v^*}{\partial x^*} + \frac{\partial F_v^*}{\partial y^*} + \frac{\partial G_v^*}{\partial z^*} \tag{3.52}$$

where

$$Q^* = \begin{bmatrix} \rho^* \\ \rho^* u^* \\ \rho^* v^* \\ \rho^* w^* \\ \rho^* e_t^* \end{bmatrix} \tag{3.53}$$

$$E^* = \begin{bmatrix} \rho^* u^* \\ \rho^* u^{*2} + p^* \\ \rho^* u^* v^* \\ \rho^* u^* w^* \\ (\rho^* e_t^* + p^*) u^* \end{bmatrix} \quad E_v^* = \begin{bmatrix} 0 \\ \tau_{xx}^* \\ \tau_{xy}^* \\ \tau_{xz}^* \\ u^* \tau_{xx}^* + v^* \tau_{xy}^* + w^* \tau_{xz}^* - q_x^* \end{bmatrix} \tag{3.54}$$

$$F^* = \begin{bmatrix} \rho^* v^* \\ \rho^* v^* u^* \\ \rho^* v^{*2} + p^* \\ \rho^* v^* w^* \\ (\rho^* e_t^* + p^*) v^* \end{bmatrix} \quad F_v^* = \begin{bmatrix} 0 \\ \tau_{yx}^* \\ \tau_{yy}^* \\ \tau_{yz}^* \\ u^* \tau_{yx}^* + v^* \tau_{yy}^* + w^* \tau_{yz}^* - q_y^* \end{bmatrix} \tag{3.55}$$

$$G^* = \begin{bmatrix} \rho^* w^* \\ \rho^* w^* u^* \\ \rho^* w^* v^* \\ \rho^* w^{*2} + p^* \\ (\rho^* e_t^* + p^*) w^* \end{bmatrix} \quad G_v^* = \begin{bmatrix} 0 \\ \tau_{zx}^* \\ \tau_{zy}^* \\ \tau_{zz}^* \\ u^* \tau_{zx}^* + v^* \tau_{zy}^* + w^* \tau_{zz}^* - q_z^* \end{bmatrix} \tag{3.56}$$

$$
\begin{aligned}
q_x^* &= -\frac{\mu^*}{PrRe_\infty(k-1)M_\infty^2}\frac{\partial T^*}{\partial x^*} \\
q_y^* &= -\frac{\mu^*}{PrRe_\infty(k-1)M_\infty^2}\frac{\partial T^*}{\partial y^*} \\
q_z^* &= -\frac{\mu^*}{PrRe_\infty(k-1)M_\infty^2}\frac{\partial T^*}{\partial z^*}
\end{aligned}
\tag{3.57}
$$

Reynolds number:

$$Re_\infty = \frac{\rho_\infty u_\infty L}{\mu_\infty}$$

Prandtl number:

$$Pr = \frac{\mu c_p}{k}$$

3.5 Heat Transfer

3.5.1 Conduction

Fourier's Law:

$$q'' = -k\nabla T = -k\text{grad}T \tag{3.58}$$

q'' is the heat flux and k is thermal conductivity.

3.5.2 Convection

Newton's Law of cooling:

$$q'' = h(T_s - T_\infty) \tag{3.59}$$

h: convection heat transfer coefficient.

3.5.3 Radiation

Stefan-Boltzmann's Law (for black body):

$$E_b = \sigma T^4 \tag{3.60}$$

E_b: the total hemispherical emissive power;

σ: Stefan-Boltzmann constant.

$$\sigma = \frac{C_1}{C_2^4}\int_0^\infty \frac{u^3 du}{e^u - 1} = \frac{C_1}{C_2^4}\frac{\pi^4}{15} = 5.67 \times 10^{-8}\mathrm{W/m^2 \cdot K^4} \tag{3.61}$$

where

$$C_1 = 2\pi hc^2 = 3.742 \times 10^{-16} \quad \mathrm{W \cdot m^2}$$

$$C_2 = \frac{hc}{k} = 1.439 \times 10^{-2} \quad \mathrm{m \cdot K}$$

c: the speed of propagation of the wave, $c = 2.998 \times 10^8$ m/s ;

h: Planck's constant, $h = 6.6256 \times 10^{-34}$J ·s ;

k: Boltzmann's constant, $k = 1.3805 \times 10^{-23}$ J/K

Chapter 4

FLUENT Introduction(Fluent,1998)

FLUENT is a state-of-the-art computer program for modeling fluid flow and heat transfer in complex geometries. It provides complete mesh flexibility, solving flow problems with unstructured meshes that can be generated from complex geometries with relative ease. Supported mesh types include 2D triangular/quadrilateral, 3D tetrahedral/hexahedral/pyramid/wedge, and mixed (hybrid) meshes. It can also refine or coarsen the grid based on various flow parameters.

FLUENT is written in the C computer language and makes full use of the flexibility and power offered by the language. Consequently, true dynamic memory allocation, efficient data structures, and flexible solver control are all made possible. In addition, FLUENT uses a client/server architecture, which allows it to run as separate simultaneous processes on client desktop workstations and powerful compute servers, for efficient execution, interactive control and complete flexibility of machine or operating system types. All functions required to compute a solution and display the results are accessible in FLUENT through an interactive, menu-driven interface.

4.1 Program Structure

The FLUENT package includes the following products:

FLUENT, the solver,
prePDF, the preprocessor for modeling PDF combustion,
GAMBIT, the preprocessor for geometry modeling and mesh generation,
TGrid, an additional preprocessor that can generate volume meshes from existing boundary meshes, and
Filters (translators) for import of surface and volume meshes from CAD/CAE packages such as ANSYS, I-DEAS, NASTRAN, PATRAN, and others.

Once a grid has been read into FLUENT, all remaining operations are performed within the solver. These include setting boundary conditions, defining fluid properties, executing the solution, refining the grid and viewing and postprocessing the results.

Fluent can use unstructured meshes which can reduce the amount of time generating a grid. FLUENT can also use block-structured meshes. Therefore it is capable of handling both triangular and quadrilateral elements (or a combination of the two) in 2D, hexahedral, pyramid, and wedge elements (or a combination of these) in 3D.

All types of meshes can be adapted in order to resolve large gradients in the flow field, but the initial mesh is generated (whatever the element types used) outside of the solver, using GAMBIT, TGrid, or one of the CAD systems for which mesh import filters exist.

4.2 Problem Solving Steps

The basic procedural steps are shown below.

1. Create the model geometry and grid,
2. Start the appropriate solver for 2D or 3D modeling,
3. Import the grid,
4. Check the grid,
5. Select the solver formulation,
6. Choose the basic equations to be solved: laminar or turbulent (or inviscid), chemical species or reaction, heat transfer models, etc. Identify additional models needed: fans, heat exchangers, porous media, etc,
7. Specify material properties,
8. Specify the boundary conditions,
9. Adjust the solution control parameters,
10. Initialize the flow field,
11. Calculate a solution,
12. Examine the results,
13. Save the results, and
14. If necessary, refine the grid or consider revisions to the numerical or physical model.

4.3 Numerical Schemes

There are two numerical methods: segregated solver and coupled solver.

Using either method, FLUENT will solve the governing integral equations for the conservation of mass and momentum, and (when appropriate) for energy and other

scalars such as turbulence and chemical species. In both cases a control-volume-based technique is used that consists of:

Division of the domain into discrete control volumes using a computational grid.

Integration of the governing equations on the individual control volumes to construct algebraic equations for the discrete dependent variables ('unknowns') such as velocities, pressure, temperature, and conserved scalars.

Linearization of the discretized equations and solution of the resultant linear equation system to yield updated values of the dependent variables.

The two numerical methods employ a similar discretization process (finite-volume), but the approach used to linearize and solve the discretized equations is different.

4.3.1 Segregated Solution Method

Using the segregated solver, the governing equations are solved sequentially (i.e., segregated from each another). Because the governing equations are non-linear (and coupled), several iterations of the solution loop must be performed before a converged solution is obtained. Each iteration consists of the steps illustrated in Figure 4.1 and outlined below:

1. Fluid properties are updated, based on the current solution. (If the calculation has just begun, the fluid properties will be updated based on the initialized solution.)

2. The u, v and w momentum equations are each solved in turn using current values for pressure and face mass fluxes, in order to update the velocity field.

3. Since the velocities obtained in Step 1 may not satisfy the continuity equation locally, a 'Poisson-type' equation for the pressure correction is derived from the continuity equation and the linearized momentum equations. This pressure correction equation is then solved to obtain the necessary corrections to the pressure and velocity fields and the face mass fluxes, such that continuity is satisfied.

4. Where appropriate, equations for scalars such as turbulence, energy, species, and radiation are solved using the previously updated values of the other variables.

5. When interphase coupling is to be included, the source terms in the appropriate continuous phase equations may be updated with a discrete phase trajectory calculation.

6. A check for convergence of the equation set is made.

These steps are continued until the convergence criterias are met.

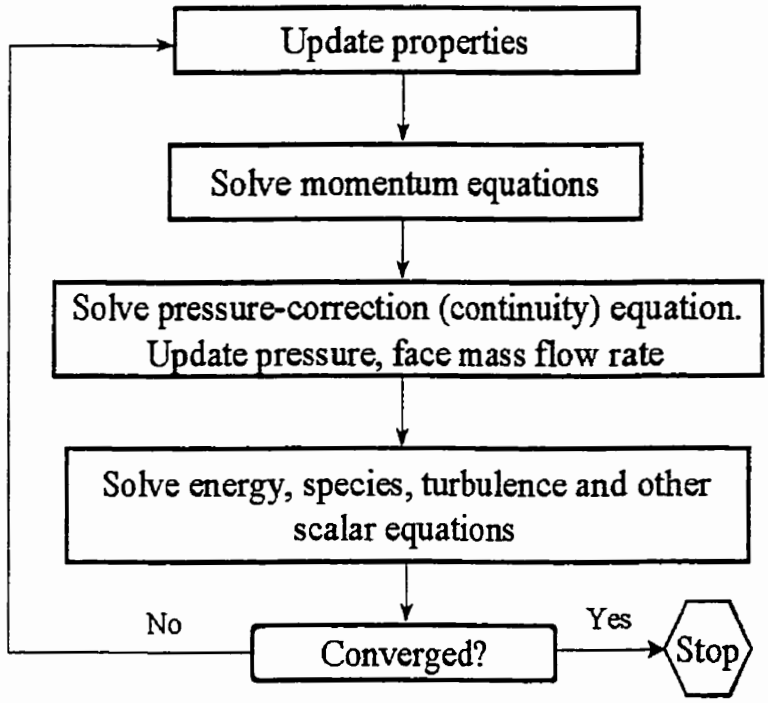

Figure 4.1 Overview of the Segregated Solution Method

4.3.2 Coupled Solution Method

Using the coupled solver, the governing equations to include continuity, momentum, and (where appropriate) energy and species transport are solved simultaneously (i.e., coupled together). Governing equations for additional scalars will be solved sequentially (i.e., segregated from one another and from the coupled set). Because the governing equations are non-linear (and coupled), several iterations of the solution loop must be performed before a converged solution is obtained. Each iteration consists of the steps illustrated in Figure 4.2 and outlined below:

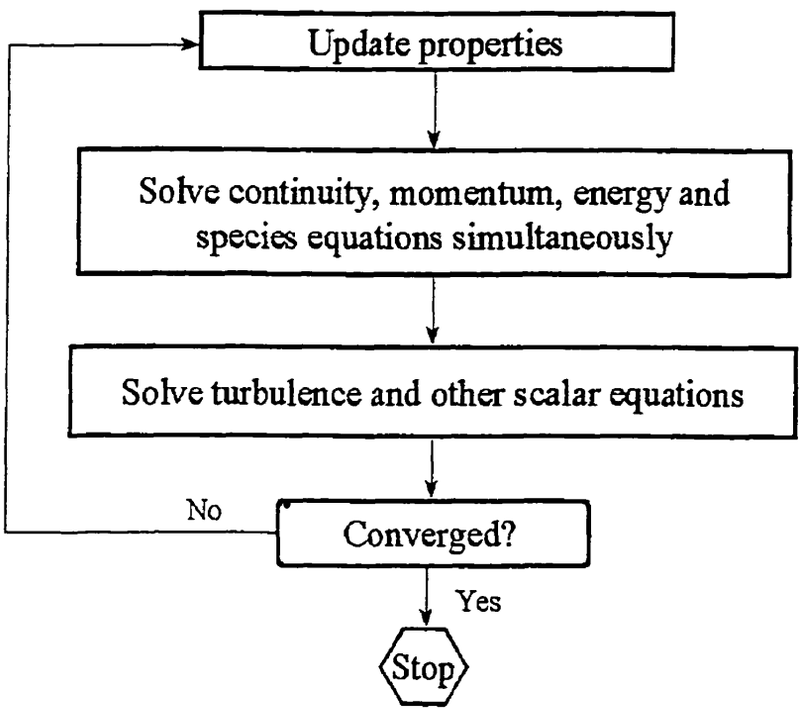

Figure 4.2 Overview of the Coupled Solution Method

1. Fluid properties are updated, based on the current solution. (If the calculation has just begun, the fluid properties will be updated based on the initialized solution.)

2. The continuity, momentum, and (where appropriate) energy and species equations are solved simultaneously.

3. Where appropriate, equations for scalars such as turbulence and radiation are solved using the previously updated values of the other variables.

4. When interphase coupling is to be included, the source terms in the appropriate continuous phase equations may be updated with a discrete phase trajectory calculation.

5. A check for convergence of the equation set is made.

These steps are continued until the convergence criterias are met.

4.4 Setting Physical Properties

An important step in the setup of the model is the definition of the physical properties of the material. Material properties include: density and molecular weights, viscosity, heat capacity, thermal conductivity, mass diffusion coefficients, standard state enthalpies and kinetic theory parameters.

Properties may be temperature- and/or composition-dependent, with temperature dependence based on a polynomial, piecewise-linear, or piecewise-polynomial function and individual component properties either defined by user or computed via kinetic theory.

Material properties can be defined as functions of temperature. For most properties, a polynomial, piecewise-linear, or piecewise-polynomial function of temperature can be used:

For piecewise-polynomial:

$$\phi(T) = A_1 + A_2 T + A_3 T^2 + \cdots \qquad \text{when } T_{min,1} < T < T_{max,1} \qquad (4.1)$$

$$\phi(T) = B_1 + B_2 T + B_3 T^2 + \cdots \qquad \text{when } T_{min,2} < T < T_{max,2} \qquad (4.2)$$

where ϕ is the property. Temperature in the function is always in Kelvin.

4.5 Mixture Materials

The concept of mixture materials has been implemented to facilitate the setup of species transport and reacting flow. A mixture material may be thought of as a set of species and a list of rules governing their interaction. The mixture material carries with the following information:

1) A list of the constituent species, referred to as "fluid" materials;

2) A list of mixing laws dictating how mixture properties (density, viscosity, specific heat, etc.) are to be derived from the properties of individual species if composition-dependent properties are desired;

3) A direct specification of mixture properties if composition-independent properties are desired;

4) Diffusion coefficients for individual species in the mixture;

5) Other material properties (e.g., absorption and scattering coefficients) that are not associated with individual species;

6) A set of reactions, including a reaction type (finite-rate, eddy-dissipation, etc.) and stoichiometry and rate constants.

Both mixture materials and fluid materials are stored in the materials database. Many common mixture materials are included (e.g., methane-air, propane-air). Generally, all reaction parameters and many physical properties of the mixture and its constituent species are defined in the database. The use of mixture materials gives the flexibility to use one of the many predefined mixtures, modify one of these mixtures, or create a new mixture material.

4.6 Physical Models

Comprehensive modeling capabilities for a wide range of incompressible and compressible, laminar and turbulent fluid flow problems are provided. A broad range of mathematical models for transport phenomena (like heat transfer and chemical reactions) is combined with the ability to model complex geometries. The range of problems that can be addressed is very wide. Applications include laminar non-newtonian flow modeling in process equipment, turbulent heat transfer in turbomachinery and automotive engine components, pulverized coal combustion in utility boilers, compressible jets in process equipment, external aerodynamics, and compressible reacting flow in solid rocket motors.

To permit modeling of fluid flow and related transport phenomena in industrial equipment and processes, various useful features are provided. These include porous media, lumped parameter (fan and heat exchanger), streamwise-periodic flow and heat transfer, swirl, and moving reference frame models. The moving reference frame family of models includes the ability to model single or multiple reference frames. A time-accurate sliding mesh method, useful for modeling multiple stages in turbomachinery applications, for example, is also provided, along with the mixing plane model for computing time-averaged flow fields.

Another very useful set of models is the set of discrete phase models. These models can be used to analyze sprays and particle-laden flows in equipment like cyclones and aircraft-engine inlets. Several models for multiphase flows are also available, and can be used, for example, to predict jet breakup, the motion of liquid after a dam break, cavitation, sedimentation, and separation.

The turbulence models provided have a broad range of applicability without the need for fine tuning to a specific application, and they include the effects of other physical phenomena, such as buoyancy and compressibility. Particular care has

been devoted to addressing issues of near-wall accuracy via the use of extended wall functions and zonal models.

Various modes of heat transfer can be modeled, including natural, forced, and mixed convection with or without added complications such as conjugate heat transfer, porous media, etc. The set of radiation models and related submodels for modeling participating media are general and can take into account the complications of combustion. A particular strength is its ability to model combustion phenomena via eddy dissipation models or probability density function models. A host of other models that are very useful for combustion applications are also available, including coal and droplet combustion and pollutant formation models.

4.7 User-Defined Functions

User-defined functions can be used to enhance the standard features in a number of ways. These functions can be used to customize: boundary conditions, source terms, property definitions, patching of initial conditions, wall heat fluxes, radiation scattering phase functions, surface and volume reaction rates, solution of user-defined scalars, and discrete phase model body force, drag, source term, etc.

User-defined functions (UDFs) are written in the C programming language. There are two types of user-defined functions: interpreted and compiled. Interpreted UDFs are translated at runtime from within a FLUENT session. Compiled UDFs are compiled and grouped in a shared library using a Makefile before beginning a FLUENT session. The shared library is then linked with the standard FLUENT executable at runtime. The standard FLUENT executable will remain unchanged, but we will be able to link one of any number of shared libraries to it to form "effective" custom executables.

One advantage of using compiled UDFs is that they run much faster than interpreted UDFs. Another advantage is that compiled UDFs are given complete access

to the solver. Interpreted UDFs, on the other hand, have limited access to the solver and, for example, do not recognize C language structures. Interpreted UDFs are architecture-independent, and as a result, are more convenient to use.

4.8 Solution-Adaptive Grid

The solution-adaptive mesh refinement feature allows to refine and/or coarsen the grid based on geometric and numerical solution data. By using solution-adaptive refinement, cells can be added where they are needed in the mesh, thus enabling the features of the flow field to be better resolved. When adaption is used properly, the resulting mesh is optimal for the flow solution because the solution is used to determine where more cells are added. In other words, computational resources are not wasted by the inclusion of unnecessary cells, as typically occurs in the structured grid approach. Furthermore, the effect of mesh refinement on the solution can be studied without completely regenerating the mesh.

Solution-adaptive grid capability is particularly useful for accurately predicting flow fields in regions with large gradients, such as free shear layers and boundary layers. In comparison to solutions on structured or block structured grids, this feature significantly reduces the time required to generate a good grid. Solution-adaptive refinement makes it easier to perform grid refinement studies and reduces the computational effort required to achieve a desired level of accuracy, since mesh refinement is limited to those regions where greater mesh resolution is needed.

The advantages of solution-adaptive refinement are significant. However, the capability must be used carefully to avoid certain pitfalls. Some guidelines for proper usage of solution-adaptive refinement are as follows:

1) The surface mesh must be fine enough to represent adequately the important features of the geometry. For example, it would be bad practice to place too few nodes on the surface of a highly-curved airfoil, and then use solution refinement

to add nodes on the surface. Clearly, the surface will always contain the facets contained in the initial mesh, regardless of the additional nodes introduced by refinement.

2) The initial mesh should contain sufficient cells to capture the essential features of the flow field. In addition to having sufficient surface resolution to represent the shape of the body, the initial mesh should also contain enough cells so that a reasonable first solution can be obtained. Subsequent gradient adaption can be used to sharpen the shock and establish a grid-independent solution.

3) A reasonably well-converged solution should be obtained before an adaption is performed. If adapt to an incorrect solution, cells will be added in the wrong region of the flow. However, careful judgment must be used in deciding how well to converge the solution before adapting, because there is a trade-off between adapting too early to an unconverged solution and wasting time by continuing to iterate when the solution is not changing significantly.

4.9 Unstructured Grids

Discretization of a domain can be accomplished either directly in the physical space or on the transformed computational space. The choice will primarily depend on the numerical scheme to be utilized as well as the domains of solution. The finite difference equations approximating the partial differential equations are solved within a rectangular grid system. For non-rectangular physical domain, a coordinate transformation to computational space is required. The grid points are defined at the intersection of equally distanced parallel lines within the rectangular (2-D) or cubical (3-D) computational domain. There are corresponding grid points within the physical space established by algebraic relations or differential

equations. The grid points can be easily identified and are usually designated by the indices i, j and k in an orderly manner along the grid lines. This type of grid is known as structured grid.

In addition to finite difference schemes, two other numerical schemes are available for the solution of the conservation laws. These schemes are finite volume schemes and finite element schemes. Both of these schemes are integral methods, that is, the original differential equations are integrated on the physical domain. Therefore, the grid system for the finite volume or finite element schemes are usually generated directly within the physical space. There exist various choices in the selection of the volumes or elements. Thus, the domain of solution is usually divided into triangles or quadrilaterals (or any other kind of polygons in 2-D, whereas pyramids or tetrahedrons are used in 3-D). It is obvious that the grid points, in general, cannot be associated with grid lines. Therefore, the identification of the grid points must be individually specified. Such a grid system is known as an unstructured grid system. The main advantage of the unstructured grid is that it can be used easily to fit irregular, singly-connected domains, as well as multiply-connected domains. The unstructured grid also can be coupled with grid refinement techniques for the adaptive methods. However, unstructured grid generation is more difficult to program, that is, the programmer needs a sound background in the data structure arrangement and experience in the data book-keeping skills.

4.10 Boundary Conditions

Boundary conditions specify the flow and thermal variables on the boundaries of physical model. They are, therefore, a critical component of simulations and it is important that they are specified appropriately.

The boundary conditions are classified as follows:

Flow inlet and exit boundaries: pressure inlet, velocity inlet, mass flow inlet, inlet

vent, intake fan, pressure outlet, pressure far-field, outflow, outlet vent, exhaust fan;

Wall, repeating and pole boundaries: wall, symmetry, periodic, axis;

Internal cell zones: fluid, solid (porous is a type of fluid zone);

Internal face boundaries: fan, radiator, porous jump, wall, interior.

Physical boundaries of a specified domain upon which boundary conditions are generally required or where the values of the dependent variables must be determined as a part of the overall solution can be categorized into five groups. They are: body surface, far-field, symmetry line (or surface in 3D), inflow, and outflow boundaries. Physical or numerical specification and implementation of the boundary conditions along various boundaries are generally challenging.

4.10.1 Using Flow Boundary Conditions

There are 10 types of boundary cell types for the specification of flow inlets and exits: velocity inlet, pressure inlet, mass flow inlet, pressure outlet, pressure far-field, outflow, inlet vent, intake fan, outlet vent and exhaust fan.

4.10.1.1 Velocity Inlet Boundary Conditions

Velocity inlet boundary conditions are used to define the flow velocity, along with all relevant scalar properties of the flow, at flow inlets. The total (or stagnation) properties of the flow are not fixed, so they will rise to whatever value is necessary to provide the prescribed velocity distribution. The inflow velocity by specifying the velocity magnitude and direction, the velocity components, or the velocity magnitude normal to the boundary can be defined.

This boundary condition is intended for incompressible flows, and its use in compressible flows will lead to a nonphysical result because it allows stagnation conditions to float to any level. One should also be careful not to place a velocity

inlet too close to a solid obstruction, since this could cause the inflow stagnation properties to become highly nonuniform.

4.10.1.2 Pressure Inlet Boundary Conditions

Pressure inlet boundary conditions are used to define the fluid pressure at flow inlets, along with all other scalar properties of the flow. They are suitable for both incompressible and compressible flow calculations. Pressure inlet boundary conditions can be used when the inlet pressure is known but the flow rate and/or velocity is not known. This situation may arise in many practical situations, including buoyancy-driven flows. Pressure inlet boundary conditions can also be used to define a "free" boundary in an external or unconfined flow.

The pressure field (p'_s) and pressure inputs (p'_s or p'_0) include the hydrostatic head, $\rho_0 gx$. That is, the pressure is defined as

$$p'_s = \rho_0 gx + p_s \tag{4.3}$$

or

$$\frac{\partial p'_s}{\partial x} = \rho_0 g + \frac{\partial p_s}{\partial x} \tag{4.4}$$

Total pressure for an incompressible fluid is defined as

$$p_0 = p_s + \frac{1}{2}\rho|\mathbf{v}|^2 \tag{4.5}$$

and for a compressible fluid as

$$p_0 = p_s \left[1 + \frac{k-1}{2} M_a^2\right]^{k/(k-1)} \tag{4.6}$$

where

p_0 total pressure

p_s static pressure

M_a Mach number

k ratio of specific heats (c_p/c_v)

4.10.1.3 Mass Inlet Boundary Conditions

Mass flow boundary conditions can be used to provide a prescribed mass flux at an inlet. The inlet total pressure is adjusted locally to achieve the velocity needed to provide the prescribed mass flux.

Mass flow inlet boundary conditions are used in compressible flows to prescribe a mass flow rate at an inlet. It is not necessary to use mass flow inlets in incompressible flows because when density is constant, velocity inlet boundary conditions will fix the mass flow. A mass flow inlet is often used when it is more important to match a prescribed mass and energy flow rate than to match the total pressure of the inflow stream. An example is the case of a small cooling jet that is bled into the main flow, while the velocity of the main flow is governed primarily by a pressure inlet/outlet boundary condition pair.

The adjustment of inlet total pressure might result in a slower convergence, so if both the pressure inlet boundary condition and the mass flow inlet boundary condition are acceptable choices, the latter should be chosen.

4.10.1.4 Pressure Outlet Boundary Conditions

Pressure outlet boundary conditions are used to define the static pressure at flow outlets (and also other scalar variables, in case of backflow). The use of a pressure outlet boundary condition instead of an outflow condition often results in a better rate of convergence when backflow occurs during iteration.

Pressure outlet boundary conditions require the specification of a static (gauge) pressure at the outlet boundary. The value of static pressure specified is used only

while the flow is subsonic. Should the flow become locally supersonic, the specified pressure is no longer used; pressure will be extrapolated from the flow in the interior. All other flow quantities are extrapolated from the interior.

4.10.1.5 Pressure Far-Field Boundary Conditions

Pressure far-field boundary conditions are used to model a free-stream compressible flow at infinity, with free-stream Mach number and static conditions specified. This boundary type is available only for compressible flows.

Pressure far-field conditions are used to model a free-stream condition at infinity, with free-stream Mach number and static conditions being specified. The pressure far-field boundary condition is often called a characteristic boundary condition, since it uses characteristic information to determine the flow variables at the boundaries.

This boundary condition is only applicable when the density is calculated using the ideal-gas law. Using it for other flows is not permitted. To effectively approximate true infinite-extent conditions, the far-field boundary must be placed far enough from the object of interest. For example, in lifting airfoil calculations, it is not uncommon for the far-field boundary to be a circle with a radius of 20 chord lengths.

4.10.1.6 Other Boundary Conditions

Outflow boundary conditions are used to model flow exits where the details of the flow velocity and pressure are not known prior to solution of the flow problem. They are appropriate where the exit flow is close to a fully developed condition, as the outflow boundary condition assumes a zero normal gradient for all flow variables except pressure. They are not appropriate for compressible flow calculations.

Inlet vent boundary conditions are used to model an inlet vent with a specified loss coefficient, flow direction, and ambient (inlet) total pressure and temperature.

Intake fan boundary conditions are used to model an external intake fan with a specified pressure jump, flow direction, and ambient (intake) total pressure and temperature.

Outlet vent boundary conditions are used to model an outlet vent with a specified loss coefficient and ambient (discharge) static pressure and temperature.

Exhaust fan boundary conditions are used to model an external exhaust fan with a specified pressure jump and ambient (discharge) static pressure.

No slip velocity boundary conditions are used at the body surface. Therefore, the surface velocity is imposed at the boundary. For most applications where there is no relative motion between the solid surface and the fluid, the velocity components are set to zero according to the no slip condition. If the surface is porous where fluid is injected or extracted at some specified velocity, the injection or extraction velocity is used. Usually the pressure at the surface is not known and must be determined as a part of the overall solution. Generally speaking, the Neumann-type boundary condition is imposed for the pressure. For this purpose a relation involving the normal pressure gradient is obtained from the appropriate momentum equation.

4.10.2 Symmetry

For applications where the configuration and the domain of solution are symmetrical, the axis of symmetry (or surface of symmetry) may be used as a boundary. The boundary location may be defined in two fashions. First, the boundary is set on the axis of symmetry. In this case the net flow across the symmetry line is zero. Therefore, the component of the velocity normal to the boundary is set to zero. Furthermore, the shear stress along the axis of symmetry may be zero in some applications. Thus, the velocity gradient is set to zero. Second, the boundary may be set below the axis of symmetry, in which case the symmetry of flow variables are used as the required boundary conditions.

4.10.3 Wall Boundary Conditions

Wall boundary conditions are used to bound fluid and solid regions. In viscous flows, the no-slip boundary condition is enforced at walls.

4.10.3.1 Shear-Stress Calculation in Laminar Flow

In a laminar flow, the wall shear stress is defined by the normal velocity gradient at the wall as

$$\tau = \mu \frac{\partial v}{\partial n} \tag{4.7}$$

When there is a steep velocity gradient at the wall, it must be sure that the grid is sufficiently fine to accurately resolve the boundary layer.

Wall functions are a collection of semi-empirical formulas and functions that in effect 'bridge' or 'link' the solution variables at the near-wall cells and the corresponding quantities on the wall. The wall functions comprise 'laws-of-the-wall for mean velocity and temperature' and 'formulas for near-wall turbulent quantities'.

Two types of wall function: standard wall functions and nonequilibrium wall functions are introduced.

4.10.3.2 Standard Wall Functions

The standard wall functions are based on the proposal of Launder and Spalding (1974), and have been most widely used for industrial flows.

The law-of-the-wall for mean velocity yields

$$U^* = \frac{1}{\kappa} \ln(Ey^*) \tag{4.8}$$

where

$$U^* \equiv \frac{U_P C_\mu^{1/4} k_P^{1/2}}{\tau_w/\rho} \tag{4.9}$$

$$y^* \equiv \frac{\rho C_\mu^{1/4} k_P^{1/2} y_P}{\mu} \tag{4.10}$$

and

κ Von Karman's constant (= 0.42)

E empirical constant (= 9.81)

U_P mean velocity of the fluid at point P

k_P turbulent kinetic energy at point P

y_P distance from point P to the wall

μ dynamic viscosity of the fluid

The logarithmic law for mean velocity is known to be valid for $y^* > 30 \sim 60$. In FLUENT, the log-law is employed when $y^* > 11.225$.

When the mesh is such that $y^* < 11.225$ at the wall-adjacent cells, the laminar stress-strain relationship is applied that can be written as

$$U^* = y^* \tag{4.11}$$

It should be noted that the laws-of-the-wall for mean velocity and temperature are based on the wall unit, y^*, rather than $y^+(\equiv \rho u_\tau y/\mu)$. These quantities are approximately equal in equilibrium turbulent boundary layers.

Reynolds' analogy between momentum and energy transport gives a similar logarithmic law for mean temperature. As in the law-of-the-wall for mean velocity, the law-of-the-wall for temperature employed comprises the following two different laws:

1) Linear law for the thermal conduction sublayer where conduction is important;

2) Logarithmic law for the turbulent region where effects of turbulence dominate conduction.

The thickness of the thermal conduction layer is, in general, different from the thickness of the (momentum) viscous sublayer, and changes from fluid to fluid. For example, the thickness of the thermal sublayer for a high-Prandtl-number fluid (e.g., oil) is much less than its momentum sublayer thickness. For fluids of low Prandtl numbers (e.g., liquid metal), on the contrary, it is much larger than the momentum sublayer thickness.

In the $k-\varepsilon$ models and in the RSM (if the option to obtain wall boundary conditions from the k equation is enabled), the k equation is solved in the whole domain including the wall-adjacent cells. The boundary condition for k imposed at the wall is

$$\frac{\partial k}{\partial n} = 0 \tag{4.12}$$

where n is the local coordinate normal to the wall.

The production of kinetic energy, G_k, and its dissipation rate, ε, at the wall-adjacent cells, which are the source terms in the k equation, are computed on the basis of the local equilibrium hypothesis. Under this assumption, the production of k and its dissipation rate are assumed to be equal in the wall-adjacent control volume.

Thus, the production of k is computed from

$$G_k \approx \tau_w \frac{\partial U}{\partial y} = \tau_w \frac{\tau_w}{\kappa \rho C_\mu^{1/4} k_P^{1/2} y_P} \tag{4.13}$$

and ε is computed from

$$\varepsilon_P = \frac{C_\mu^{3/4} k_P^{3/2}}{\kappa y_P} \tag{4.14}$$

Note that, as shown here, the wall boundary conditions for the solution variables including mean velocity, temperature, k and ε are all taken care of by the wall functions. Therefore, one do not need to be concerned about the boundary conditions at the walls.

The standard wall functions work reasonably well for a broad range of wall-bounded flows. However, they tend to become less reliable when the flow situations depart too much from the ideal conditions that are assumed in their derivation. Among others, the constant-shear and local equilibrium hypotheses are the ones that most restrict the universality of the standard wall functions. Accordingly, when the near-wall flows are subjected to severe pressure gradients, and when the flows are in strong nonequilibrium, the quality of the predictions is likely to be compromised.

The nonequilibrium wall functions offered as an additional option can improve the results in such situations.

4.10.3.3 Nonequilibrium Wall Functions

The key elements in the nonequilibrium wall functions (Kim, 1995) are as follows:

1. Launder and Spalding's log-law for mean velocity is sensitized to pressure-gradient effects.

2. The two-layer-based concept is adopted to compute the budget of turbulent kinetic energy ($\overline{G_k}, \overline{\varepsilon}$) in the wall-neighboring cells.

The law-of-the-wall for mean temperature remains the same as in the standard wall function. The log-law for mean velocity sensitized to pressure gradients is

$$\frac{\tilde{U}\, C_\mu^{1/4} k^{1/2}}{\tau_w/\rho} = \frac{1}{\kappa} \ln\left(E \frac{\rho C_\mu^{1/4} k^{1/2} y}{\mu}\right) \tag{4.15}$$

where

$$\tilde{U} = U - \frac{1}{2}\frac{dp}{dx}\left[\frac{y_v}{\rho\kappa^* k^{1/2}} ln\left(\frac{y}{y_v}\right) + \frac{y - y_v}{\rho\kappa^* k^{1/2}} + \frac{y_v^2}{\mu}\right] \tag{4.16}$$

and y_v is the physical viscous sublayer thickness, and is computed from

$$y_v \equiv \frac{\mu y_v^*}{\rho C_\mu^{1/4} \kappa_P^{1/2}} \tag{4.17}$$

where $y_v^* = 11.225$.

The nonequilibrium wall function employs the two-layer concept in computing the budget of turbulent kinetic energy at the wall-adjacent cells, which is needed to solve the k equation at the wall-neighboring cells. The wall-neighboring cells are assumed to consist of a viscous sublayer and a fully turbulent layer. The following profile assumptions for turbulence quantities are made:

$$\tau_t = \begin{cases} 0, & y < y_v \\ \tau_w, & y > y_v \end{cases} \tag{4.18}$$

$$k = \begin{cases} \left(\frac{y}{y_v}\right)^2 k_P, & y < y_v \\ k_P, & y > y_v \end{cases} \tag{4.19}$$

$$\varepsilon = \begin{cases} \frac{2\upsilon k}{y^2}, & y < y_v \\ \frac{k^{3/2}}{C_l y}, & y > y_v \end{cases} \tag{4.20}$$

where $C_l = \kappa C_\mu^{-3/4}$, and y_v is defined in Equation (4.17).

Using these profiles, the cell-averaged production of k, $\overline{G_k}$, and the cell-averaged dissipation rate, $\bar{\varepsilon}$, can be computed from the volume average of G_k and ε of the wall-adjacent cells. For quadrilateral and hexahedral cells for which the volume average can be approximated with a depth-average,

$$\begin{aligned}\overline{G_k} &\equiv \frac{1}{y_n}\int_0^{y_n} \tau_t \frac{\partial U}{\partial y} dy \\ &= \frac{1}{\kappa y_n} \frac{\tau_w^2}{\rho C_\mu^{1/4} k_P^{1/2}} ln\left(\frac{y_n}{y_v}\right) \end{aligned} \tag{4.21}$$

and

$$\begin{aligned}\overline{\epsilon} &= \frac{1}{y_n}\int_0^{y_n} \epsilon dy \\ &\equiv \frac{1}{y_n}\left[\frac{2v}{y_v} + \frac{k_P^{1/2}}{C_l} ln\left(\frac{y_n}{y_v}\right)\right] k_P \end{aligned} \tag{4.22}$$

where y_n is the height of the cell ($y_n = 2y_p$). For cells with other shapes (e.g., triangular and tetrahedral grids), the appropriate volume averages are used.

Chapter 5

Mathematical and Physical Models

5.1 Introduction

The purpose of this chapter is to present and discuss the solution of turbulent reaction flow problems with the use of various kinds of numerical methods and turbulent models. Turbulence is commonplace. At high Reynolds number the flow becomes turbulent. When chemical reactions occur in turbulence, the situation is more chaotic. In order to achieve closure of the equations for turbulence in reacting flow systems, various models have been proposed. Among them, the most popular is the $k - \varepsilon$ two-equation model. Recently, direct numerical simulations and large eddy simulations have been applied to study chemically reacting flow. In numerical methods, finite difference methods have been used most widely but other methods such as finite volumes, finite element and spectral methods have been applied increasingly in computational combustion.

5.2 Turbulence Models

Various models have been proposed to achieve closure of the equations of turbulence in reacting flow system. The most popular model is the standard $k-\varepsilon$ model of Launder and Spalding (1974), the turbulence kinetic energy k and its dissipation rate ε are calculated from transport equations in the fully turbulent flow region, and the Reynolds-stress tensor is represented by an eddy viscosity model constructed from k, ε and mean flow field. The turbulent eddy viscosity can be determined from the transport equation of k and ε. For wall bound flows, wall functions are added to blend the fully turbulent region with the near wall region, because of the predominance of viscous effects in that region. Used in conjunction with wall functions, the $k-\varepsilon$ model is reasonably well behaved, and has been applied to the solution of many practical problems with a moderate amount of success.

5.2.1 Zero Equation Models

The zero equation models are equations wherein the turbulent fluctuating correlations are related to the mean flow field quantities by algebraic relations. The underlying assumption in zero-equation models is that local rate of production of turbulence and the rate of dissipation of turbulence are approximately equal. However, they do not include the convection of turbulence. Obviously, it is contrary to the physics of most flow fields, since the past history of the flow must be accounted for. Nevertheless, these models are mathematically simple and their incorporation into a numerical code can be accomplished with relative ease.

Generally, most models employ an inner region/outer region formulation to represent mixing length. A commonly used model utilizes an exponential function (van Driest damping function) for the inner region, whereas the outer region is proportional to the boundary layer thickness. Mathematically they are expressed as

$$l_i = k(1 - e^{-y^+/A^+})y \tag{5.1}$$

and

$$l_o = C_o\delta \tag{5.2}$$

where k is the Von Karman constant (~ 0.41), and A^+ is a parameter which depends on the streamwise pressure gradient. For a zero-pressure gradient flow, it has a value of 26. The constant C_o in the equation is usually assigned a value of $0.08 \sim 0.09$, whereas δ is the boundary layer thickness.

Another formulation commonly used for the outer region turbulent viscosity is the Cebeci/Smith model expressed as

$$\nu_t = \alpha\bar{u}_e\delta^* \tag{5.3}$$

where α is usually assigned a value of 0.0168 for flows where Re_θ (momentum thickness Reynolds number) is greater than 5000 and δ^* is the kinetic displacement thickness defined as

$$\delta^+ = \int_o^\infty \left(1 - \frac{u}{u_e}\right) dy \tag{5.4}$$

Recall that the Reynolds number based on momentum thickness is defined as

$$Re_\theta = \frac{\rho_e u_e \theta}{\mu_e} \tag{5.5}$$

where the momentum thickness θ is

$$\theta = \int_o^\infty \frac{u}{u_e}\left(1 - \frac{u}{u_e}\right) dy \tag{5.6}$$

The algebraic model described above requires information regarding the boundary layer thickness and flow properties at the boundary layer edge. When the

Navier-Stokes equations are being solved, it may be a difficult task to determine the boundary layer thickness and the required properties at the edge. That is especially the case when flow separation exists within the domain. However, when it is necessary to determine the extent of the viscous region within the domain, the total enthalpy is usually used.

A turbulence model which is not written in terms of the boundary layer quantities was introduced by Baldwin and Lomax (1978). The inner region is approximated by

$$\mu_t = \rho l^2 |\omega| \tag{5.7}$$

where ω is the vorticity defined as

$$\omega = \frac{\partial u}{\partial y} - \frac{\partial v}{\partial x} \tag{5.8}$$

The outer region is approximated by

$$\mu_t = \alpha \bar{\rho} C_{cp} F_{wake} F_{Kleb} \tag{5.9}$$

where α is assigned a value of 0.0168 (as in the Cebeci/Smith model) and

$$F_{wake} = min \left[(y_{max} G_{max}) , \left(C_{wake} y_{max} \frac{(\Delta V)^2}{G_{max}} \right) \right] \tag{5.10}$$

A typical value for C_{wake} is 0.25. In the above equation, the following definitions are employed,

$$G_{max} = max \left(\frac{l}{k} |\omega| \right) \tag{5.11}$$

where l is the mixing length and determined by the Van Driest function. The difference between the absolute values of the maximum and minimum velocities within the viscous region is denoted by ΔV. F_{Kleb} is the intermittence factor defined as

$$F_{Kleb} = \left[l + 5.5 \left(\frac{C_{Kleb} y}{y_{max}} \right)^6 \right]^{-1} \tag{5.12}$$

and y_{max} is the y location where G_{max} occurs.

The Klebanoff constant C_{Kleb} is determined from the following expression,

$$C_{Kleb} = \frac{2}{3} - \frac{0.01312}{0.1724 - \beta^*} \tag{5.13}$$

where

$$\beta^* = \frac{y_{max}}{v*} \frac{\partial V}{\partial x} \tag{5.14}$$

and v^* is the friction velocity. The velocity gradient in β^* is calculated outside the viscous region. Once the Klebanoff constant is evaluated, C_{CP} is determined from

$$C_{CP} = \frac{3 - 4C_{Kleb}}{2C_{Cleb}(2 - 3C_{Kleb} + C_{Kleb}^3)} \tag{5.15}$$

To model the eddy diffusivity, the Reynolds analogy may be used. Recall that the Reynolds analogy assumes a similarity between the momentum transfer and heat transfer. Therefore, a turbulent Prandtl number is defined as

$$Pr_t = \frac{\nu_t}{\alpha_t} = \frac{\mu_t c_p}{k_t} \tag{5.16}$$

For most flows, it is assumed that the turbulent Prandtl number remains constant across the boundary layer. For air, $Pr_t = 0.9$. Thus, the turbulent conductivity is determined as

$$k_t = \frac{\mu_t c_p}{Pr_t} \tag{5.17}$$

where μ_t is provided by the turbulence models.

5.2.2 Spalart-Allmaras One Equation Model

5.2.2.1 Spalart-Allmaras Model

In turbulence models that employ the Boussinesq approach, the central issue is how the eddy viscosity is computed. The model proposed by Spalart and Allmaras (1992) solves a transport equation for a quantity that is a modified form of the turbulent kinematic viscosity. The transported variable in the Spalart-Allmaras model, $\tilde{\upsilon}$, is identical to the turbulent kinematic viscosity except in the near-wall (viscous-affected) region. The transport equation for $\tilde{\upsilon}$ is

$$\rho\frac{D\,\tilde{\upsilon}}{Dt} = G_{\upsilon} + \frac{1}{\sigma_{\tilde{\upsilon}}}\left[\frac{\partial}{\partial x_j}\left\{(\mu+\rho\,\tilde{\upsilon})\frac{\partial\,\tilde{\upsilon}}{\partial x_j}\right\} + C_{b2}\rho\left(\frac{\partial\,\tilde{\upsilon}}{\partial x_j}\right)^2\right] - Y_{\upsilon} \tag{5.18}$$

where G_{υ} is the production of turbulent viscosity and Y_{υ} is the destruction of turbulent viscosity that occurs in the near-wall region due to wall blocking and viscous damping. $\sigma_{\tilde{\upsilon}}$ and C_{b2} are constants and υ is the molecular kinematic viscosity.

The turbulent viscosity, μ_t, is computed from

$$\mu_t = \rho\,\tilde{\upsilon}\,f_{\upsilon 1} \tag{5.19}$$

where the viscous damping function, $f_{\upsilon 1}$, is given by

$$f_{\upsilon 1} = \frac{\chi^3}{\chi^3 + C_{\upsilon 1}^3} \tag{5.20}$$

and

$$\chi \equiv \frac{\tilde{\upsilon}}{\upsilon} \tag{5.21}$$

The production term, G_υ, is modeled as

$$G_\upsilon = C_{b1}\rho\,\tilde{S}\tilde{\upsilon} \tag{5.22}$$

where

$$\tilde{S} \equiv S + \frac{\tilde{\upsilon}}{\kappa^2 d^2} f_{\upsilon 2} \tag{5.23}$$

and

$$f_{\upsilon 2} = 1 - \frac{\chi}{1 + \chi f_{\upsilon 1}} \tag{5.24}$$

C_{b1} and κ are constants, d is the distance from the wall, and S is a scalar measure of the deformation tensor. As in the original model proposed by Spalart and Allmaras, S is based on the magnitude of the vorticity:

$$S \equiv \sqrt{2\Omega_{ij}\Omega_{ij}} \tag{5.25}$$

where Ω_{ij} is the mean rate-of-rotation tensor and is defined by

$$\Omega_{ij} = \frac{1}{2}\left(\frac{\partial u_j}{\partial x_i} - \frac{\partial u_i}{\partial x_j}\right) \tag{5.26}$$

The justification for the default expression for S is that, for the wall-bounded flows that were of most interest when the model was formulated, turbulence is found only where vorticity is generated near walls. However, it has been acknowledged that one should also take into account the effect of mean strain on the turbulence production, and a modification to the model has been proposed (Dacles-Mariani et al, 1995).

This modification combines measures of both rotation and strain tensors in the definition of S:

$$S \equiv |\Omega_{ij}| + C_{prod}\, min(0, |S_{ij}| - |\Omega_{ij}|) \tag{5.27}$$

where

$$C_{prod} = 2.0, \quad |\Omega_{ij}| \equiv \sqrt{2\Omega_{ij}\Omega_{ij}}, \quad |S_{ij}| \equiv \sqrt{2S_{ij}S_{ij}}$$

with the mean strain rate, S_{ij}, defined as

$$S_{ij} = \frac{1}{2}\left(\frac{\partial u_j}{\partial x_i} + \frac{\partial u_i}{\partial x_j}\right) \tag{5.28}$$

Including both the rotation and strain tensors reduces the production of eddy viscosity and consequently reduces the eddy viscosity itself in regions where the measure of vorticity exceeds that of strain rate.

The destruction term is modeled as

$$Y_v = C_{w1}\rho f_w \left(\frac{\tilde{v}}{d}\right)^2 \tag{5.29}$$

where

$$f_w = g\left[\frac{1 + C_{w3}^6}{g^6 + C_{w3}^6}\right]^{1/6} \tag{5.30}$$

$$g = r + C_{w2}\left(r^6 - r\right) \tag{5.31}$$

$$r \equiv \frac{\tilde{v}}{\tilde{S}\,\kappa^2 d^2} \tag{5.32}$$

The model constants $C_{b1}, C_{b2}, \sigma_{\tilde{v}}, C_{v1}, C_{w1}, C_{w2}, C_{w3}$, and κ have the following default values (Spalart and Allmaras, 1992):

$$C_{b1} = 0.1335, \quad C_{b2} = 0.622, \quad \sigma_{\tilde{v}} = 22/3, \quad C_{v1} = 7.1,$$

$$C_{w1} = C_{b1}/\kappa^2 + (1 + C_{b2})/\sigma_{\tilde{v}}, \quad C_{w2} = 0.3, \quad C_{w3} = 2.0, \quad \kappa = 0.41$$

5.2.2.2 Wall Boundary Conditions

At walls, the modified turbulent kinematic viscosity, $\tilde{\upsilon}$, is set to zero.

When the mesh is fine enough to resolve the laminar sublayer, the wall shear stress is obtained from the laminar stress-strain relationship:

$$\frac{u}{u_\tau} = \frac{\rho u_\tau y}{\mu} \tag{5.33}$$

If the mesh is too coarse to resolve the laminar sublayer, it is assumed that the centroid of the wall-adjacent cell falls within the logarithmic region of the boundary layer, and the law-of-the-wall is employed:

$$\frac{u}{u_\tau} = \frac{1}{\kappa} \ln E \frac{u_\tau y}{\upsilon} \tag{5.34}$$

where $\kappa = 0.419$ and E = 9.793.

5.2.3 $k - \varepsilon$ Two-Equation Model

The convection of turbulence is not modeled in zero-equation models. Therefore, the physical effect of past history of the flow is not included in simple algebraic models. In order to account for this physical effect, a transport equation based on the Navier-Stokes equation may be derived. When two such equations are employed, it is referred to as a two-equation model. A commonly used two-equation turbulence model is the $k - \varepsilon$ model. The partial differential equations are derived for kinetic energy of turbulence (k), and the dissipation of turbulence (ε), where

$$k = \frac{1}{2}\left[\overline{u'^2} + \overline{v'^2} + \overline{w'^2}\right] \tag{5.35}$$

and

$$\varepsilon = \nu_t \overline{\left(\frac{\partial u_i'}{\partial x_j}\right)\left(\frac{\partial u_i'}{\partial x_j}\right)} \tag{5.36}$$

5.2.3.1 The Standard $k-\varepsilon$ Model

The standard $k-\varepsilon$ model(Launder and Spalding, 1972) is a semi-empirical model based on model transport equations for the turbulent kinetic energy (k) and its dissipation rate (ε). The model transport equation for k is derived from the exact equation, while the model transport equation for ε was obtained using physical reasoning and bears little resemblance to its mathematically exact counterpart.

In the derivation of the $k-\varepsilon$ model, it was assumed that the flow is fully turbulent, and the effects of molecular viscosity are negligible. The standard $k-\varepsilon$ model is therefore valid only for fully turbulent flows.

The turbulent kinetic energy, k, and its rate of dissipation, ε, are obtained from the following transport equations:

$$\rho\frac{Dk}{Dt} = \frac{\partial}{\partial x_i}\left[\left(\mu + \frac{\mu_t}{\sigma_k}\right)\frac{\partial k}{\partial x_i}\right] + G_k + G_b - \rho\varepsilon - Y_M \tag{5.37}$$

and

$$\rho\frac{D\varepsilon}{Dt} = \frac{\partial}{\partial x_i}\left[\left(\mu + \frac{\mu_t}{\sigma_\varepsilon}\right)\frac{\partial \varepsilon}{\partial x_i}\right] + C_{1\varepsilon}\frac{\varepsilon}{k}(G_k + C_{3\varepsilon}G_b) - C_{2\varepsilon}\rho\frac{\varepsilon^2}{k} \tag{5.38}$$

In these equations, G_k represents the generation of turbulent kinetic energy due to the mean velocity gradients. G_b is the generation of turbulent kinetic energy due to buoyancy. Y_M represents the contribution of the fluctuating dilatation in compressible turbulence to the overall dissipation rate. $C_{3\varepsilon}$ is the constant considering buoyancy. The turbulent viscosity, μ_t, is computed by combining k and ε as follows:

$$\mu_t = \rho C_\mu \frac{k^2}{\varepsilon} \tag{5.39}$$

According to Launder and Spalding, the model constants

$$C_{1\epsilon} = 1.44, \quad C_{2\epsilon} = 1.92, \quad C_\mu = 0.09, \quad \sigma_k = 1.0, \quad \sigma_\epsilon = 1.3, \quad C_{3\epsilon} = 1$$

These values have been determined from experiments with air and water for fundamental turbulent shear flows including homogeneous shear flows and decaying isotropic grid turbulence. They have been found to work fairly well for a wide range of wall-bounded and free shear flows.

5.2.3.2 Transport Equations for the RNG $k-\varepsilon$ Model

The RNG $k-\varepsilon$ model was derived using a rigorous statistical technique called renormalization group theory (RNG). It is similar in form to the standard $k-\varepsilon$ model, but includes the following refinements:

1) The RNG model has an additional term in its ε equation that significantly improves the accuracy for rapidly strained flows.

2) The effect of swirl on turbulence is included in the RNG model, enhancing accuracy for swirling flows.

3) The RNG theory provides an analytical formula for turbulent Prandtl numbers, while the standard $k-\varepsilon$ model uses user-specified, constant values.

4) While the standard $k-\varepsilon$ model is a high-Reynolds-number model, the RNG theory provides an analytically-derived differential formula for effective viscosity that accounts for low-Reynolds-number effects. Effective use of this feature does, however, depend on an appropriate treatment of the near-wall region.

These features make the RNG $k-\varepsilon$ model more accurate and reliable for a wider class of flows than the standard $k-\varepsilon$ model. A more comprehensive description of RNG theory and its application to turbulence can be found in (Choudhury, 1993).

The RNG $k-\varepsilon$ model has a similar form to the standard $k-\varepsilon$ model:

$$\rho\frac{Dk}{Dt} = \frac{\partial}{\partial x_i}\left(\alpha_k \mu_{eff}\frac{\partial k}{\partial x_i}\right) + G_k + G_b - \rho\varepsilon - Y_M \tag{5.40}$$

and

$$\rho\frac{D\varepsilon}{Dt} = \frac{\partial}{\partial x_i}\left(\alpha_\varepsilon \mu_{eff}\frac{\partial \varepsilon}{\partial x_i}\right) + C_{1\varepsilon}\frac{\varepsilon}{k}(G_k + C_{3\varepsilon}G_b) - C_{2\varepsilon}\rho\frac{\varepsilon^2}{k} - R \tag{5.41}$$

In these equations, G_k represents the generation of turbulent kinetic energy due to the mean velocity gradients. G_b is the generation of turbulent kinetic energy due to buoyancy. Y_M represents the contribution of the fluctuating dilatation in compressible turbulence to the overall dissipation rate. The quantities α_k and α_ε are the inverse effective Prandtl numbers for k and ε, respectively. R will be discussed later on in 5.2.3.5.

5.2.3.3 Modeling the Effective Viscosity

The scale elimination procedure in RNG theory results in a differential equation for turbulent viscosity:

$$d\left(\frac{\rho^2 k}{\sqrt{\varepsilon\mu}}\right) = 1.72\frac{\hat{\upsilon}}{\sqrt{\hat{\upsilon}^3 - 1 + C_\upsilon}}d\,\hat{\upsilon} \tag{5.42}$$

where

$$\hat{\upsilon} = \mu_{eff}/\mu, \qquad C_\upsilon \approx 100$$

Equation (5.42) is integrated to obtain an accurate description of how the effective turbulent transport varies with the effective Reynolds number (or eddy scale), allowing the model to better handle low-Reynolds-number and near-wall flows.

In the high-Reynolds-number limit,

$$\mu_t = \rho C_\mu \frac{k^2}{\varepsilon} \tag{5.43}$$

where C_μ equals to 0.0845, derived using RNG theory. It is interesting to note that this value of C_μ is very close to the empirically-determined value of 0.09 used in the standard $k-\varepsilon$ model.

5.2.3.4 Calculating the Inverse Effective Prandtl Numbers

The inverse effective Prandtl numbers α_k and α_ε are computed using the following formula derived analytically by the RNG theory:

$$\left|\frac{\alpha-1.3929}{\alpha_o-1.3929}\right|^{0.6321}\left|\frac{\alpha+2.3929}{\alpha_o+2.3929}\right|^{0.3679}=\frac{\mu_{mol}}{\mu_{eff}} \tag{5.44}$$

where $\alpha_o = 1.0$. In the high-Reynolds-number limit ($\mu_{mol}/\mu_{eff} \ll 1$), $\alpha_k = \alpha_\varepsilon \approx 1.393$.

5.2.3.5 The R Term in the ε Equation

The main difference between the RNG and standard $k-\varepsilon$ models lies in the additional term in the ε equation given by

$$R=\frac{C_\mu\rho\eta^3(1-\eta/\eta_o)}{1+\beta\eta^3}\frac{\varepsilon^2}{k} \tag{5.45}$$

where $\eta \equiv Sk/\varepsilon$, $\eta_o = 4.38$, $\beta = 0.012$.

The effects of this term in the RNG ε equation can be seen more clearly by rearranging ε equation as

$$\rho\frac{D\varepsilon}{Dt}=\frac{\partial}{\partial x_i}\left(\alpha_\varepsilon\mu_{eff}\frac{\partial\varepsilon}{\partial x_i}\right)+C_{1\varepsilon}\frac{\varepsilon}{k}(G_k+C_{3\varepsilon}G_b)-C_{2\varepsilon}^*\rho\frac{\varepsilon^2}{k} \tag{5.46}$$

where $C_{2\varepsilon}^*$ is given by

$$C_{2\varepsilon}^{*} \equiv C_{2\varepsilon} + \frac{C_{\mu}\rho\eta^{3}(1-\eta/\eta_{o})}{1+\beta\eta^{3}} \tag{5.47}$$

In regions where $\eta < \eta_o$, the R term makes a positive contribution, and $C_{2\varepsilon}^{*}$ becomes larger than $C_{2\varepsilon}$. In the logarithmic layer, for instance, it can be shown that $\eta \approx 3.0$, giving $C_{2\varepsilon}^{*} \approx 2.0$, which is close in magnitude to the value of $C_{2\varepsilon}$ in the standard $k-\varepsilon$ model. As a result, for weakly to moderately strained flows, the RNG model tends to give results largely comparable to the standard $k-\varepsilon$ model.

In regions of large strain rate ($\eta > \eta_o$), however, the R term makes a negative contribution, making the value of $C_{2\varepsilon}^{*}$ less than $C_{2\varepsilon}$. In comparison with the standard $k-\varepsilon$ model, the smaller destruction of ε augments ε, reducing k and eventually the effective viscosity. As a result, in rapidly strained flows, the RNG model yields a lower turbulent viscosity than the standard $k-\varepsilon$ model.

Thus, the RNG model is more responsive to the effects of rapid strain and streamline curvature than the standard $k-\varepsilon$ model, which explains the superior performance of the RNG model for certain classes of flows. The model constants $C_{1\varepsilon}$ and $C_{2\varepsilon}$ are

$$C_{1\varepsilon} = 1.42, \qquad C_{2\varepsilon} = 1.68$$

5.2.4 Reynolds Stress Model

Reynolds-averaged Navier-Stokes (RANS) equations are:

$$\frac{\partial \rho}{\partial t} + \frac{\partial}{\partial x_i}(\rho u_i) = 0 \tag{5.48}$$

$$\rho\frac{Du_i}{Dt} = \frac{\partial p}{\partial x_i} + \frac{\partial}{\partial x_j}\left[\mu\left(\frac{\partial u_i}{\partial x_j} + \frac{\partial u_j}{\partial x_i} - \frac{2}{3}\delta_{ij}\frac{\partial u_l}{\partial x_l}\right)\right] + \frac{\partial}{\partial x_j}(-\rho\overline{u_i'u_j'}) \tag{5.49}$$

They have the same general form as the instantaneous Navier-Stokes equations,

with the velocities and other solution variables now representing ensemble-averaged (or time-averaged) values. Additional terms now appear that represent the effects of turbulence. The Reynolds stress model (Gibson and Launder 1978, Launder 1989, Launder et al 1975) involves calculation of the individual Reynolds stresses, $\overline{u_i' u_j'}$, using differential transport equations. The individual Reynolds stresses are then used to obtain closure of the Reynolds-averaged momentum Equation (5.49).

The exact form of the Reynolds stress transport equations may be derived by taking moments of the exact momentum equation. This is a process wherein the exact momentum equations are multiplied by a fluctuating property, the product then being Reynolds-averaged. Unfortunately, several of the terms in the exact equation are unknown and modeling assumptions are required in order to close the equations.

In this section, the Reynolds stress transport equations are presented together with the modeling assumptions required to attain closure.

5.2.4.1 The Reynolds Stress Transport Equations

The exact transport equations for the transport of the Reynolds stresses, $\rho\overline{u_i' u_j'}$, may be written as follows:

$$\underbrace{\frac{\partial}{\partial t}(\rho\overline{u_i u_j})}_{Local\ Time\ Derivative} + \underbrace{\frac{\partial}{\partial x_k}(\rho U_k \overline{u_i u_j})}_{C_{ij}\equiv Convection} = \underbrace{-\frac{\partial}{\partial x_k}\left[\rho\overline{u_i u_j u_k} + \overline{p(\delta_{kj}u_i + \delta_{ik}u_j)}\right]}_{D_{ij}^T\equiv Turbulent\ Diffusion} +$$

$$\underbrace{\frac{\partial}{\partial x_k}\left[\mu\frac{\partial}{\partial x_k}(\overline{u_i u_j})\right]}_{D_{ij}^L\equiv Molecular\ Diffusion} - \underbrace{\rho\left(\overline{u_i u_k}\frac{\partial U_j}{\partial x_k} + \overline{u_j u_k}\frac{\partial U_i}{\partial x_k}\right)}_{P_{ij}\equiv Stress\ Production} - \underbrace{\rho\beta(g_i\overline{u_j\theta} + g_j\overline{u_i\theta}}_{G_{ij}\equiv Buoyancy Production} +$$

$$\underbrace{\overline{p\left(\frac{\partial u_i}{\partial x_j} + \frac{\partial u_j}{\partial x_i}\right)}}_{\phi_{ij}\equiv Pressure\ Strain} - \underbrace{2\mu\overline{\frac{\partial u_i}{\partial x_k}\frac{\partial u_j}{\partial x_k}}}_{\varepsilon_{ij}\equiv Dissipation} \underbrace{-2\rho\Omega_k(\overline{u_j u_m}\varepsilon_{ikm} + \overline{u_i u_m}\varepsilon_{jkm})}_{F_{ij}\equiv Production\ by\ System Rotation} \qquad (5.50)$$

Of the various terms in these exact equations, $C_{ij}, D_{ij}^{L}, P_{ij}$, and F_{ij} do not require any modeling. However, $D_{ij}^{T}, G_{ij}, \phi_{ij}$ and ε_{ij} need to be modeled to close the equations.

5.2.4.2 Modeling Turbulent Diffusive Transport

D_{ij}^{T} can be modeled by the generalized gradient-diffusion model:

$$D_{ij}^{T} = C_s \frac{\partial}{\partial x_k}\left(\rho \frac{k\overline{u_k u_l}}{\varepsilon}\frac{\partial \overline{u_i u_j}}{\partial x_l}\right) \tag{5.51}$$

However, this equation can result in numerical instabilities, so it has been simplified to use a scalar turbulent diffusivity as follows (Lien and Leschziner, 1994):

$$D_{ij}^{T} = \frac{\partial}{\partial x_k}\left(\frac{\mu_t}{\sigma_k}\frac{\partial \overline{u_i u_j}}{\partial x_k}\right) \tag{5.52}$$

where μ_t is the turbulent viscosity.

A value of $\sigma_k = 0.82$ is derived by applying the generalized gradient-diffusion model to the case of a plane homogeneous shear flow. Note that this value of σ_k is different from that in the standard and realizable $k-\varepsilon$ models, in which σ= 1.0.

5.2.4.3 Linear Pressure-Strain Model

The classical approach to modeling ϕ_{ij} uses the following decomposition:

$$\phi_{i,j} = \phi_{ij,1} + \phi_{ij,2} + \phi_{ij}^{w} \tag{5.53}$$

where $\phi_{ij,1}$ is the "slow pressure-strain" term, also known as the return-to-isotropy term, $\phi_{ij,2}$ is called the rapid pressure-strain term, and ϕ_{ij}^{w} is the wall-reflection term.

5.2.4.4 Boundary Conditions for the Reynolds Stresses

At walls, the near-wall values of the Reynolds stresses and ε are computed from wall functions. Explicit wall boundary conditions are applied for the Reynolds stresses by using the log-law and the assumption of equilibrium, disregarding convection and diffusion in the transport equations for the stresses.

Alternatively, the Reynolds stresses can be explicitly specified in terms of wall-shear stress, instead of k:

$$\frac{\overline{u_{\tau\tau}'^2}}{u_\tau^2} = 5.1, \quad \frac{\overline{u_\eta'^2}}{u_\tau^2} = 1.0, \quad \frac{\overline{u_\lambda'^2}}{u_\tau^2} = 2.3, \quad \frac{\overline{u_\tau' u_\lambda'}}{u_\tau^2} = 1.0$$

where u_t is the friction velocity defined by $u_t \equiv \sqrt{\tau_w/\rho}$, τ_w is the wall-shear stress.

5.2.5 Computational Effort

In terms of computation, the zero equation model is the least expensive turbulence model, since no turbulence transport equation is solved. In Spalart-Allmaras model, only one turbulence transport equation is solved.

The standard $k-\varepsilon$ model clearly requires more computational effort than the Spalart-Allmaras model since an additional transport equation is solved. The realizable $k-\varepsilon$ model requires very little more computational effort than the standard $k-\varepsilon$ model. However, due to the extra terms and functions in the governing equations and a greater degree of nonlinearity, computations with the RNG $k-\varepsilon$ model tend to take 10-15% more CPU time than with the standard $k-\varepsilon$ model. Compared with the $k-\varepsilon$ models, the RSM requires additional memory and CPU time due to the increased number of the transport equations for Reynolds stresses.

The standard $k-\varepsilon$ model is known to be slightly over-diffusive in certain sit-

uations, while the RNG $k-\varepsilon$ model is designed such that the turbulent viscosity is reduced in response to high rates of strain. Since diffusion has a stabilizing effect on the numerics, the RNG model is more likely to be susceptible to instability in steady-state solutions. However, this should not necessarily be seen as a disadvantage of the RNG model, since these characteristics make it more responsive to important physical instabilities such as time-dependent turbulent vortex shedding.

5.2.6 Direct Numerical Simulation

Direct numerical simulation (DNS) refers to a class of three-dimensional, time-dependent numerical solutions of the equations that govern the velocity, pressure, temperature and species concentrations in a turbulent flow. In general, DNS resolves the dynamics of all of the length and times scales of the turbulence, and thus introduces no modeling assumptions in its implementation. Since the pioneering studies by Lily (1972) and Patterson (1971), DNS has grown into an important tool for analyzing a broad range of complex turbulent processes because it provides the investigator with information that may be difficult if not impossible to obtain from a conventional experiment.

In direct numerical simulation, the instantaneous Navier-Stokes equations are solved numerically by means of spectral and pseudospectral techniques. Frequently, these simulations assume that the flow is periodic in one, two, or three directions, which are treated by means of spectral Fourier methods. The results of these simulations are not realistic because turbulent flows evolve in both space and time, and the use of periodic boundary conditions implies that only the temporal evolution of the flow is important. In addition, direct numerical simulation has been mainly applied to simple flows such as mixing layers with simple chemistry and low Reynolds number flows (Givi et al. 1988). Direct numerical simulation of diffusion turbulent flames may be found in Vervisch' review (1998).

DNS has to take into account explicitly all scales of motion. It is theoretically possible to resolve the whole spectrum of turbulent scales directly. DNS is

not, however, feasible for practical engineering problems. To understand the large computational cost of DNS, consider that the ratio of the large (energy-containing) scales to the small (energy-dissipating) scales is proportional to $Re_t^{3/4}$, where Re_t is the turbulent Reynolds number. Therefore, to resolve all the scales, the mesh size in three dimensions will be proportional to $Re_t^{9/4}$. Simple arithmetic shows that, for high Reynolds numbers, the mesh sizes required for DNS are prohibitive. Adding to the computational cost is the fact that the simulation will be a transient one with very small time steps, since the temporal resolution requirements are governed by the dissipating scales, rather than the mean flow or the energy-containing eddies.

5.2.7 The Large Eddy Simulations

Turbulent flows are characterized by eddies with a wide range of length and time scales. The largest eddies are typically comparable in size to the characteristic length of the mean flow. The smallest scales are responsible for the dissipation of turbulent kinetic energy.

The conventional approach to flow simulations employs the solution of the Reynolds-averaged Navier-Stokes (RANS) equations. In the RANS approach, all the turbulent motions are modeled, resulting in a significant savings in computational effort.

Conceptually, LES is situated somewhere between DNS and the RANS approach. Basically, in LES, large eddies are resolved directly, while small eddies are modeled. The rationale behind LES can be summarized as follows:

- Momentum, mass, energy, and other passive scalars are transported mostly by large eddies.
- Large eddies are more problem-dependent. They are dictated by the geometries and boundary conditions of the flow involved.
- Small eddies are less dependent on the geometry, tend to be more isotropic, and are consequently more universal.

- The chance of finding a universal model is much higher when only small eddies are modeled.

Solving only for the large eddies and modeling the smaller scales results in mesh resolution requirements that are much less restrictive than with DNS. Typically, mesh sizes can be at least one order of magnitude smaller than with DNS. Furthermore, the time step sizes will be proportional to the eddy-turnover time, which is much less restrictive than with DNS. In practical terms, however, extremely fine meshes are still required. It is only due to the explosive increases in computer hardware performance coupled with the availability of parallel processing that LES can even be considered as a possibility for engineering calculations.

The following sections give details of the governing equations for LES, present the two options for modeling the subgrid-scale stresses (necessary to achieve closure of the governing equations), and discuss the relevant boundary conditions.

5.2.7.1 Filtered Navier-Stokes Equations

The governing equations employed for LES are obtained by filtering the time-dependent Navier-Stokes equations in either Fourier (wave-number) space or configuration (physical) space. The filtering process effectively filters out the eddies whose scales are smaller than the filter width or grid spacing used in the computations. The resulting equations thus govern the dynamics of large eddies.

A filtered variable (denoted by an overbar) is defined by

$$\overline{\phi}(x) = \int_D \phi(x')G(x,x')dx' \tag{5.54}$$

where D is the fluid domain, and G is the filter function that determines the scale of the resolved eddies.

The finite-volume discretization provides the filtering operation:

$$\overline{\phi}(x) = \frac{1}{V}\int_V \phi(x')dx', x' \in V \tag{5.55}$$

where V is the volume of a computational cell. The filter function, $G(x, x')$, implied here is then

$$G(x, x') = \begin{cases} 1/V & \text{for} \quad x' \in V \\ 0 & \text{otherwise} \end{cases} \tag{5.56}$$

Since the application of LES to compressible flows is still in its infancy, the theory is presented here for incompressible flows. Filtering the incompressible Navier-Stokes equations, one obtains

$$\frac{\partial \rho}{\partial t} + \frac{\partial \rho \overline{u}_i}{\partial x_i} = 0 \tag{5.57}$$

and

$$\frac{\partial}{\partial t}(\rho \overline{u}_i) + \frac{\partial}{\partial x_j}(\rho \overline{u}_i \overline{u}_j) = \frac{\partial}{\partial x_j}\left(\mu \frac{\partial \overline{u}_i}{\partial x_j}\right) - \frac{\partial \overline{p}}{\partial x_i} - \frac{\partial \tau_{ij}}{\partial x_j} \tag{5.58}$$

where τ_{ij} is the subgrid-scale stress defined by

$$\tau_{ij} \equiv \rho \overline{u_i u_j} - \rho \overline{u}_i \overline{u}_j \tag{5.59}$$

5.2.7.2 Subgrid-Scale Models

The subgrid-scale stresses resulting from the filtering operation are unknown, and require modeling. The majority of subgrid-scale models in use today are eddy viscosity models of the following form:

$$\tau_{ij} - \frac{1}{3}\tau_{kk}\delta_{ij} = -2\mu_t \overline{S}_{ij} \tag{5.60}$$

where μ_t is the subgrid-scale turbulent viscosity, and $\overline{S}_{ij}$ is the rate-of-strain tensor for the resolved scale defined by

$$\overline{S}_{ij} \equiv \left(\frac{\partial \overline{u}_i}{\partial x_j} + \frac{\partial \overline{u}_j}{\partial x_i} \right) \tag{5.61}$$

There are two models for μ_t: the Smagorinsky-Lilly model and the RNG-based subgrid-scale model.

5.2.7.3 Smagorinsky-Lilly Model

The most basic of subgrid-scale models was proposed by Smagorinsky (1963) and further developed by Lilly (1966). In the Smagorinsky-Lilly model, the eddy viscosity is modeled by

$$\mu_t = \rho L_s^2 |\overline{S}| \tag{5.62}$$

where L_s is the mixing length for subgrid scales and $|\overline{S}| \equiv \sqrt{(2\overline{S}_{ij}\overline{S}_{ij})}$.

5.2.7.4 RNG-based Subgrid-Scale Model

Renormalization group (RNG) theory can be used to derive a model for the subgrid-scale eddy viscosity (Yakhot et al, 1989). The RNG procedure results in an effective subgrid viscosity, $\mu_{eff} = \mu + \mu_t$, given by

$$\mu_{eff} = \mu \left[1 + H \left(\frac{\mu_s^2 \mu_{eff}}{\mu^3} - C \right) \right]^{1/3} \tag{5.63}$$

where

$$\mu_s = (C_{rng} V^{1/3})^2 \sqrt{2\overline{S}_{ij}\overline{S}_{ij}} \tag{5.64}$$

H(x) is the Heaviside function:

$$H(x) = \begin{cases} x, & x > 0 \\ 0, & x \leq 0 \end{cases} \tag{5.65}$$

V is the volume of the computational cell. The theory gives $C_{rng} = 0.157$ and C=100.

In highly turbulent regions of the flow ($\mu_t >> \mu$), $\mu_{eff} = \mu_s$, and the RNG-based subgrid-scale model reduces to the Smagorinsky-Lilly model with a different model constant. In low-Reynolds-number regions of the flow, the argument of the ramp function becomes negative and the effective viscosity recovers molecular viscosity. This enables the RNG-based subgrid-scale eddy viscosity to model the low-Reynolds-number effects encountered in transitional flows and near-wall regions.

5.2.7.5 Boundary Conditions for the LES Model

The stochastic components of the flow at the velocity-specified inlet boundaries are accounted for by superposing random perturbations on individual velocity components as

$$\overline{u}_i = < \overline{u}_i > + I\psi|\overline{u}| \tag{5.66}$$

where I is the intensity of the fluctuation, ψ is a Gaussian random number satisfying $\overline{\psi} = 0$, and $\sqrt{\overline{\psi'}} = 1$.

5.3 Computational Methods

The numerical methodologies are used to solve the partial differential equations governing combustion phenomenon that include fluid dynamics, chemical thermodynamics, chemical kinetics and heat transfer. The solution techniques must be selected to achieve the best result. The most prominent computational methods are finite difference methods, finite volume methods, finite element methods and spectral methods. The finite difference methods, specially SIMPLE (semi-implicit

method for pressure-linked equations), are the most popular techniques in combustion simulation. The spectral methods are a new class of numerical algorithms. The widespread application of spectral methods has been motivated because their relatively higher numerical accuracy as compared to more conventional approaches.

5.3.1 The SIMPLE and SIMPLEC Techniques

A fully implicit method is the one described by Patankar (1980). In this technique, which was originally developed for incompressible flows, the momentum and continuity equations are manipulated in such a manner that a Poisson equation is obtained for the pressure. The resulting pressure equation replaces the continuity equation, while the momentum equations are used to determine the velocity field. The pressure and momentum equations are coupled through the pressure and velocity components. Because of the coupling between the pressure and momentum equations, the discretized forms of these equations are solved iteratively.

The SIMPLE method (Patankar, 1980) employs a sequential iteration in which the equations for each variable are solved repeatedly in succession. Point or line block iterative methods (Vanka, 1986) can also be used to solve for all the dependent variables simultaneously.

The advantage gained by implicit discretization is no time-step limitation. It is somewhat offset by the use of iterations that make time-dependent calculations rather expensive because iterations must be performed at each time step. Moreover, the iterative process may be slow or nonconvergent and under-relaxation may be required.

SIMPLE technique is applicable to both incompressible and compressible flows, since the pressure, rather than the density, is treated as a dependent variable. Because the density in incompressible flows does not appear at all in the continuity equation as it does in compressible flows, the methods that calculate the pressure from the equation of state and use the density as a dependent variable are not valid

for incompressible flows. With SIMPLE, a Poisson equation for the pressure is obtained, the continuity equation reduces to a compatibility condition for the velocity field. The SIMPLE algorithm uses a relationship between velocity and pressure corrections to enforce mass conservation and to obtain the pressure field.

If the momentum equation is solved with a guessed pressure field p^*, the resulting face flux J_f^*

$$J_f^* = \hat{J}_f^* + d_f(p_{c0}^* - p_{c1}^*) \tag{5.67}$$

does not satisfy the continuity equation.

where

$$d_f = \frac{\rho A_f^2}{\overline{a}_p} \tag{5.68}$$

Consequently, a correction J_f' is added to the face flow rate J_f^* so that the corrected face flow rate J_f

$$J_f = J_f^* + J_f' \tag{5.69}$$

satisfies the continuity equation. The SIMPLE algorithm postulates that J_f' be written as

$$J_f' = d_f(p_{c0}' - p_{c1}') \tag{5.70}$$

where p' is the cell pressure correction.

The SIMPLE algorithm substitutes the flux correction equations into the discrete continuity equation to obtain a discrete equation for the pressure correction p' in the cell:

$$a_p p' = \sum_{nb} a_{nb} p_{nb}' + b \tag{5.71}$$

where the source term b is the net flow rate into the cell:

$$b = \sum_{nb}^{N_{faces}} J_f^* \tag{5.72}$$

The pressure-correction equation may be solved using the algebraic multigrid(AMG) method. Once a solution is obtained, the cell pressure and the face flow rate are corrected using

$$p = p^* + \alpha_p p^* \tag{5.73}$$

$$J_f = J_f^* + d_f(p'_{c0} - p'_{c1}) \tag{5.74}$$

Here a_p is the under-relaxation factor for pressure. The corrected face flow rate J_f satisfies the discrete continuity equation identically during each iteration.

With SIMPLEC, the pressure-correction under-relaxation factor is generally set to 1.0, which aids in convergence speed-up. The SIMPLEC procedure is similar to the SIMPLE procedure outlined in SIMPLE. The only difference lies in the expression used for the face flow rate correction J'_f. As in SIMPLE, the correction equation may be written as

$$J_f = J_f^* + d_c(p'_{c0} - p'_{c1}) \tag{5.75}$$

where the coefficient d_c is defined as

$$d_c = \rho A_f^2 / \overline{(a_P - \sum_{nb} a_{nb})} \tag{5.76}$$

The use of this modified correction equation has been shown to accelerate convergence in problems where pressure-velocity coupling is the main deterrent to obtaining a solution.

5.3.2 Spectral Methods

The spectral methods (SPM) have been introduced and widely utilized in the field of combustion, mostly in the area of turbulent combustion. The improved accuracy can, in some cases, allow the physical phenomenon to be "captured" with fewer computational points, thereby allowing the physics of the problem to be simulated with less severe restrictions on the degree of numerical discretization. In simulating turbulence, this feature is particularly appealing because there exists at high Reynolds numbers a wide range of physical scales (Tennekes 1972) that must be accurately and efficiently accommodated in order to achieve a successful simulation (Zang et al. 1989).

Spectral solution of a partial differential equation involves the approximation of the solution of the equation as a truncated series of known and predetermined smoothing functions. For example, the approximate solution of a mixed initial boundary value problem describing the transport of a variable $U(x,t)$ involves the approximation of the dependent variable U in terms of the Nth order-series expansion of the type:

$$U(x,t) = \sum_{n=0}^{N} a_n(t)\phi_n(x) \tag{5.77}$$

In this approximation, N is the truncation cut-off and represents a measure of the resolution or the accuracy of the approximation. $\{\phi_n(x)\}$, $n = 0, 1, \ldots N$ are call the basis functions (also referred to as the expansion functions or the trial functions) and are prescribed a priori in such a way that the differential equation is satisfied as closely as possible by the truncated series expansion. $\{a_n(t)\}$ are the expansion coefficients, and their determination is the subject of spectral approximation.

The most familiar spectral approximations are those that represent the depen-

dent variable in terms of Fourier-series expansion. For a one-dimensional function, $U(x)$ on $x \in [0, 2\pi]$, the Fourier expansion is given by:

$$U(x) = \sum_{n=-\infty}^{n=\infty} \hat{a}_n \exp(inx) \tag{5.78}$$

with the test functions being the same as the basic functions but normalized to satisfy the orthonormality condition;

$$\hat{a}_n = \frac{1}{2\pi} \int_0^{2\pi} U(x) \exp(-inx) dx \tag{5.79}$$

The Fourier expansion function exp (inx) is primarily applied to periodic functions in a normalized domain, $x \in [0, 2\pi]$ (i.e., $U(x + 2\pi l) = U(x), l = 0, \pm 1, \pm 2, \ldots$) and exhibits a unique feature in that the nth coefficient of expansion a_n decreases more rapidly than any inverse power of n when U is sufficiently smooth. In the numerical approximation of Equation (5.78) by a truncating method the infinite-series expansion is truncated as

$$U_s(x) = \sum_{n=-N/2}^{N/2-1} \hat{a}_n \exp(inx) \tag{5.80}$$

Note that the expansion coefficients used in this truncated expansion are essentially the same as those obtained by infinite-series expansion. In Fourier spectral methods the derivatives of the function can be calculated rather easily. They are expressed by the analytic derivatives of the finite series that approximate the dependent variable. For example, in both truncating and interpolating series the first derivative is represented by

$$\frac{dU_s(x)}{dx} = \sum_{n=-N/2}^{N/2-1} ina_n \exp(inx) \tag{5.81}$$

This procedure can be generalized for the evaluation of higher derivatives:

$$\frac{d^m U(x)}{dx^m} = \sum_{n=-N/2}^{N/2-1} (in)^m a_n \exp(inx) \tag{5.82}$$

Those equations provide more accurate estimate of the derivatives than the one of the finite-difference discretization. The limitation of spectral approximations is the difficulty in simulating complex geometries. By the way, this method is invoked only for spatial discretization and not for temporal. This is similar to finite element procedures. In numerical simulations of boundary-value, ordinary differential equations, elliptic partial differential equations and spectral methods may be implemented directly. For initial-value ordinary differential equations as well as parabolic and hyperbolic partial differential equations, a complete algorithm may include the combination of a spectral approximation for the spatial variations and an appropriate finite difference procedure for representing the time derivatives.

Chapter 6

Chemical Reaction Dynamics

Non-reacting turbulent flows are highly challenging to model. When chemical reactions occur, the problems become even more complex, since the turbulent fluid flow is further coupled with chemical kinetics and quite often with phase changes. This is why the study of turbulent reacting flows is one of the most challenging fields of engineering science. In this chapter, several combustion models for turbulent diffusion flames are summarized and a simplified EBU model is presented.

6.1 Probability Density Function Model

In many problems of practical interest, the chemical reaction rates are fast so that the reaction is completed as soon as the reactants are mixed. The classical approach to the solution of these problems is to describe the mixing by obtaining the solution for a conserved scalar. The fast chemistry assumption implies that the instantaneous molecular species concentrations and temperature are functions only of the conserved scalar concentration at that instant. The functions are nonlinear,

however, and the central problem becomes that of linking the means and higher moments of the species and temperature to those of the conserved scalar. This is usually accomplished by considering the complete probability density function of the conserved scalar.

Linear relationships among all the conserved scalars exist only when there are two uniform reactant feeds. This restriction on the reactant feed only extends to elemental composition; each feed may be in several streams each of which may have any state of chemical aggregation, e.g., it may be partially reacted or pyrolyzed. If enthalpies are to be included in the conserved scalar set, then the enthalpies of the two feeds must be uniform. Uniformity here implies spatial and temporal constancy. When there are three feeds there are two independent conserved scalars and so on.

6.1.1 Probability Density Function Modeling Approach

The mixture fraction/PDF modeling approach involves the solution of transport equations for one or two conserved scalars (the mixture fractions). In this approach, transport equations for individual species are not solved. Instead, individual component concentrations for the species of interest are derived from the predicted mixture fraction distribution. Reaction mechanisms, which may be unknown or exceedingly complex, are not explicitly defined. Instead the reacting system is treated using infinitely fast chemistry (the flame sheet or "mixed-is-burned" approach), or chemical equilibrium calculations. Physical properties of chemical species and equilibrium data are obtained from the chemical database. Finally, the interaction of turbulence and chemistry is accounted for with a probability density function or PDF.

6.1.2 Mixture Fraction

The basis of the mixture fraction modeling approach is that under a certain set of simplifying assumptions the instantaneous thermochemical state of the fluid

is related to a conserved scalar quantity known as the mixture fraction f. For a binary system consisting of fuel and oxidizer, the mixture fraction can be written in terms of the elemental mass fraction as Sivathanu and Faeth (1990):

$$f = \frac{\xi_k - \xi_{kO}}{\xi_{kF} - \xi_{kO}} \tag{6.1}$$

where ξ_k is the elemental mass fraction for some element, k. Subscript O denotes the value at the oxidizer (or air) stream inlets and subscript F denotes the value at the fuel stream inlets. ξ_k might represent elemental carbon, for example. For simple fuel/oxidizer systems, the mixture fraction can be stated more simply as the local mass fraction of burned and unburned fuel.

If a secondary stream (another fuel or oxidant, or a nonreacting stream) is included, the fuel and secondary mixture fractions are simply the mass fractions of the fuel and secondary streams. The sum of all three mixture fractions in the system (fuel, secondary stream, and oxidizer) is always equal to 1:

$$f_{fuel} + f_{sec} + f_{ox} = 1 \tag{6.2}$$

6.1.3 Transport Equations for the Mixture Fraction

As noted above, the mixture fraction, f, is a conserved quantity. Its value at each point in the flow domain is computed through solution of the following conservation equation for the mean (time averaged) value of f in the turbulent flow field:

$$\frac{\partial}{\partial t}(\rho \overline{f}) + \frac{\partial}{\partial x_i}(\rho u_i \overline{f}) = \frac{\partial}{\partial x_i}\left(\frac{\mu_t}{\sigma_t}\frac{\partial \overline{f}}{\partial x_i}\right) + S_m \tag{6.3}$$

The source term, S_m, is due solely to transfer of mass into the gas phase from liquid fuel droplets or reacting particles. In all other cases there are no sources of $\overline{f}$.

In addition to solving for the mean mixture fraction, a conservation equation for

the mixture fraction variance, $\overline{f'^2}$, is solved (Jones and Whitelaw, 1982):

$$\frac{\partial}{\partial t}(\rho\overline{f'^2}) + \frac{\partial}{\partial x_i}(\rho u_i\overline{f'^2}) = \frac{\partial}{\partial x_i}\left(\frac{\mu_t}{\sigma_t}\frac{\partial\overline{f'^2}}{\partial x_i}\right) + C_g\mu_t\left(\frac{\partial\overline{f}}{\partial x_i}^2\right) - C_d\rho\frac{\varepsilon}{k}\overline{f'^2} \qquad (6.4)$$

where the constants σ_t, C_g and C_d take the values 0.7, 2.86, and 2.0, respectively. The mixture fraction variance is used in the closure model describing turbulence-chemistry interactions.

6.1.4 Various Forms of PDF Used in Turbulent Flames

Various forms of PDF have been adopted by different investigators in turbulent combustion calculations. The commonly used ones are the following:

6.1.4.1 The Double Delta Function

The double delta function is given by

$$p(f) = \begin{cases} 0.5, & f = \overline{f} - \sqrt{\overline{f'^2}} \\ 0.5, & f = \overline{f} + \sqrt{\overline{f'^2}} \\ 0, & \text{elsewhere} \end{cases} \qquad (6.5)$$

with suitable bounding near $f = 1$ and $f = 0$. One example of the double delta function is illustrated in Figure 6.1. As noted above, the double delta function PDF is very easy to compute but may be less accurate than the alternate β-function PDF.

The double delta function is the most easily computed, while the β-function is thought to represent most closely experimentally observed PDFs. The shape produced by these functions depends solely on the mean mixture fraction, $\overline{f}$, and its variance, $\overline{f'^2}$.

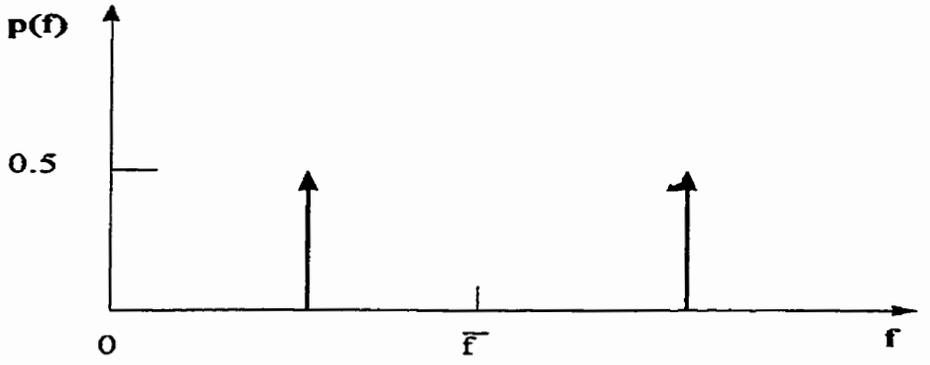

Figure 6.1 Example of the Double Delta Function PDF Shape

6.1.4.2 Clipped Gaussian Distribution

Lockwood and Naguib (1975) proposed and used a clipped Gaussian distribution. This model can be divided into three regions:

Region 1: $(f = 0)$

$$P(f, x_i) = \int_{-\infty}^{0} \frac{1}{\sigma(2\pi)^{1/2}} \exp\left[-\frac{1}{2}\left(\frac{f-\mu}{\sigma}\right)^2\right] df \tag{6.6a}$$

Region 2: $(0 < f < 1)$

$$\frac{1}{\sigma(2\pi)^{1/2}} \exp\left[-\frac{1}{2}\left(\frac{f-\mu}{\sigma}\right)^2\right] \tag{6.6b}$$

Region 3: $(f = 1)$

$$\int_1^{\infty} \frac{1}{\sigma(2\pi)^{1/2}} \exp\left[-\frac{1}{2}\left(\frac{f-\mu}{\sigma}\right)^2\right] df \tag{6.6c}$$

The distribution is represented by the Gaussian function for the range $0 < f < 1.$, but the tails of the distribution are represented by δ-function at f=0 and 1. It should be noted that Lockwood and Naguib used Reynolds averaging in their work instead of Favre averaging.

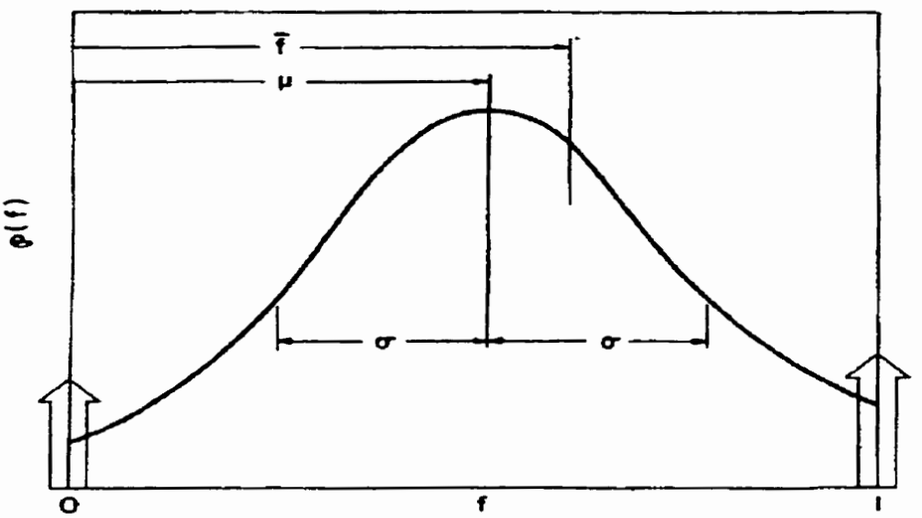

Figure 6.2 Clipped Gaussian pdf in terms of mixture fraction

6.1.4.3 The β-Function

The β-function PDF shape is given by the following function of $\overline{f}$ and $\overline{f'^2}$:

$$p(f) = \frac{f^{\alpha-1}(1-f)^{\beta-1}}{\int_0^1 f^{\alpha-1}(1-f)^{\beta-1} df} \tag{6.7}$$

where

$$\alpha = \overline{f}\left[\frac{\overline{f}(1-\overline{f})}{\overline{f'^2}} - 1\right] \tag{6.8}$$

and

$$\beta = (1 - \overline{f}) \left[\frac{\overline{f}(1 - \overline{f})}{\overline{f'^2}} - 1 \right] \tag{6.9}$$

The integral in the denominator is called Beta function $B(\alpha, \beta)$, which can be expressed in terms of several Gamma functions as $\Gamma(\alpha)\Gamma(\beta)/\Gamma(\alpha + \beta)$.

Figures 6.3 and 6.4 show the form of the β function for two conditions of $\overline{f}$ and $\overline{f'^2}$.

6.1.4.4 Student's t-Distribution

Student's t-distribution (Speigel, 1975) can sometimes be used to assess experimental uncertainties. The pdf of Student's t-distribution has the following form:

$$p(t) = \frac{\Gamma\left(\frac{n+1}{2}\right)}{\sqrt{n\pi}\Gamma\left(\frac{n}{2}\right)\left(1 + \frac{t^2}{n}\right)^{(n+1)/2}} \tag{6.10}$$

for $-\infty < t < \infty$. In the above equation, n is the number of degrees of freedom, the mean $\mu = 0$, the variance

$$\sigma^2 = \frac{n}{n-2} \quad \text{for} \quad n > 2 \tag{6.11}$$

and

$$t \equiv \frac{\chi^* \sqrt{n}}{Y} \tag{6.12}$$

where χ^* is an independent random variable which has mean equal to zero and variance equal to σ^2. As n approaches ∞, the Student's t-distribution approaches the normal distribution.

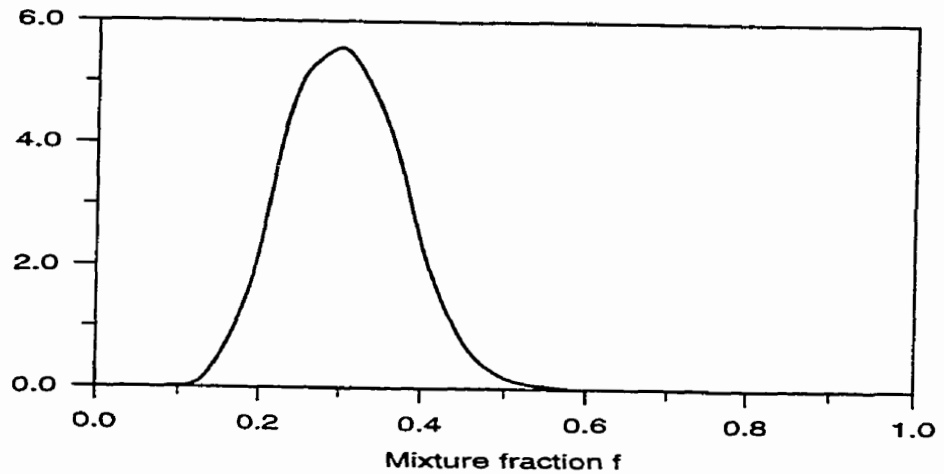

Figure 6.3 The β function ($\overline{f} = 0.3$ and $\overline{f'^2} = 0.005$)

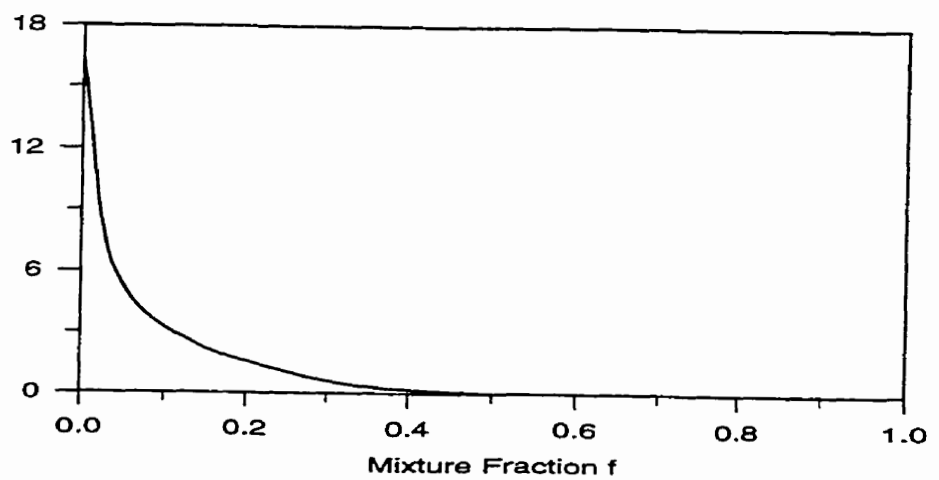

Figure 6.4 The β function ($\overline{f} = 0.1$ and $\overline{f'^2} = 0.01$)

6.1.4.5 Alternative Formulation of the Clipped Gaussian PDF

Kent and Bilger (1977) considered an alternative formulation of the clipped Gaussian pdf whereby intermittence was utilized. They proposed the following formula:

$$p(f, x_i) = [1 - I(x_i)]\delta(f) + I(x_i)p_1(f, x_i) \tag{6.13}$$

where $p_1(f, x_i)$ is the pdf for turbulent flow, for which a clipped Gaussian distribution was used, and $I(x_i)$ is the intermittence obtained from empirical correlation. They found that nitric oxide concentrations are particularly sensitive to the form of the pdf used.

6.1.5 Evaluation of PDF Model

The mixture fraction modeling approach has been specifically developed for the simulation of turbulent diffusion flames and similar reaction processes in which turbulent mixing is the limiting rate for reaction progress. For such systems, the PDF method offers many benefits over the finite rate formulation. The mixture fraction method allows intermediate species formation, dissociation effects, and the coupling between turbulence and chemistry to be accounted for in a rigorous way. The method is computationally efficient in that it does not require the solution of a large number of species transport equations. The approach has the additional benefit of allowing a more accurate estimation of the flow field mean density than is possible using the finite rate formulation. Note that the mixture fraction approach can be applied to reacting or non-reacting turbulent flows.

The mixture fraction approach can be used only when reacting flow system meets several requirements. First, the mixture fraction approach requires that the flow be

incompressible and turbulent. Second, the mixture fraction approach can only be applied to diffusion reaction systems; it is not applicable to premixed or partially premixed systems.

6.2 Chemical Equilibrium Model

The conservation species transport equation takes the following general form:

$$\frac{\partial}{\partial t}(\rho Y_{i'}) + \frac{\partial}{\partial x_i}(\rho u_i Y_{i'}) = -\frac{\partial}{\partial x_i} J_{i',i} + \hat{R}_{i'} + S_{i'} \tag{6.14}$$

where $Y_{i'}$ is the mass fraction of species i'. An equation of this form will be solved for N-1 species where N is the total number of fluid phase chemical species present in the system. $S_{i'}$ is the rate of creation by addition from. $J_{i',i}$ is the diffusion flux of species i', which arises due to concentration gradients. The diffusion flux in laminar flows can be written as

$$J_{i',i} = -\rho D_{i',m} \frac{\partial Y_{i'}}{\partial x_i}$$

Here $D_{i',m}$ is the diffusion coefficient for species i' in the mixture.

In turbulent flows, the mass diffusion is in the following form:

$$J_{i',i} = -\left(\rho D_{i',m} + \frac{\mu_t}{Sc_t}\right) \frac{\partial Y_{i'}}{\partial x_i}$$

where Sc_t is the turbulent Schmidt number, $(\mu_t/\rho D_t)$ (with a default setting of 0.7).

The reaction rates that appear in Equation (6.14) as source terms $\hat{R}_{i'}$ can be computed from Arrhenius rate expressions. Models of this type are suitable for a wide range of applications including laminar or turbulent reaction systems, and combustion systems including premixed or diffusion flames.

6.2.1 Reaction Rate Calculations

The source of chemical species i' due to reaction, $\hat{R}_{i'}$, is computed as the sum of the reaction sources over the N_R reactions that the species may participate in:

$$\hat{R}_{i'} = M_{i'} \sum_{k=1}^{N_R} \hat{R}_{i',k} \tag{6.15}$$

where $M_{i'}$ is the molecular mass of species i' and $\hat{R}_{i',k}$ is the molar rate of creation/destruction of species i' in reaction k. Reaction may occur in the continuous phase between continuous phase species only, or at surfaces resulting in the surface deposition or evolution of a continuous-phase species. The reaction rate, $R_{i',k}$, is controlled either by an Arrhenius kinetic rate expression or by the mixing of the turbulent eddies containing fluctuating species concentrations.

6.2.2 The Arrhenius Rate

Consider the kth reaction written in general form as follows:

$$\sum_{i'=1}^{N} v'_{i',k} A_{i'} \underset{k_{b,k}}{\overset{k_{f,k}}{\rightleftharpoons}} \sum_{i'=1}^{N} v''_{i',k} A_{i'} \tag{6.16}$$

where

N	number of chemical species
$v'_{i',k}$	stoichiometric coefficient for reactant i' in reaction k
$v''_{i',k}$	stoichiometric coefficient for product i' in reaction k
$A_{i'}$	symbol denoting species i'
$k_{f,k}$	forward rate constant for reaction k
$k_{b,k}$	backward rate constant for reaction k

Equation (6.15) is valid for both reversible and non-reversible reactions. For non-reversible reactions, the backward rate constant $k_{b,k}$ is simply omitted.

The summations in Equation (6.15) are for all chemical species in the system, but only species involved as reactants or products will have non-zero stoichiometric coefficients; species that are not involved will drop out of the equation except for third-body reaction species.

The molar rate of creation/destruction of species i' in reaction k, $\hat{R}_{i',k}$, in Equation (6.14) is given by

$$\hat{R}_{i',k} = \Gamma(v''_{i',k} - v'_{i',k}) \left(k_{f,k} \prod_{j'=1}^{N} [C_{j'}]^{\eta'_{j',k}} - k_{b,k} \prod_{j'=1}^{N} [C_{j'}]^{\eta''_{j',k}} \right) \tag{6.17}$$

where

$C_{j'}$ molar concentration of each reactant or product species j' (kmol/m^3)

$\eta'_{j',k}$ rate exponent for reactant j' in reaction k

$\eta''_{j',k}$ rate exponent for product j' in reaction k

and Γ represents the net effect of third bodies on the reaction rate. This term is given by

$$\Gamma = \sum_{j'}^{N} \gamma_{j'k} C_{j'} \tag{6.18}$$

where $\gamma_{j'k}$ is the third-body efficiency of the j'th species in the kth reaction.

The forward rate constant for reaction k, $k_{f,k}$, is computed using the Arrhenius expression

$$k_{f,k} = A_k T^{\beta_k} \exp(-E_k/RT) \tag{6.19}$$

where

A_k pre-exponential factor (consistent units)

β_k temperature exponent (dimensionless)

E_k activation energy for the reaction (J/kmol)

R universal gas constant (J/kmol-K)

The values of $v'_{i',k}, v''_{i',k}, \eta'_{i',k}, \eta''_{i',k}, \beta_k, A_k, E_k$ and $\gamma_{j',k}$ can be provided during the problem definition.

If the reaction is reversible, the backward rate constant for reaction k, $k_{b,k}$, is computed from the forward rate constant using the following relation:

$$k_{b,k} = \frac{k_{f,k}}{K_k} \tag{6.20}$$

where K_k is the equilibrium constant for the kth reaction, computed from

$$K_k = \exp\left(\frac{\Delta S_k^o}{R} - \frac{\Delta H_k^o}{RT}\right)\left(\frac{p}{RT}\right)^{\sum_{k=1}^{N_R} \eta'_{j',k}} \tag{6.21}$$

The term within the exponential represents the change in Gibbs free energy, and its components are computed as follows:

$$\frac{\Delta S_k^o}{R} = \sum_{i'=1}^{N} (v''_{i',k} - v'_{i',k}) \frac{S_{i'}^o}{R} \tag{6.22}$$

$$\frac{\Delta H_k^o}{RT} = \sum_{i'=1}^{N} (v''_{i',k} - v'_{i',k}) \frac{h_{i'}^o}{R} \tag{6.23}$$

where $S_{i'}^o$ and $h_{i'}^o$ are, respectively, the standard-state entropy and standard-state enthalpy (including heat of formation). These values are specified as properties of the mixture material.

6.3 Eddy Dissipation Model

The influence of turbulence on the reaction rate is taken into account by employ-

ing the Magnussen and Hjertager model (1977). In this model, the rate of reaction $R_{i',k}$ is given by the smaller (i.e., limiting value) of the two expressions below:

$$\hat{R}_{i',k} = v'_{i',k} M_{i'} A \rho \frac{\varepsilon}{k} \frac{Y_R}{v'_{R,k} M_R} \tag{6.24}$$

$$\hat{R}_{i',k} = v'_{i',k} M_{i'} AB \rho \frac{\varepsilon}{k} \frac{\sum_P Y_P}{\sum_{j'}^{N} v''_{j',k} M_{j'}} \tag{6.25}$$

where

Y_P represents the mass fraction of any product species

Y_R represents the mass fraction of a particular reactant

M represents the molecular mass of species

A an empirical constant equal to 4.0

B an empirical constant equal to 0.5

The eddy-dissipation model relates the rate of reaction to the rate of dissipation of the reactant- and product-containing eddies. (k/ε) represents the time scale of the turbulent eddies following the eddy-dissipation model of Spalding (1970). The model is useful for the prediction of premixed and diffusion problems as well as for partially premixed reacting flows.

6.4 Varied Coefficient EBU Model

Three eddy-break-up models are presented respectively by Spalding (1970) and Magnussen-Hjertager (1976). It is true that the Magnussen and Hjertager model is more widely used. In this model there is a parameter A which is given a value of 4. In this section, this EBU coefficient A may be presented more adequately as a PDF function to reflect its dependence with the local turbulence interaction with combustion. The calculating accuracy is improved.

Givi (1984) pointed out that there is no single constant value of A (in Givi's paper, it serves as H^{-1}) that can be employed throughout the whole flow field both axially and radially. Their results show that the value of A is a function of radial distance and there is a peak at the shear layer where reactant consumption is most important. The peak takes place at $r = D_0 = 2R_i$ where R_i is the inner jet radius.

Brizuela and Bilger (1996) suggested that the EBU coefficient A may be computed explicitly as a function of the mean and standard deviation of mixture fraction. Higher accuracy is obtained.

6.4.1 Basic Principle

For a one-step chemical reaction such as

$$\mathrm{F} + r\mathrm{O} \rightarrow (r+1)\mathrm{P} \tag{6.26}$$

where r is the air:fuel ratio on a mass basis, O is the oxidant, F the fuel and P the product.

$$\beta_{FO} \equiv Y_F - Y_O/r \tag{6.27}$$

$$\beta_{FP} \equiv Y_F + Y_P/(r+1) \tag{6.28}$$

$$\beta_{OP} \equiv Y_O + rY_P/(r+1) \tag{6.29}$$

are conserved scalars. Y is the mass fraction.

The general mixture fraction can be defined as

$$f \equiv \frac{\beta - \beta_1}{\beta_1 - \beta_2} \tag{6.30}$$

The subscripts 1 and 2 refer to the composition in the two feeds and β is a Shvab-Zeldovich function. $\tilde{f}$ is the mean of f.

When the feed materials are in exact stoichiometric proportion, let Equation (6.30) $\beta = \beta_{FO}$, and notice $Y_F = Y_O = 0$

$$\beta_{FO} = 0 \text{ (stoichiometric reaction)} \tag{6.31}$$

$$(\beta_{FO})_1 = Y_F \text{ (pure fuel)} \tag{6.32}$$

$$(\beta_{FO})_2 = Y_O/r \text{ (pure oxidant)} \tag{6.33}$$

so,

$$f_s = \frac{Y_O}{rY_F + Y_O} \tag{6.34}$$

For fast chemistry or the one-step irreversible reaction, there will be no oxidant present for mixtures richer than stoichiometric ($f > f_s$) and no fuel present when the mixture is weaker than stoichiometric ($f < f_s$). Both will be zero when the mixture is stoichiometric. This yields the functional relationships shown in Figure 6.5.

The constant

$$Y_B \equiv Y_F + \frac{1}{r}Y_O = Y_F/(1 - f_s) \tag{6.35}$$

The standard deviation

$$g = \sqrt{\widetilde{f'^2}} \tag{6.36}$$

The Heaviside function is defined as

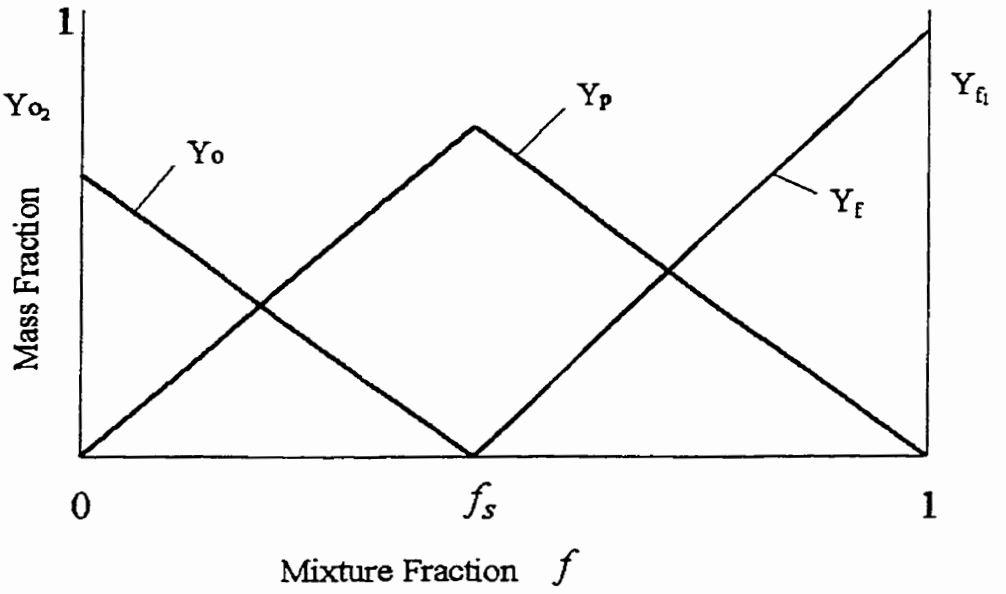

Figure 6.5 Composition structure functions

$$H(\delta) = \begin{cases} 1 & \text{if} \quad \delta \geq 0 \\ 0 & \text{if} \quad \delta < 0 \end{cases} \tag{6.37}$$

The chemical-species conservation equation

$$\rho \frac{\partial Y_i}{\partial t} + \rho u_k \frac{\partial Y_i}{\partial x_k} - \frac{\partial}{\partial x_k}\left(\rho D_i \frac{\partial Y_i}{\partial x_k}\right) = w_i \tag{6.38}$$

Here Y_i is the mass fraction of chemical species i that has a net chemical production rate w_i, ρ the density and u_k the component of velocity in the coordinate direction x_k.

6.4.2 Mean Properties

6.4.2.1 Parameter J_1

In Bilger's model, J_1 is an important parameter. Its definition is:

$$J_1\left(\frac{f_s-\tilde{f}}{g}\right)=\int_0^{f_s}\left(\frac{f_s-f}{g}\right)\tilde{P}(f;x)df-\frac{(f_s-\tilde{f})}{g}H(f_s-\tilde{f}) \tag{6.39}$$

where $\tilde{P}(f;x)$ is the probability density function, g is standard deviation.

$$\begin{aligned}
J_1\left(\frac{f_s-\tilde{f}}{g}\right) &= \left[\int_0^1\left(\frac{f_s-f}{g}\right)\tilde{P}(f;x)df-\int_{f_s}^1\left(\frac{f_s-f}{g}\right)\tilde{P}(f;x)df\right] \\
&\quad -\frac{f_s-\tilde{f}}{g}H(f_s-\tilde{f}) \\
&= \left[\frac{f_s-\tilde{f}}{g}-\int_{f_s}^1\left(\frac{f_s-f}{g}\right)\tilde{P}(f;x)df\right]-\frac{f_s-\tilde{f}}{g}H(f_s-\tilde{f}) \\
&= \frac{f_s-\tilde{f}}{g}[1-H(f_s-\tilde{f})]+\int_{f_s}^1\left(\frac{f-f_s}{g}\right)\tilde{P}(f;x)df \\
&= \frac{f_s-\tilde{f}}{g}H(\tilde{f}-f_s)+\int_{f_s}^1\left(\frac{f-f_s}{g}\right)\tilde{P}(f;x)df
\end{aligned} \tag{6.40}$$

when $\tilde{f}>f_s, H(f_s-\tilde{f})=0$, from (6.39)

$$J_1=\int_0^{f_s}\left(\frac{f_s-f}{g}\right)\tilde{P}(f;x)df\geq 0 \tag{6.41}$$

when $\tilde{f}<f_s, H(\tilde{f}-f_s)=0$, from (6.40)

$$J_1 = \int_{f_s}^{1} \left(\frac{f - f_s}{g} \right) \widetilde{P}(f;x)df \geq 0 \tag{6.42}$$

Totally

$$J_1 \geq 0 \tag{6.43}$$

So, J_1 is non-negative.

6.4.2.2 The Mass Fraction with f and J_1

The general Favre averaging form of mass fraction(Bilger, 1980):

$$\widetilde{Y_i}(x) = \int_0^1 Y_i^e(f)\widetilde{P}(f;x)df \tag{6.44}$$

for $\widetilde{Y_o}$

$Y_o = rY_B(f_s - f)$ when $f \leq f_s$

$Y_o = 0$ when $f > f_s$

or

$$Y_o^e(\tilde{f}) = rY_B(f_s - \tilde{f})H(f_s - \tilde{f}) \tag{6.45}$$

$$\begin{aligned} \widetilde{Y_o} &= \int_0^1 Y_o^e(f)\widetilde{P}(f;x)df \\ &= \int_0^{f_s} rY_B(f_s - f)\widetilde{P}(f;x)df + \int_{f_s}^1 0 \cdot \widetilde{P}(f;x)df \\ &= rY_B \int_0^{f_s} (f_s - f)\widetilde{P}(f;x)df \end{aligned} \tag{6.46}$$

add to Equation(6.45)

$$\begin{aligned}
\widetilde{Y_o} &= Y_o^e(\tilde{f}) - rY_B(f_s - \tilde{f})H(f_s - \tilde{f}) + rY_B\int_0^{f_s}(f_s - f)\tilde{P}(f;x)df \\
&= Y_o^e(\tilde{f}) + rY_B\left[\int_0^{f_s}(f_s - f)\tilde{P}(f;x)df - (f_s - \tilde{f})H(f_s - \tilde{f})\right] \\
&= Y_o^e(\tilde{f}) + rY_B g\left[\int_0^{f_s}\left(\frac{f_s - f}{g}\right)\tilde{P}(f;x)df - \frac{f_s - \tilde{f}}{g}H(f_s - \tilde{f})\right] \\
&= Y_o^e(\tilde{f}) + rY_B g J_1\left(\frac{f_s - \tilde{f}}{g}\right) \qquad (6.47)
\end{aligned}$$

for $\widetilde{Y_F}$

$$Y_F = 0 \qquad \text{when } f \le f_s$$

$$Y_F = Y_B(f - f_s) \qquad \text{when } f > f_s$$

or

$$Y_F^e(\tilde{f}) = Y_B(\tilde{f} - f_s)H(\tilde{f} - f_s) \qquad (6.48)$$

$$\begin{aligned}
\widetilde{Y_F} &= \int_0^1 Y_F^e(f)\tilde{P}(f;x)df \\
&= \int_0^{f_s} 0 \cdot \tilde{P}(f;x)df + \int_{f_s}^1 Y_B(f - f_s)\tilde{P}(f;x)df \\
&= Y_B\int_{f_s}^1 (f - f_s)\tilde{P}(f;x)df \qquad (6.49)
\end{aligned}$$

notice

$$H(\tilde{f} - f_s) + H(f_s - \tilde{f}) \equiv 1 \qquad (6.50)$$

In spite of what $\tilde{f}$ equals to, always there is one H and only one H equals 1, the other equals 0.

$$H(\tilde{f} - f_s) = 1 - H(f_s - \tilde{f}) \tag{6.51}$$

into Equation(6.48)

$$\begin{aligned} Y_F^e(\tilde{f}) &= Y_B(\tilde{f} - f_s)[1 - H(f_s - \tilde{f})] \\ &= Y_B\left[(\tilde{f} - f_s) - (\tilde{f} - f_s)H(f_s - \tilde{f})\right] \\ &= Y_B\left[(\tilde{f} - f_s) + (f_s - \tilde{f})H(f_s - \tilde{f})\right] \end{aligned} \tag{6.52}$$

$$\begin{aligned} \int_{f_s}^{1}(f - f_s)\tilde{P}(f;x)df &= \int_0^1 (f - f_s)\tilde{P}(f;x)df - \int_0^{f_s}(f - f_s)\tilde{P}(f;x)df \\ &= (\tilde{f} - f_s) + \int_0^{f_s}(f - f_s)\tilde{P}(f;x)df \end{aligned} \tag{6.53}$$

from (6.52) (6.53) into (6.49)

$$\begin{aligned} \widetilde{Y_F} &= Y_F^e(\tilde{f}) - Y_B[(\tilde{f} - f_s) + (f_s - \tilde{f})H(f_s - \tilde{f})] + Y_B[(\tilde{f} - f_s) \\ &\quad + \int_0^{f_s}(f_s - f)\tilde{P}(f;x)df \\ &= Y_F^e(\tilde{f}) + Y_B g\left[\int_0^{f_s}\left(\frac{f_s - f}{g}\right)\tilde{P}(f;x)df - \frac{f_s - \tilde{f}}{g}H(f_s - \tilde{f})\right] \\ &= Y_F^e(\tilde{f}) + Y_B g J_1\left(\frac{f_s - \tilde{f}}{g}\right) \end{aligned} \tag{6.54}$$

for $\widetilde{Y_P}$

$$Y_P = (r+1)Y_B f(1 - f_s) \qquad \text{when } f \le f_s$$

$$Y_F = (r+1)Y_B f_s(1 - f) \qquad \text{when } f > f_s$$

or

$$Y_P^e(\tilde{f}) = (r+1)Y_B[\tilde{f}(1-f_s)H(f_s-\tilde{f}) + f_s(1-\tilde{f})H(\tilde{f}-f_s)] \qquad (6.55)$$

$$\widetilde{Y_P} = (r+1)Y_B\left[(1-f_s)\int_0^{f_s} f\tilde{P}(f;x)df + f_s\int_{f_s}^1 (1-f)\tilde{P}(f;x)df\right] \qquad (6.56)$$

$$\begin{aligned}
\widetilde{Y_P} &= (r+1)Y_B\left[(1-f_s)\int_0^{f_s} f\tilde{P}(f;x)df\right. \\
&\quad \left. + f_s\left(\int_0^1 (1-f)\tilde{P}(f;x)df - \int_0^{f_s}(1-f)\tilde{P}(f;x)df\right)\right] \\
&= (r+1)Y_B\left[\int_0^{f_s} f\tilde{P}(f;x)df - f_s\int_0^{f_s} f\tilde{P}(f;x)df - f_s\int_0^{f_s}(1-f)\tilde{P}(f;x)df\right] + \\
&\quad (r+1)Y_B\left[f_s\int_0^1 (1-f)\tilde{P}(f;x)df\right] \\
&= (r+1)Y_B\left[\int_0^{f_s} f\tilde{P}(f;x)df - f_s\int_0^{f_s}(f+1-f)\tilde{P}(f;x)df + f_s(1-\tilde{f})\right] \\
&= (r+1)Y_B\left[\int_0^{f_s} f\tilde{P}(f;x)df - f_s\int_0^{f_s}\tilde{P}(f;x)df + f_s(1-\tilde{f})\right] \\
&= -(r+1)Y_B\left[\int_0^{f_s}(f_s-f)\tilde{P}(f;x)df - f_s(1-\tilde{f})\right] \qquad (6.57)
\end{aligned}$$

into (6.56)

$$\begin{aligned}
\widetilde{Y_P} &= Y_P^e(\tilde{f}) - (r+1)Y_B\left[\tilde{f}(1-f_s)H(f_s-\tilde{f}) + f_s(1-\tilde{f})H(\tilde{f}-f_s)\right] - \\
&\quad (r+1)Y_B\left[\int_0^{f_s}(f_s-f)\tilde{P}(f;x)df - f_s(1-\tilde{f})\right] \\
&= Y_P^e(\tilde{f}) - (r+1)Y_B\left[\tilde{f}(1-f_s)H(f_s-\tilde{f}) + f_s(1-\tilde{f}) - f_s(1-\tilde{f})H(f_s-\tilde{f})\right. \\
&\quad \left. - f_s(1-\tilde{f})\right] + (r+1)Y_B\left[\int_0^{f_s}(f_s-f)\tilde{P}(f;x)df\right] \\
&= Y_P^e(\tilde{f}) - (r+1)Y_B\left[\int_0^{f_s}(f_s-f)\tilde{P}(f;x)df - H(f_s-\tilde{f})(f_s - f_s\tilde{f} - \tilde{f} + \tilde{f}f_s)\right] \\
&= Y_P^e(\tilde{f}) - (r+1)Y_B\left[\int_0^{f_s}(f_s-f)\tilde{P}(f;x)df - H(f_s-\tilde{f})(f_s-\tilde{f})\right] \\
&= Y_P^e(\tilde{f}) - (r+1)Y_B g J_1\left(\frac{f_s-\tilde{f}}{g}\right) \qquad (6.58)
\end{aligned}$$

As J_1 is non-negative it is seen from Equations (6.47), (6.54) and (6.58) that the effect of the turbulence is to increase the mean concentration of reactants above the

"laminar" value at the mean mixture fraction. The mean product concentration is correspondingly reduced.

6.4.3 Bilger Model

The result of Bilger (1976) shows that the mixing-limited reaction rate is proportional to the probability density of the mixture being stoichiometric.

In the EBU model, the rate of consumption of fuel,

$$\overline{\dot{w}_f} = -A\bar{\rho}\tilde{Y}_L\frac{\varepsilon}{k} \tag{6.59}$$

where $\tilde{Y}_L$ is the limiting reactant mass fraction, i.e., the lowest of either mass fraction $\tilde{Y}_f$ or $\tilde{Y}_o/r$. Bilger used the preceding theory and got

$$A = \frac{C_{g2}}{2}\frac{p_z(z_s)}{J_1(z_s)} \tag{6.60}$$

where $z_s = (f_s - \tilde{f})/g$ and p_z is the pdf expressed in terms of the variable z, which is a form of the mixture fraction f, centered and normalized using mean and standard deviation. A typical value for C_{g2} is 2.0, so

$$A = \frac{p_z(z_s)}{J_1(z_s)} \tag{6.61}$$

6.4.4 Simplified Model

There exists a difficulty in FLUENT to apply Bilger's model. In order to input the coefficient A "Finite-Rate Reaction" must be chosen, when Equation (6.60) is used to calculate A, the mean f and standard deviation g are needed which only are obtained in "PDF". But in FLUENT only one model, "Finite-Rate Reaction" or "PDF", is permitted to be used. By the way, in every iteration, the transport equations about f and g are solved and get new A value, it spends a lot of CPU time. There are several methods to overcome the difficulty.

6.4.4.1 The Constant

In Magnussen (1977) model, A equals 4. Brizuela (1996) suggests that a value of $A = 2$ may be taken as a flame brush average. He thought that this value will be particularly accurate in the slightly rich region of the flame.

6.4.4.2 Brizuela Empirical Fit

Brizuela (1996) adopted an empirical fit method. Two equations are obtained with satisfactory approximation.

$$\frac{\overline{\dot{w}_f}}{\bar{\rho}\frac{\varepsilon}{k}Y_B} = A^* \breve{Y}_f^m \breve{Y}_o^{-n} \left(\frac{1}{\breve{Y}_f} + \frac{1}{\breve{Y}_o}\right)^{-p} \tag{6.62}$$

where m-n+p should be of order unity.

One more simplified form is:

$$\overline{\dot{w}_f} = 4\bar{\rho}\frac{\varepsilon}{k}\frac{\tilde{Y}_f}{\left(1+\frac{r\tilde{Y}_f}{\tilde{Y}_o}\right)}\sqrt{\frac{r\tilde{Y}_f}{\tilde{Y}_o}} \tag{6.63}$$

6.4.4.3 The Improved Model

Since it is difficult to calculate $J_1(z_s)$, it is of interest to eliminate $J_1(z_s)$ in the equation. In user-defined function file, we use the rate of consumption fuel $\overline{\dot{w}_f}$ to find a suitable expression to eliminate the parameter A. We can directly solve for $\overline{\dot{w}_f}$.

In Equation(6.59) $\tilde{Y}_L = gY_B J_1(z_s)$, added into Equation(6.61)

$$\begin{aligned}\overline{\dot{w}_f} &= -\frac{p_z(z_s)}{J_1(z_s)}\bar{\rho}gY_B J_1(z_s)\frac{\varepsilon}{k} \\ &= -p_z(z_s)\bar{\rho}gY_B\frac{\varepsilon}{\kappa}\end{aligned} \tag{6.64}$$

where Y_B is a constant.

$$p_z(z_s) = gP_f(f_s) \tag{6.65}$$

$$\overline{\dot{w}_f} = -g^2P_f(f_s)\bar{\rho}Y_B\frac{\varepsilon}{k} \tag{6.66}$$

Now, Equation(6.66) does not include $J_1(z_s)$.

Differing from Equation(6.60), Equation(6.66) is not a function of the mean f. Owing to a typical value of $f_s = 0.06$ for the combustion of hydrocarbon fuels in air, then in Equation(6.66), $P_f(f_s)$ is a constant if P_f is given. We just need to know the value of g. We assume the mixture standard deviation to be constant across the flame brush, for example, $g = 0.5, f_s = 0.03$. Then Equation(6.65) becomes

$$\overline{\dot{w}_f} = -0.0009P_f(f_s)\bar{\rho}Y_B\frac{\varepsilon}{k} \tag{6.67}$$

P_f may be:

1) The Gaussian form

$$p(f) = \frac{1}{\sqrt{2\pi}g}e^{-\frac{(f-f_s)^2}{2g^2}} \tag{6.68}$$

and

$$p(f_s) = \frac{1}{\sqrt{2\pi}g} \tag{6.69}$$

when $g = 0.03$

$$p(f_s) = \frac{1}{\sqrt{2\pi} \times 0.03} = 13.298 \tag{6.70}$$

2) β function

$$p(f) = \frac{\Gamma(\beta_1 + \beta_2)}{\beta_1 \beta_2} f^{\beta_1 - 1}(1 - f)^{\beta_2 - 1} \tag{6.71}$$

where the Γ-function is defined as

$$\Gamma = \int_0^1 x^{\beta - 1} e^{-x} dx \tag{6.72}$$

When $f_s = 0.06, g = 0.03$, we get

$$p(f_s) = 12.897 \tag{6.73}$$

The values of $p(f_s)$ are almost the same using a Gaussian or β form. We can let $p(f_s) = 13.0$. Finally

$$\bar{\dot{w}}_f = -0.0117 \bar{\rho} \tilde{Y}_B \frac{\varepsilon}{k} \tag{6.74}$$

It is pointed out that we calculate simultaneously the user-defined rate, finite chemical reaction rate and standard EBU rate. The slowest rate is used as the reaction rate and the contributions to the source terms in the species conservation and energy equations are calculated from this reaction rate. When Bilger's model is used, large values of the coefficient A such as 200 may be obtained. But this is meaningless. The larger coefficient means the faster mixing. The time scale of the chemical reaction, t_c, may reach same order of the time scale for molecular mixing, t_m. So when the Damköhler number $\mathrm{Da} \equiv t_m/t_c \approx 1$, the chemical reaction rate must be considered. When $t_c > t_m$, the chemical reaction rate is the source terms and the variation of A does not affect the calculating results.

Chapter 7

Computational Results and Discussion

In this chapter, the different combustion models are used to calculate laminar and turbulent reacting flows. The results are compared with experimental data. For turbulent flow, three kinds of turbulent models, $k-\varepsilon$, Reynolds stress and large eddy simulation are tested. Magnussen and Hjertager(1977) model extended the eddy-break-up model of Spalding (1971) to a turbulent diffusion flame.

7.1 Laminar combustion

7.1.1 Problem Description

The vertical cylindrical diffusion-flame burner is shown in Fig. 7.1. The burner consists of two concentric tubes of radii 6.35 mm and 25.4 mm. The geometry for

this test is shown in Figure 7.2. Fuel issues through the inner tube and air issues through the outer. Methane is supplied at 5.7 mL/s, or the uniform inlet fuel velocity is 0.0455 m/s, with a temperature of 300 K. Air is supplied at 187.7 mL/s, or the uniform inlet velocity is 0.0988 m/s, with a temperature of 300 K. The experimental apparatus and results are fully described by Mitchell (1980).

Mitchell (1980) points out that several investigators had analyzed the burner and in most cases these simulations were partial and did not provide a complete representation of the concentration, temperature and velocity fields established in the laminar diffusion flame.

In the present computation, the reaction rates are computed by finite-rate for laminar flow. The one-step, two-step and six-step reactions are used in methane combustion.

for the one-step model

$$CH_4 + 2\ O_2 \rightarrow CO_2 + 2H_2O \tag{7.1}$$

for the two-step model (Westbrook, 1981)

$$CH_4 + \tfrac{3}{2}\ O_2 \rightarrow CO + 2H_2O \tag{7.2}$$

$$CO + \tfrac{1}{2}\ O_2 \rightarrow CO_2 \tag{7.3}$$

for the six-step model (Hyer, 1991)

$$CH_4 + \tfrac{1}{2}\ O_2 \rightarrow CO + 2H_2 \tag{7.4}$$

$$CH_4 + H_2O \rightarrow CO + 3H_2 \tag{7.5}$$

$$CO + H_2O \rightarrow CO_2 + H_2 \tag{7.6}$$

$$CO_2 + H_2 \rightarrow CO + H_2O \tag{7.7}$$

$$H_2 + \tfrac{1}{2}\, O_2 \rightarrow H_2O \tag{7.8}$$

$$H_2O \rightarrow H_2 + \tfrac{1}{2}\, O_2 \tag{7.9}$$

The coefficients (Hyer, 1991) for the Arrhenius rate are as shown in Table 7.1.

No. of Eq.	A_k	E_k	β_k
7.1	1.e+12	1.e+08	0
7.2	5.012e+11	2.e+08	0
7.3	2.239e+12	1.7e+08	0
7.4	4.4e+09	1.26e+08	0
7.5	3.0e+08	1.26e+08	0
7.6	2.75e+10	8.37e+07	0
7.7	9.62e+10	1.26e+08	-0.85
7.8	7.45e+13	1.67e+08	-0.91
7.9	3.83e+14	4.12e+08	-1.05

Table 7.1 The Arrhenius rate coefficients

7.1.2 Results

The computed mesh is shown in Figures 7.3 and 7.4. It involves 9000 nodes. The under-relaxation factors are different for different variables varying from 0.25 to 0.8. The calculating results for a two-step reaction are very close to the one-step, so, in the figures only the one-step, six-step and experimental results are shown.

Radial composition profiles of CH_4, O_2, CO_2, H_2O, CO, H_2 and N_2 at several axial locations are shown on Figures 7.5 - 7.10 and the test results for Mitchell(1980) are also shown. Owing that the one-step method can not calculate CO and H_2, the comparison is done only between the six-step and test data.

Analysis of the CH_4 (Figure 7.5) shows that the two methods overpredict CH_4 and the calculated flame position is further from the burner plate than in the real case. For O_2, both results are the same (Figure 7.6) and the one-step model and the six-step model overpredict the CO_2 concentration (Figure 7.7). From Figure 7.8, the H_2O profile first increases with radial distance, peaks at 8 mm in predicted result and at 7 mm in experimental result, then decreases to zero. The comparison of CO, H_2 and N_2 is shown in Figures 7.9-7.11. In general, the result of the six-step is slightly better than the one-step results. The one-step model neglects the energy-absorbing pyrolysis reaction and overpredicts the temperature by about 200-250K. The six-step model is lower than the experimental result by 50-100K (Figure 7.12). The chemical reaction model mainly affects the species and the temperature distribution and has a little effect on velocity. Figures 7.13-7.17 show the temperature and velocity field of the one-step model. Figures 7.18-7.21 depict the temperature and velocity fields for the six-step model. It is pointed out that experimental CH_4 concentration at 1.2 cm is 30%, seems very low; but N_2 one is 50%, seems over-high.

It is observed that the predicted maximum temperature in the one-step model is 2326K, but in the six-step model, it is 1942K. The one-step mechanism assumes that the reaction products are CO_2 and H_2O, the total heat of reaction is overpredicted. In the actual situation, some CO and H_2 exist in the combustion products with CO_2 and H_2O. This lowers the total heat of reaction and decreases the flame temperature. The six-step mechanism includes CO and H_2, so we can get more detailed chemical species distribution. But in the six-step mechanism, more reaction equations are computed, then more CPU time is spent and more difficult it is to convergence. In our examples, for one-step and six-step, the numbers of iterations are respectively 626 and 5502.

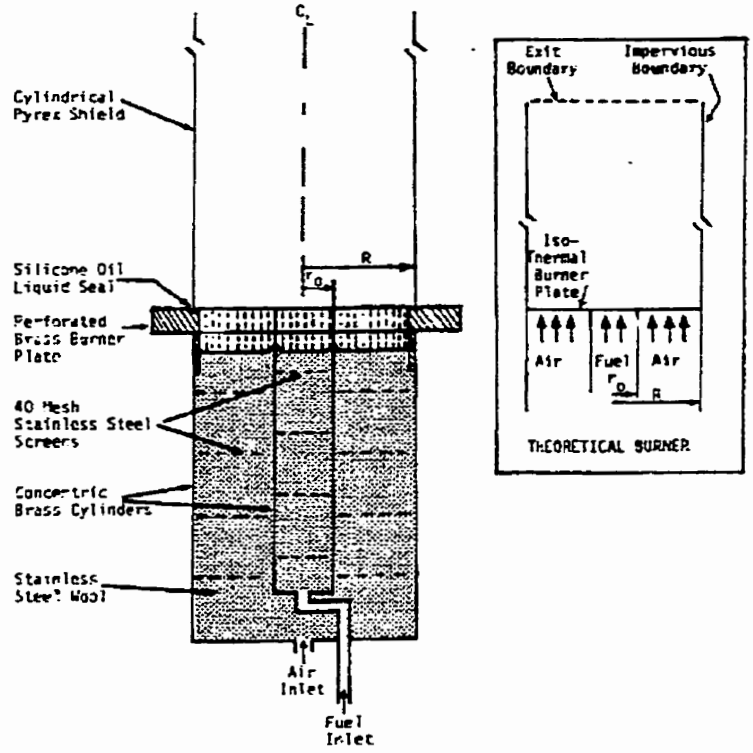

Figure 7.1 Schematic of laboratory burner (Mitchell, 1980)

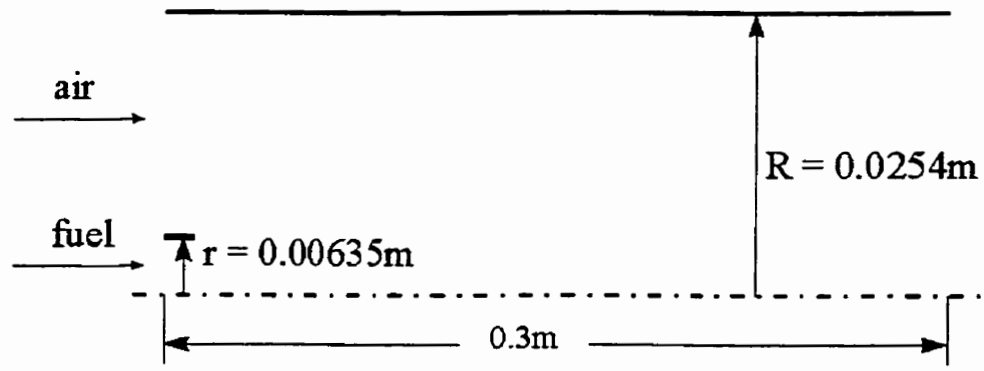

Figure 7.2 Burner Geometry

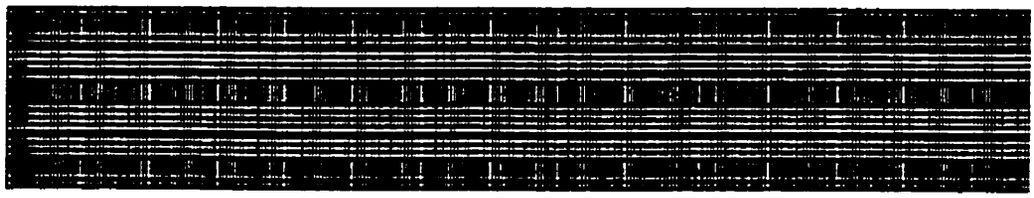

Figure 7.3 The structured grid

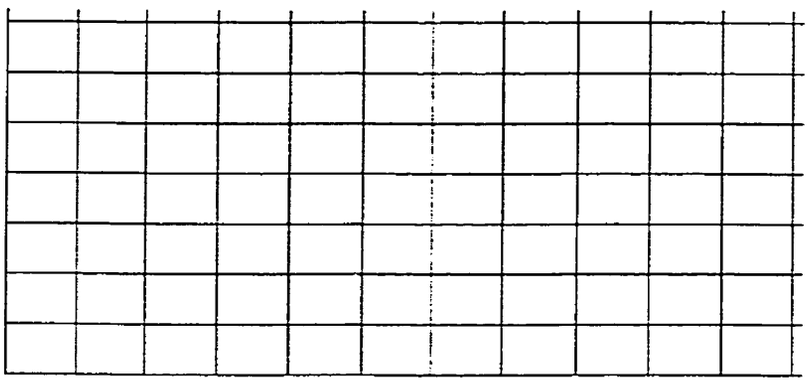

Figure 7.4 Detailed grid

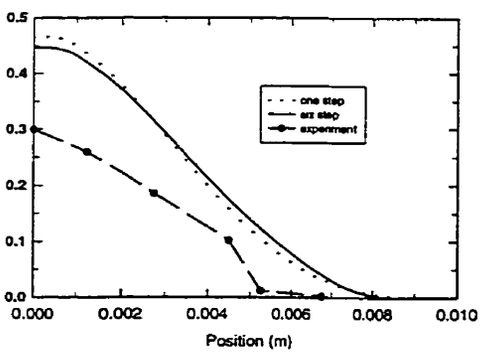

(1.2 cm)

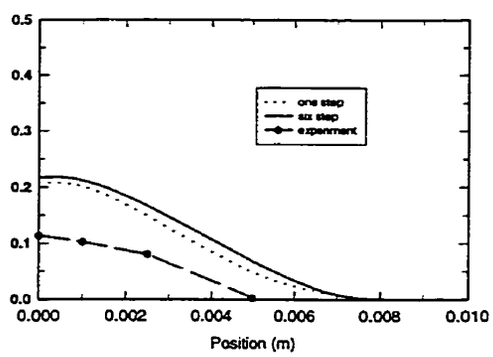

(2.4 cm)

Figure 7.5 Radial CH_4 mole fraction profiles at several axial locations

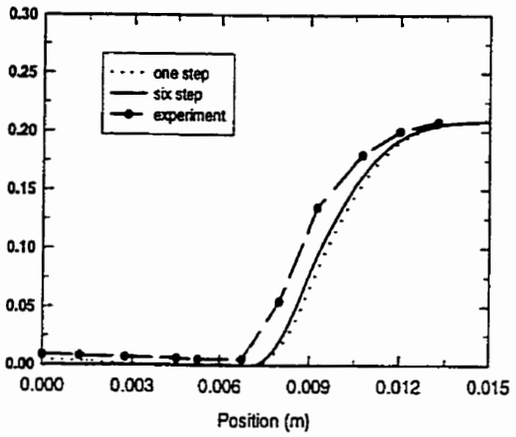

(1.2 cm)

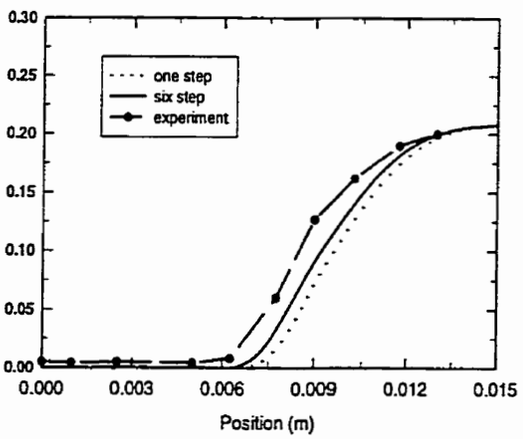

(2.4 cm)

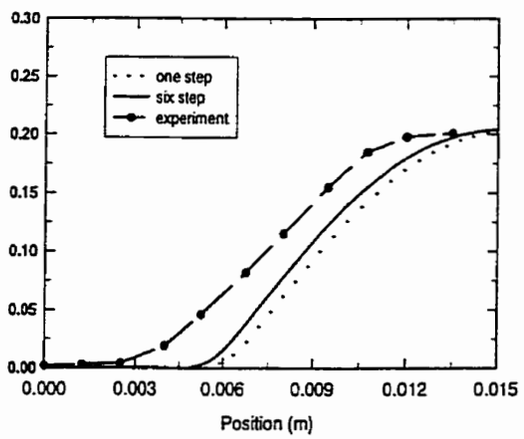

(5 cm)

Figure 7.6 Radial O_2 mole fraction profiles at several axial locations

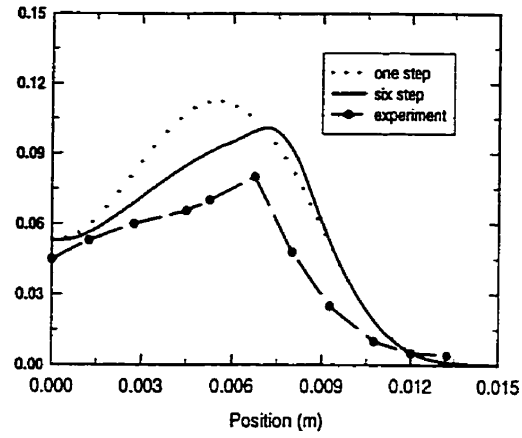

(1.2 cm)

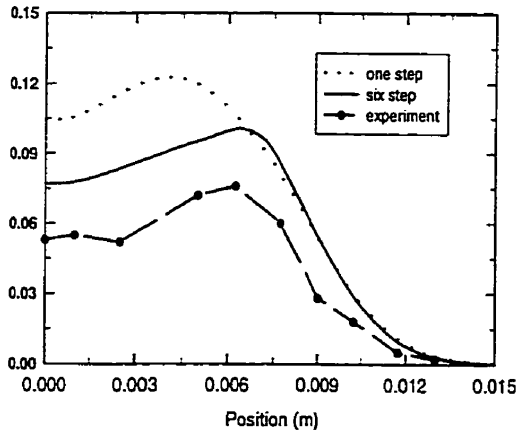

(2.4 cm)

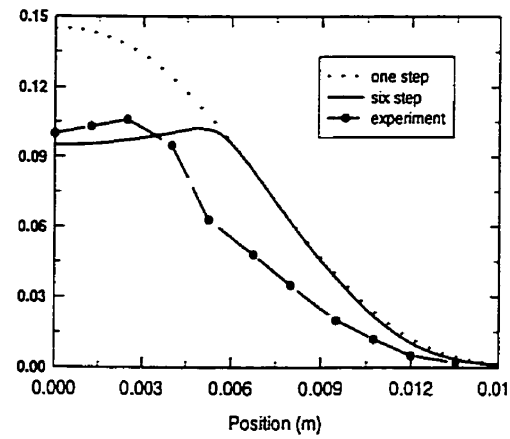

(5 cm)

Figure 7.7 Radial CO_2 mole fraction profiles at several axial locations

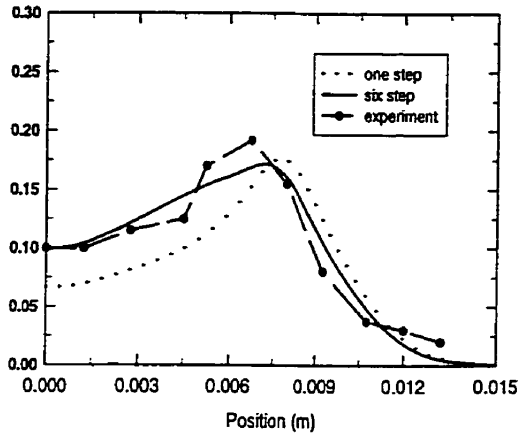

(1.2 cm)

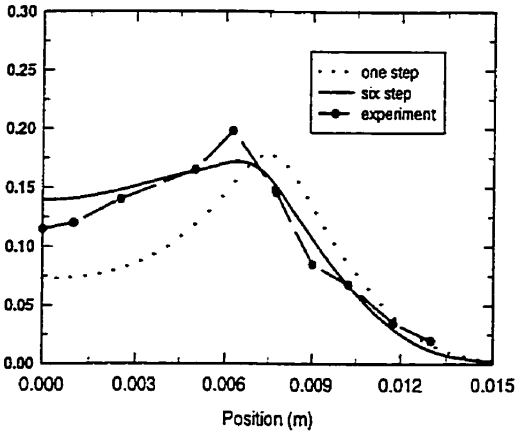

(2.4 cm)

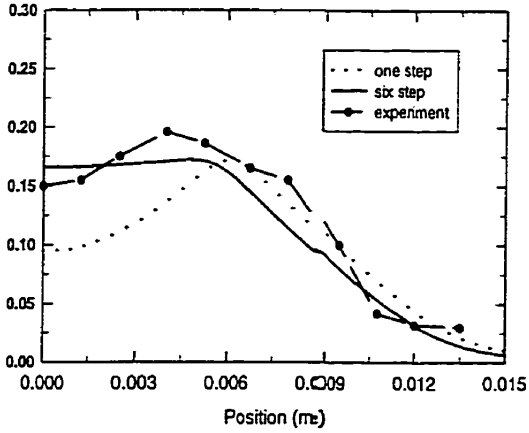

(5 cm)

Figure 7.8 Radial H_2O mole fraction profiles at several axial locations

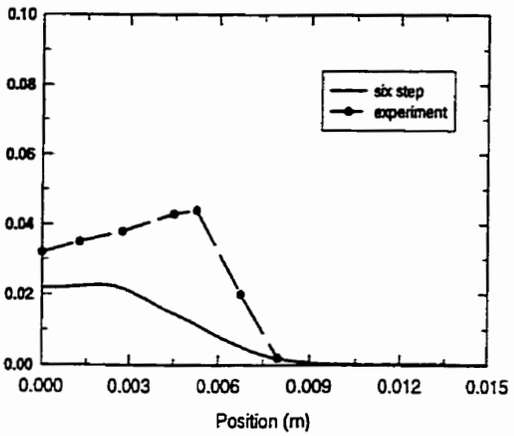

(1.2 cm)

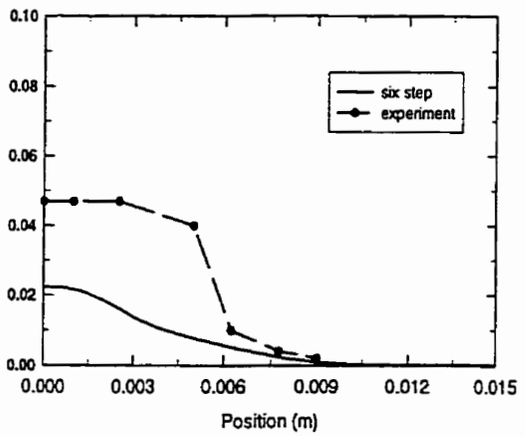

(2.4 cm)

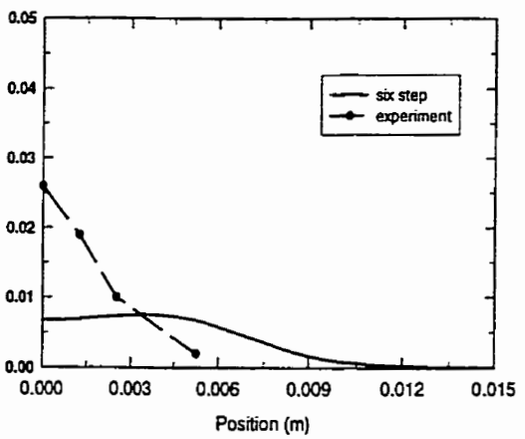

(5 cm)

Figure 7.9 Radial CO mole fraction profiles at several axial locations

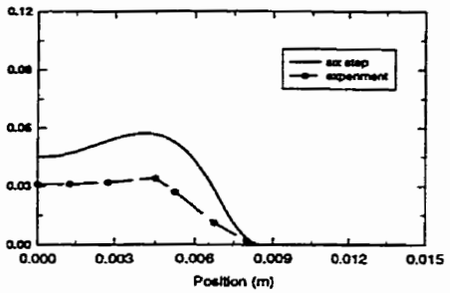

(1.2 cm)

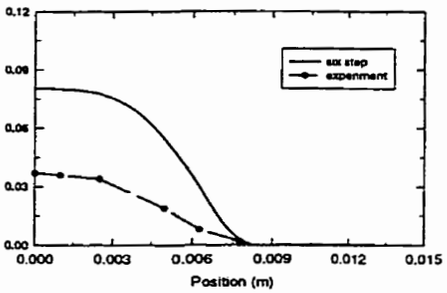

(2.4 cm)

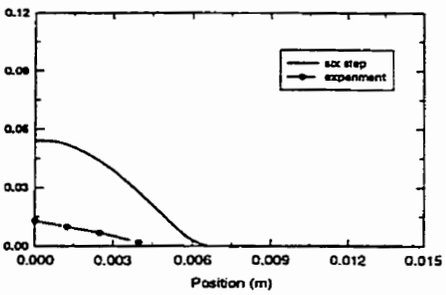

(5 cm)

Figure 7.10 Radial H_2 mole fraction profiles at several axial locations

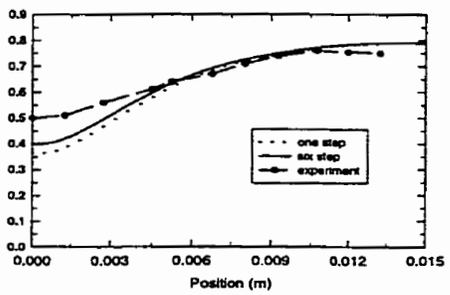

Figure 7.11 Radial profiles of N_2 mole fraction at 1.2 cm

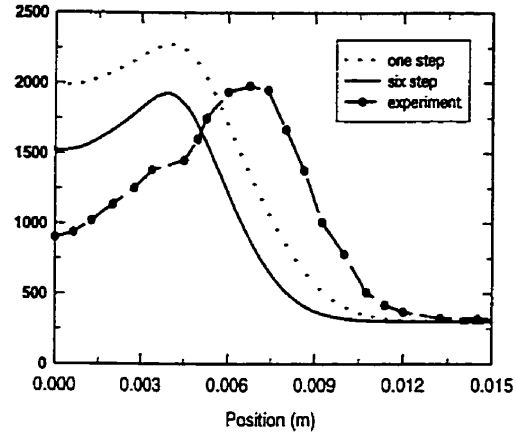

(1.2 cm)

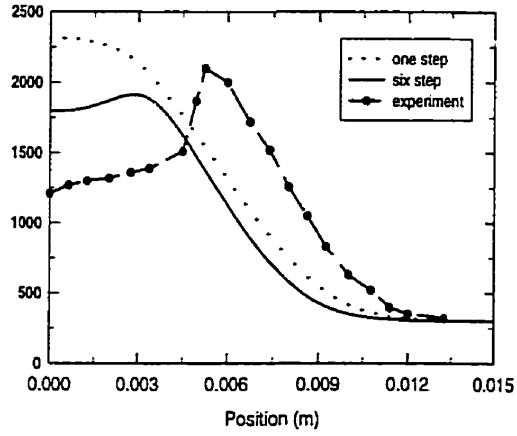

(2.4 cm)

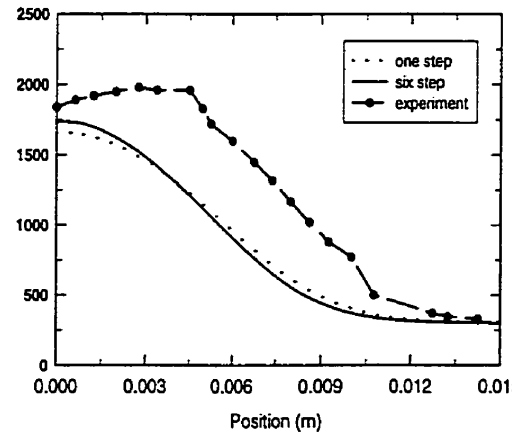

(5 cm)

Figure 7.12 Radial temperature profiles at several axial locations

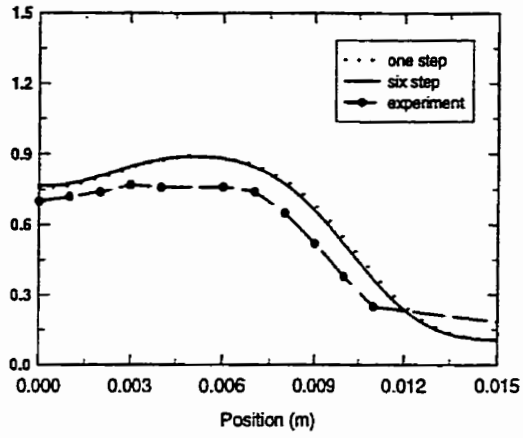

(1.2 cm)

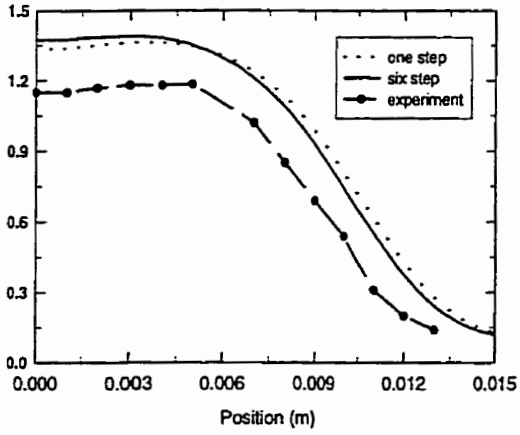

(2.4 cm)

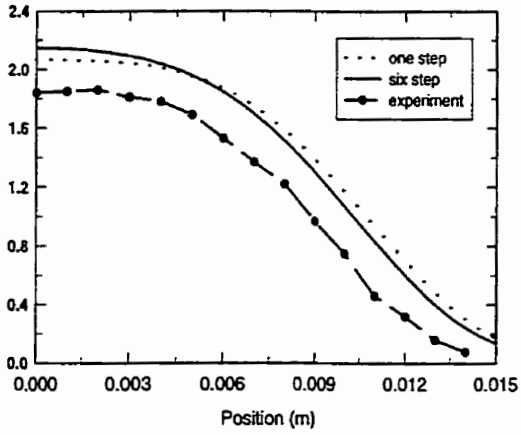

(5 cm)

Figure 7.13 Radial velocity profiles at several axial locations

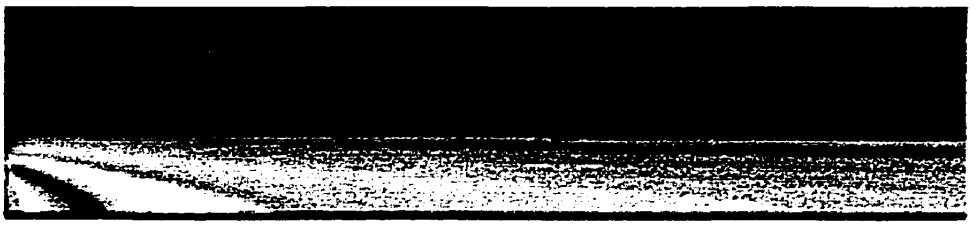

Figure 7.14 Temperature field for the one-step reaction

Figure 7.15 The core of temperature field, T_{max}=2326K, one-step

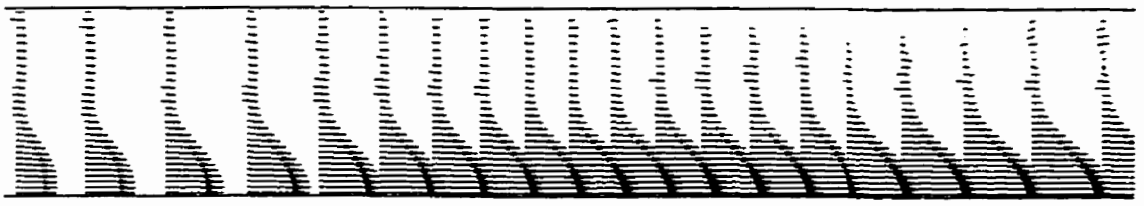

Figure 7.16 Velocity field for the one-step reaction

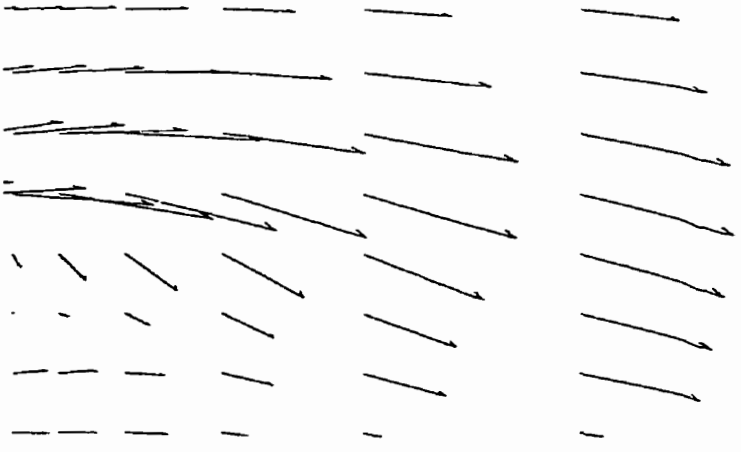

Figure 7.17 The detailed part of velocity field, one-step

Figure 7.18 Temperature field for the six-step reaction

Figure 7.19 The core of temperature field, T_{max}=1942K, six-step

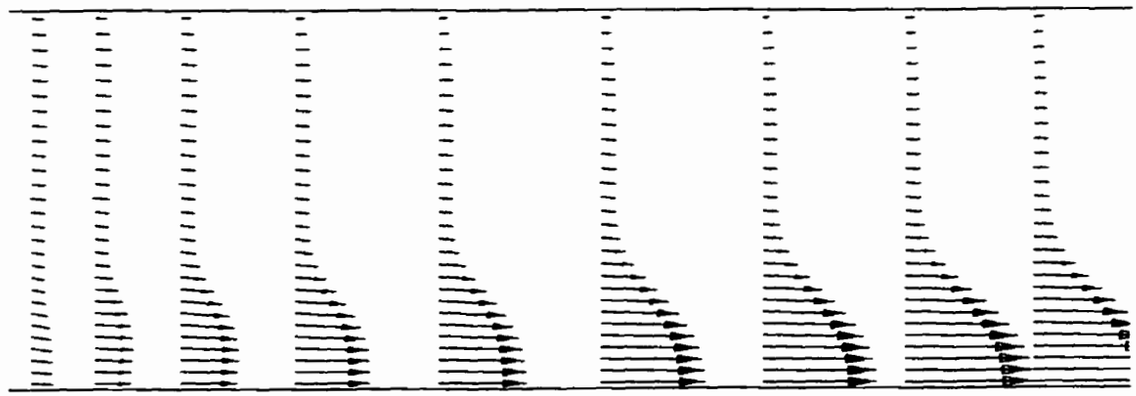

Figure 7.20 Velocity field for the six-step reaction

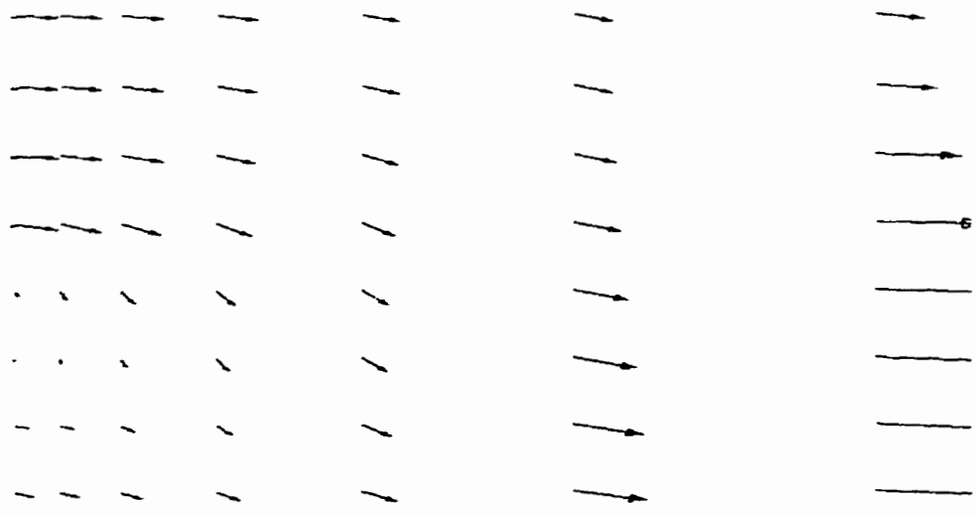

Figure 7.21 The detailed part for the velocity field, six-step

7.2 Unstructured Grid

7.2.1 Problem Description

In this section, we will compare the results of structured and unstructured grids with the same example as in Section 7.1. Both methods use the six-step chemical reaction model. Figures 7.22 and 7.23 show the geometry and the unstructured mesh which involves 2337 nodes. In comparison, there are 9000 nodes in the structured mesh. This is because a triangular mesh allows cells to be clustered in selected regions of the flow domain, whereas structured quadrilateral meshes will generally force cells to be placed in regions where they are not needed. So a triangular mesh can often be created with far fewer cells than the equivalent mesh consisting of quadrilateral elements.

7.2.2 Comparison with Structured Grid

From Figure 7.24, the comparison with the CH_4 experimental result shows that the unstructured and structured methods overpredict the CH_4 profile. It can be seen that the unstructured method is better. Similarly, on the predicted O_2 distribution along the radial direction, the magnitude of both methods has the same qualitative trends as the experimental data (Figure 7.25). But the structured grid is closer to experiment. The comparisons of CO_2 and H_2O are given in Figures 7.26 and 7.27. It is seen that the structured result is slightly better than the unstructured one. In Figures 7.28-7.29, the predicted radial profiles of CO and H_2 are compared with the test data. It is noted that at 1.2 cm, the maximum temperature location for the unstructured is slightly closer to the experimental result (Figure 7.30). It is shown that the velocity follows the trend of the test data (Figure 7.31). Figures 7.32-7.33 show the temperature distribution for the unstructured method. In general, the results with the structured and unstructured grids are a bit different, maybe it causes this difference that different nodes are used.

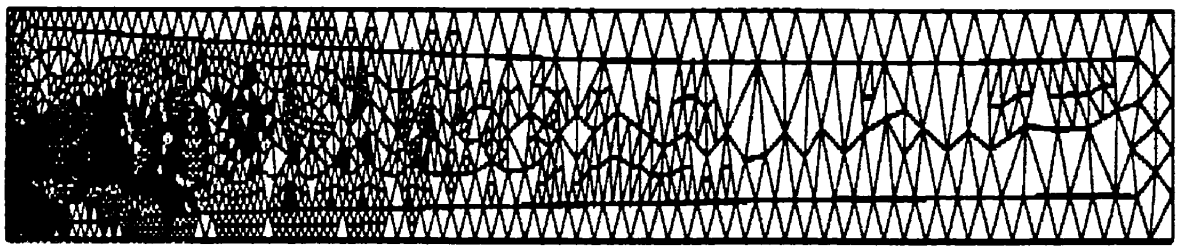

Figure 7.22 The unstructured grid

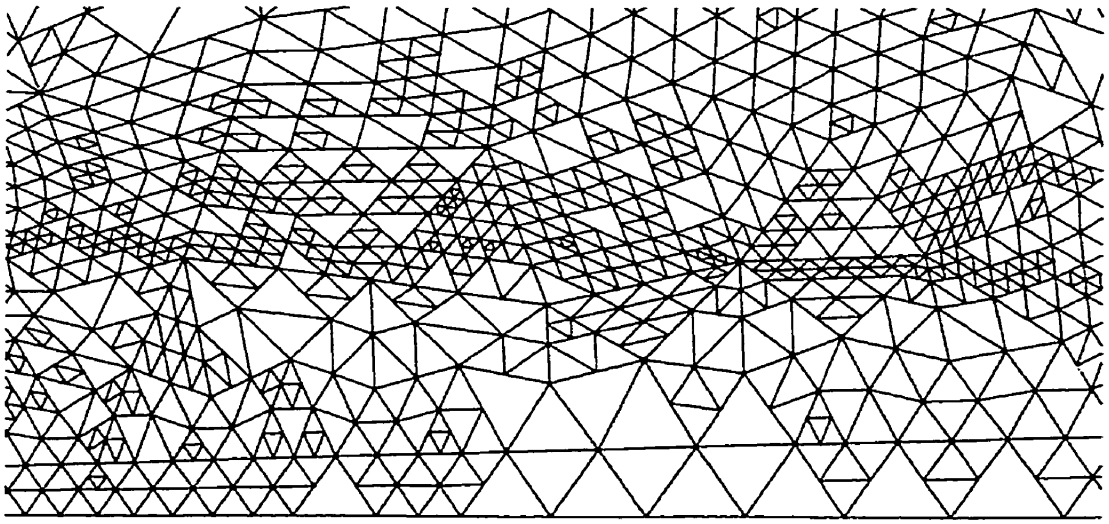

Figure 7.23 The detailed part for the grid

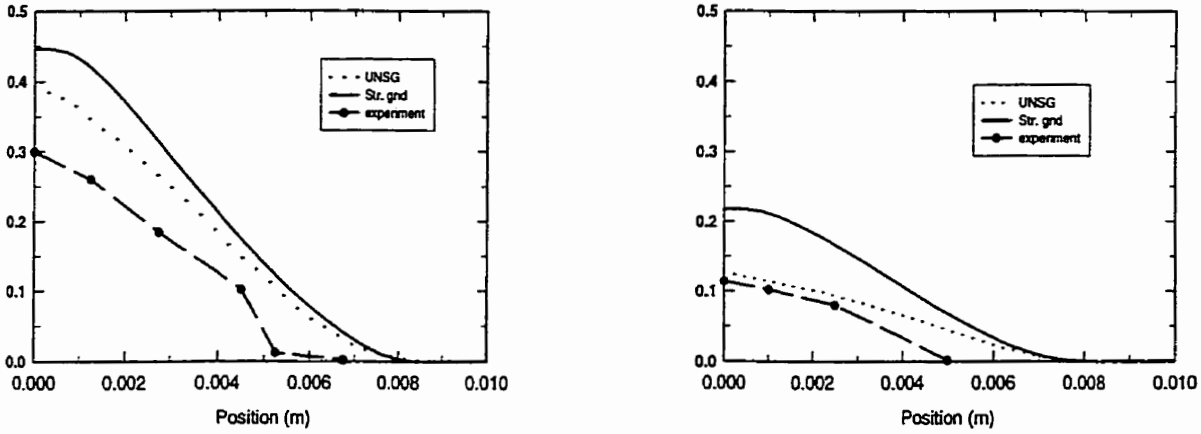

(1.2 cm) (2.4 cm)

Figure 7.24 Radial CH_4 mole fraction profiles at several axial locations

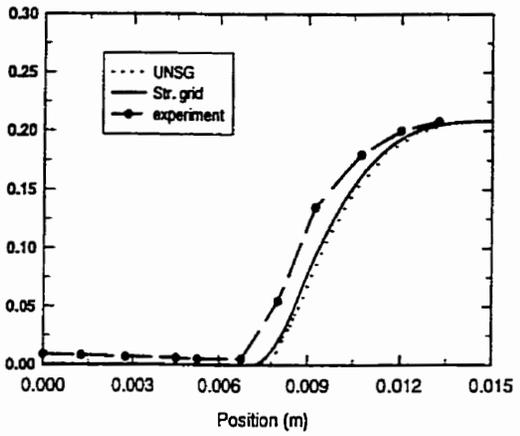

(1.2 cm)

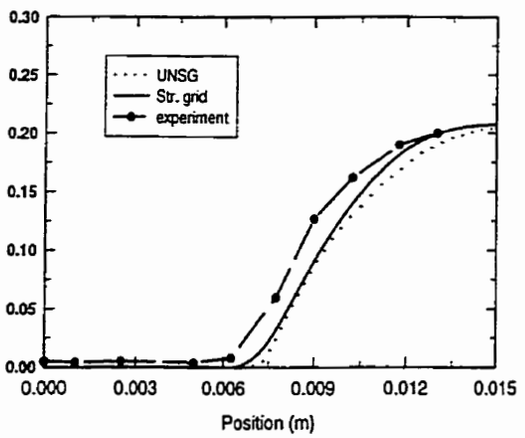

(2.4 cm)

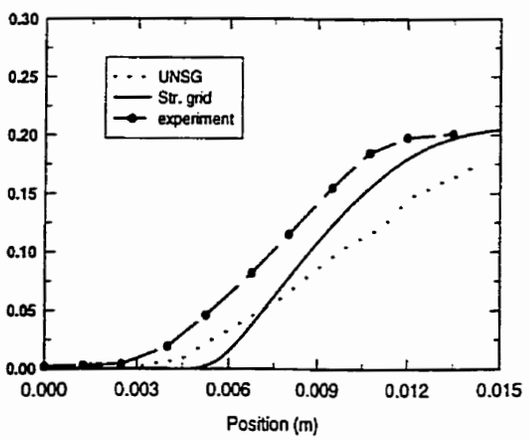

(5 cm)

Figure 7.25 Radial O_2 mole fraction profiles at several axial locations

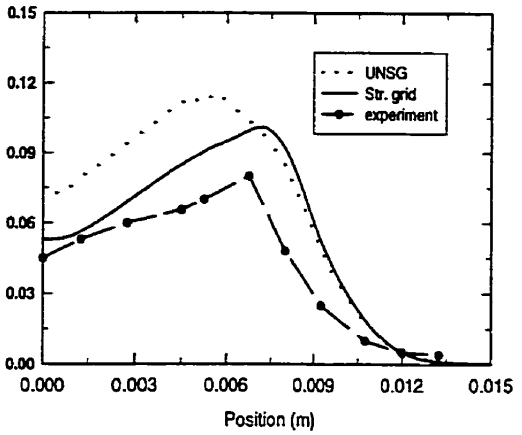

(1.2 cm)

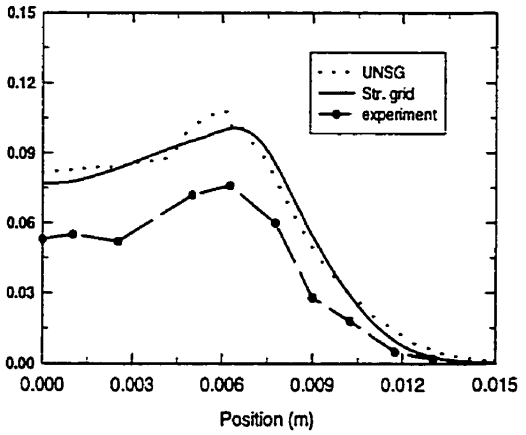

(2.4 cm)

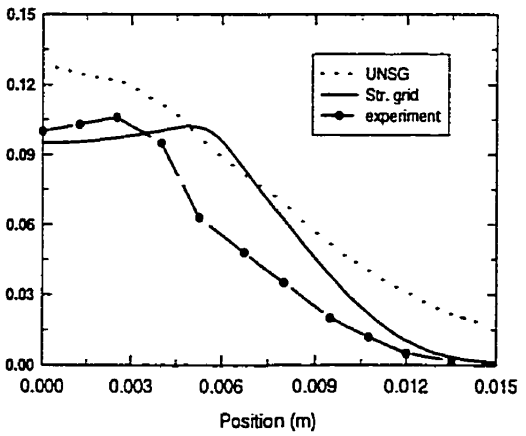

(5 cm)

Figure 7.26 Radial CO_2 mole fraction profiles at several axial locations

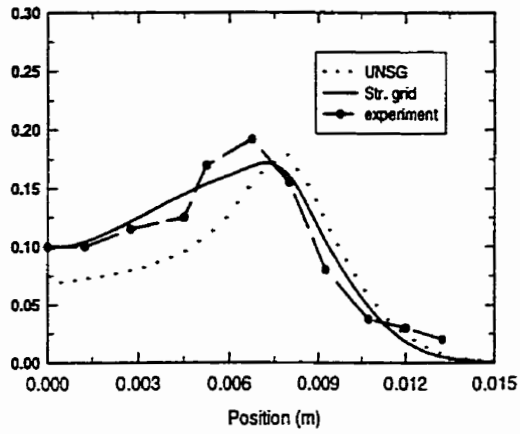

(1.2 cm)

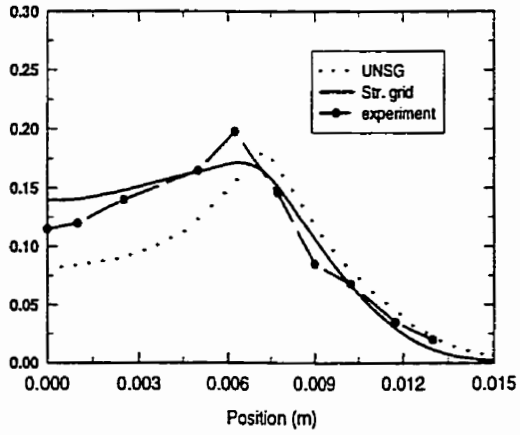

(2.4 cm)

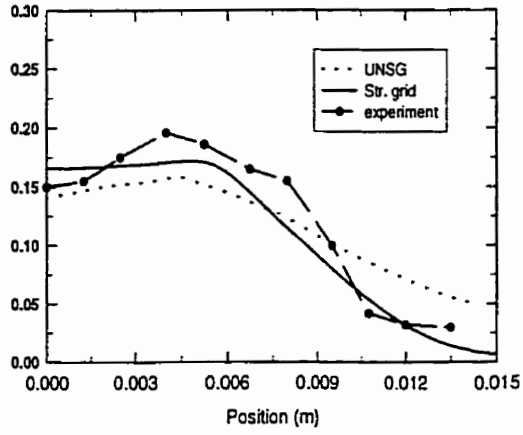

(5 cm)

Figure 7.27 Radial H_2O mole fraction profiles at several axial locations

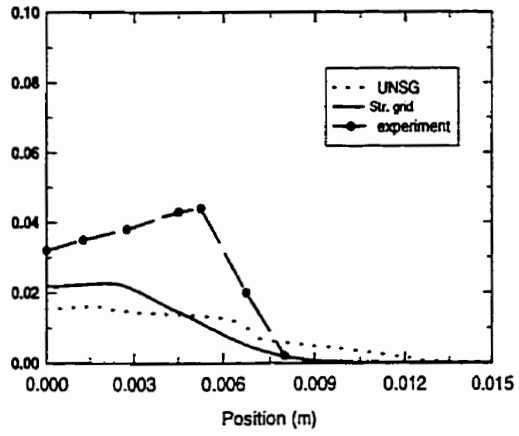

(1.2 cm)

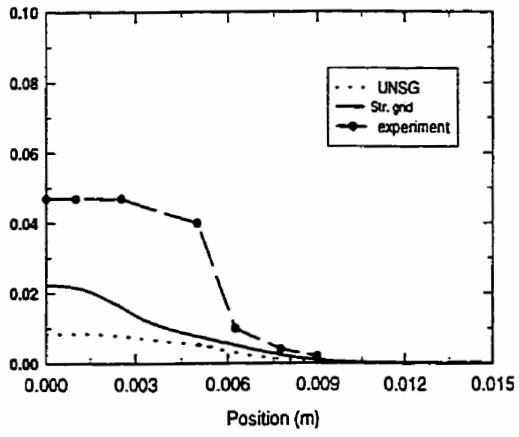

(2.4 cm)

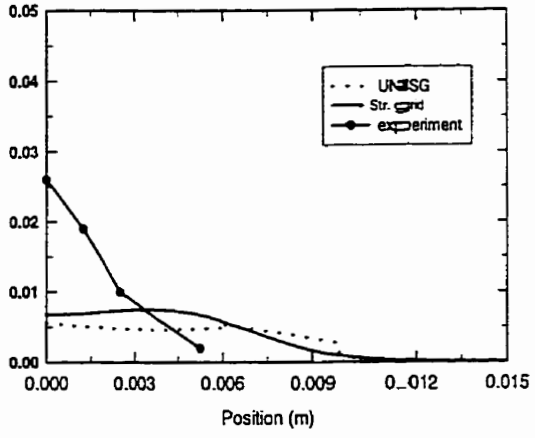

(5 cm)

Figure 7.28 Radial CO mole fraction profiles at several axial locations

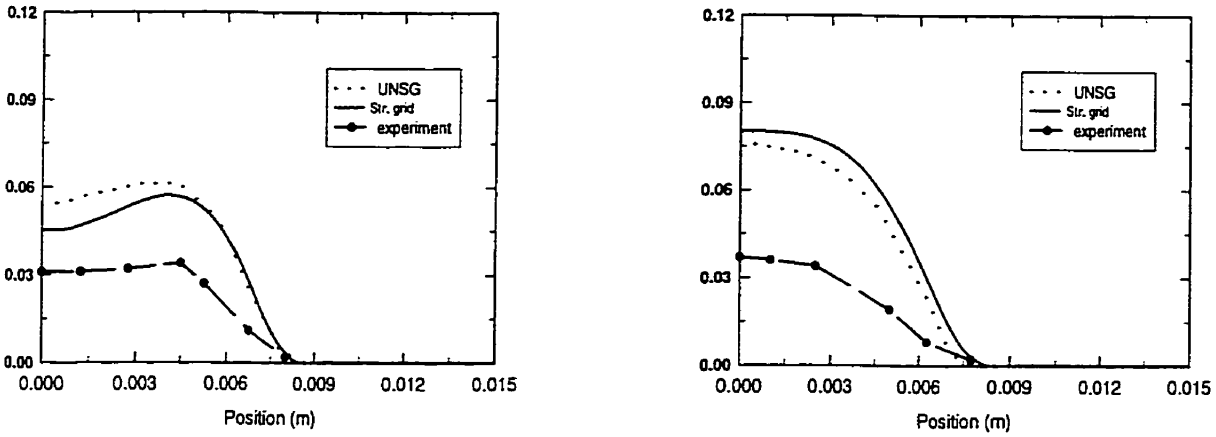

(1.2 cm) (2.4 cm)

Figure 7.29 Radial H_2 mole fraction profiles at several axial locations

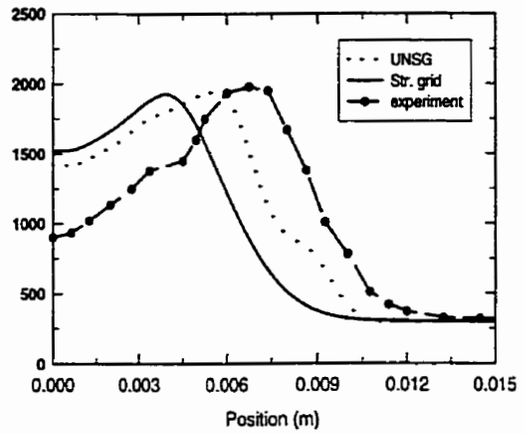

(1.2 cm)

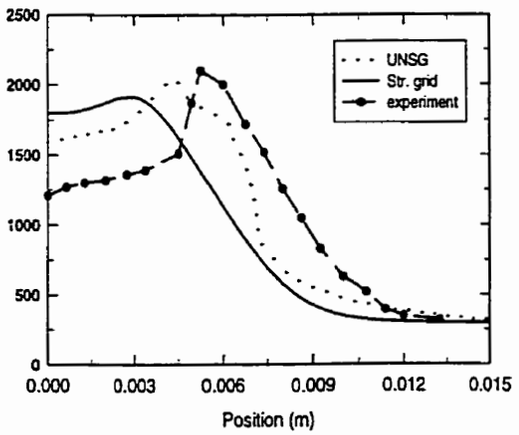

(2.4 cm)

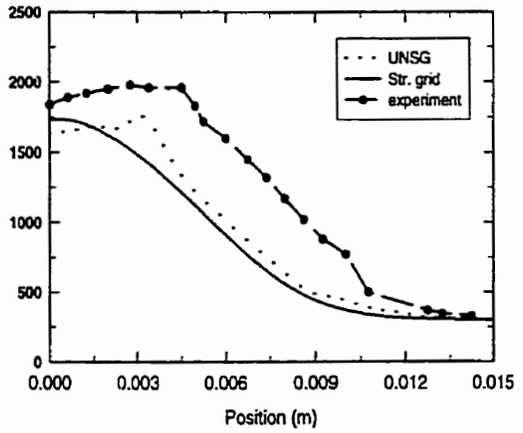

(5 cm)

Figure 7.30 Radial temperature profiles at several axial locations

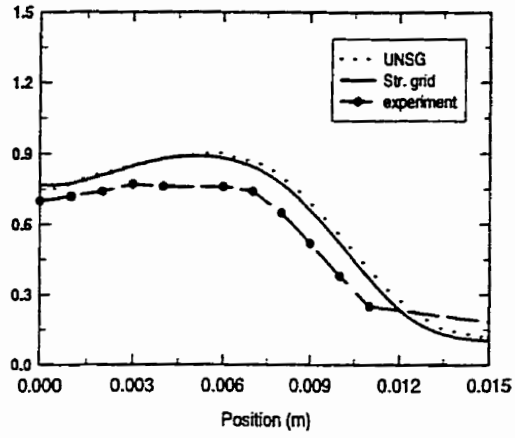

(1.2 cm)

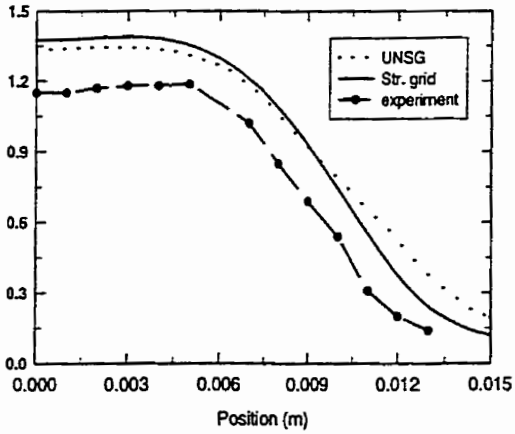

(2.4 cm)

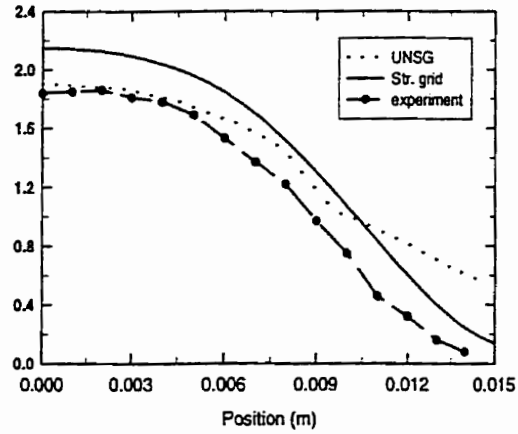

(5 cm)

Figure 7.31 Radial velocity profiles at several axial locations

Figure 7.32 Temperature field for the unstructured grid calculation

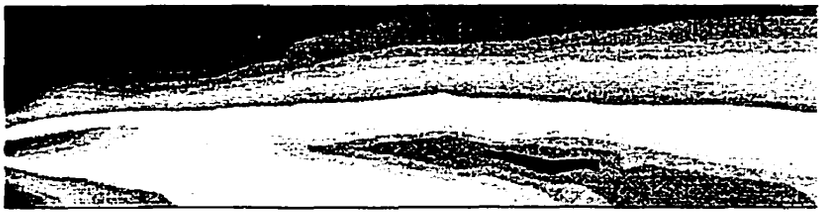

Figure 7.33 The core of temperature field, T_{max}=1930K

7.3 Turbulent Combustion

7.3.1 Problem Description

The test facility is shown in Figure 7.34. The combustor was oriented vertically to minimize three-dimensional effects. The geometry for this test is a cylindrical combustor with coaxial injectors, where the natural gas is injected by the primary tube and the air through the secondary annulus, as shown in Figure 7.35. The total pressure of the combustor is 94 kPa. In the fuel stream, the uniform inlet gas velocity is 21.3 m/s and the flow rate is 2.982 g/s, with a temperature of 300 K. In the air stream, the uniform inlet air velocity is 29.9 m/s and the flow rate is 36.3 g/s, with a preheated temperature of 589 K. The detailed test conditions to specify boundary are given in Table 7.2. The compositions of fuel and air are shown in Tables 7.3 and 7.4.

Inlet parameters	Air	Natural gas
Temperature (K)	589	300
Pressure (kPa)	94	94
M (kg/kmol)	28.9534	18.8766
ρ(kg/m^3)	0.48634	0.7114
r (m)	0.0286	0.008
$\dot{m}$ (kg/s)	0.0363	0.002982
Velocity (m/s)	29.9	21.3

Table 7.2 The summary for the test conditions at the inlet of the combustor

	Mole fraction	Mass fraction
CH_4	0.84314	0.71857
C_2H_6	0.070857	0.11319
N_2	0.024286	0.036142
CO_2	0.013238	0.030951
H_2	0.00085714	9.1793E-05
Ar	0.047619	0.10106

Table 7.3 The fuel composition

	Mole fraction	Mass fraction
N_2	0.7827	0.75729
O_2	0.208	0.22988
Ar	0.0093	0.01283

Table 7.4 The air composition

The available experimental measurements for the natural gas combustion have been carried out by Lewis and Smoot (1981) together with the numerical predictions of Smith and Smoot (1981) using the chemical equilibrium combustion model with a finite difference method. Nikjooy et al. (1988) have used the fast chemistry reaction model and the finite-rate chemistry model with the finite volume method, Elkaim et al. (1993) and McKenty et al. (1993) with the fast chemistry, PDF, eddy dissipation, chemical equilibrium and micro-flame models with CVFEM, Meng (1994) has used the classical approximation method and the direct iteration method with four combustion models, i.e. fast chemistry, eddy dissipation, chemical equilibrium and micro-flame model with SCVFEM.

In the present computation, a basic scheme is first built and named as "standard" to compare with other ones. The steady-state, Reynolds averaged Navier-Stokes

equations for mass, momentum, energy and scalar transport are used to describe the flow physics. The density is obtained from the ideal gas law. The reaction rates are computed by finite-rate/eddy-dissipation, i.e. for turbulent flows, both the Arrhenius rate and the mixing rate are computed and the smaller of the two is used. The standard $k-\varepsilon$ turbulence closure model is adopted. The specific heat values for the species are defined as piecewise-polynomial function of temperature. The eight chemical reaction equations are (Hyer, 1991):

$$CH_4 + \tfrac{1}{2}\, O_2 \rightarrow CO + 2H_2 \tag{7.10}$$

$$CH_4 + H_2O \rightarrow CO + 3H_2 \tag{7.11}$$

$$CO + H_2O \rightarrow CO_2 + H_2 \tag{7.12}$$

$$CO_2 + H_2 \rightarrow CO + H_2O \tag{7.13}$$

$$H_2 + \tfrac{1}{2}\, O_2 \rightarrow H_2O \tag{7.14}$$

$$H_2O \rightarrow H_2 + \tfrac{1}{2}\, O_2 \tag{7.15}$$

$$C_2H_6 + O_2 \rightarrow 2CO + 3H_2 \tag{7.16}$$

$$C_2H_6 + 2H_2O \rightarrow 2CO + 5H_2 \tag{7.17}$$

The coefficients (Hyer, 1991) for the Arrhenius rate are as shown in Table 7.5.

No. of Eq.	Pre-expo. Factor	Acti. Energy	Temp. Expo.
7.10	4.4e+09	1.26e+08	0
7.11	3.0e+08	1.26e+08	0
7.12	2.75e+10	8.37e+07	0
7.13	9.62e+10	1.26e+08	-0.85
7.14	7.45e+13	1.67e+08	-0.91
7.15	3.83e+14	4.12e+08	-1.05
7.16	4.2e+11	1.256e+08	0
7.17	3.0e+08	1.256e+08	0

Table 7.5 The coefficients of Arrhenius rate in standard computation

The $k-\varepsilon$ model constants are:

$$C_{1\varepsilon} = 1.44, \quad C_{2\varepsilon} = 1.92, \quad C_{\mu} = 0.09, \quad \sigma_{k} = 1.0, \quad \sigma_{\varepsilon} = 1.3$$

These values have been found to work fairly well for a wide range of wall-bounded and free shear flows.

7.3.2 Results

The computational mesh is shown in Figures 7.36 and 7.37. It involves 4014 nodes. The under-relaxation factors are different for different variables varying from 0.15 to 0.5. For example, the energy equation is very difficult to converge, so the factor is taken as 0.25. The inlet turbulent specification method is "intensity and length scale". "Turbulence intensity" is 10% and "Turbulence length scales" are 0.8 cm for fuel and 1.75 cm for air.

Radial composition profiles for CH_4, O_2, CO_2, H_2O, CO and H_2 at several axial locations are shown in Figures 7.38 - 7.43 and the test results of Lewis and Smoot (1981) are also shown. Those figures show that the calculated results are in agree-

ment with experimental data. The error comes from two sides. Firstly, the models include a 2D assumption, while the reaction rate equations and the $\kappa - \varepsilon$ turbulence closure are not perfect. Secondly, test data accuracy is limited. According to Lewis and Smoot (1981), the oxygen atom balance errors ranged from -6% to +13% and the carbon balance errors ranged from -26% to +30%. In brief, the results are reasonable on the whole to use the base for more analysis and comparison with the other models. Figures 7.44 and 7.45 show the temperature contours. For the mixing region near the inlet, the temperature rises quickly. In the latter half of the combustor, the temperature is mostly uniform. The comparison with experiment is in Figure 7.46. In the Lewis paper, the C_2H_6 radial concentration profile is not available. Figure 7.47 shows the calculated C_2H_6 distribution along the radial direction. Figures 7.48 and 7.49 depict the velocity field.

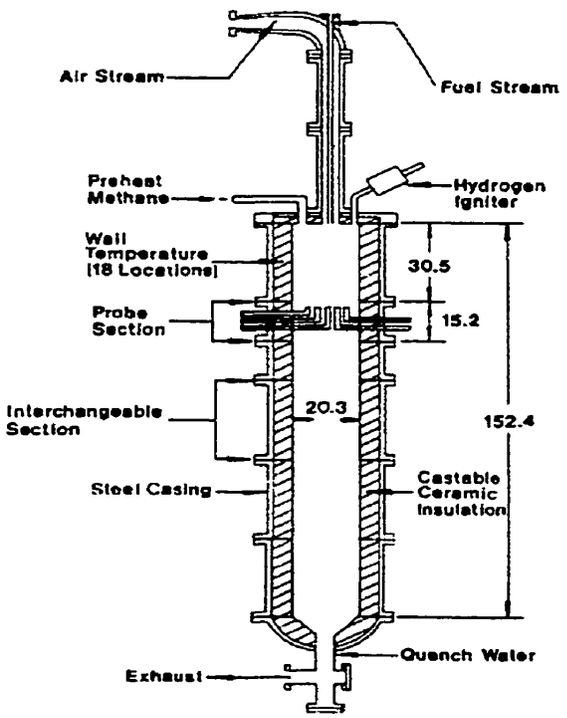

Figure 7.34 Laboratory combustor (Lewis 1981, dimension in cm)

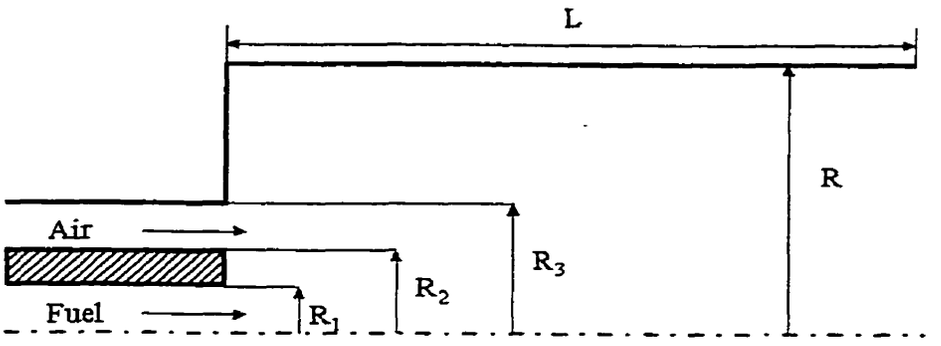

Figure 7.35 Geometry of the coaxial combustor in Lewis (1981)
(R_1 = 0.8cm, R_2 = 1.11cm, R_3 = 2.86cm, R = 10.16cm, L = 1.525m)

Figure 7.36 The computational mesh

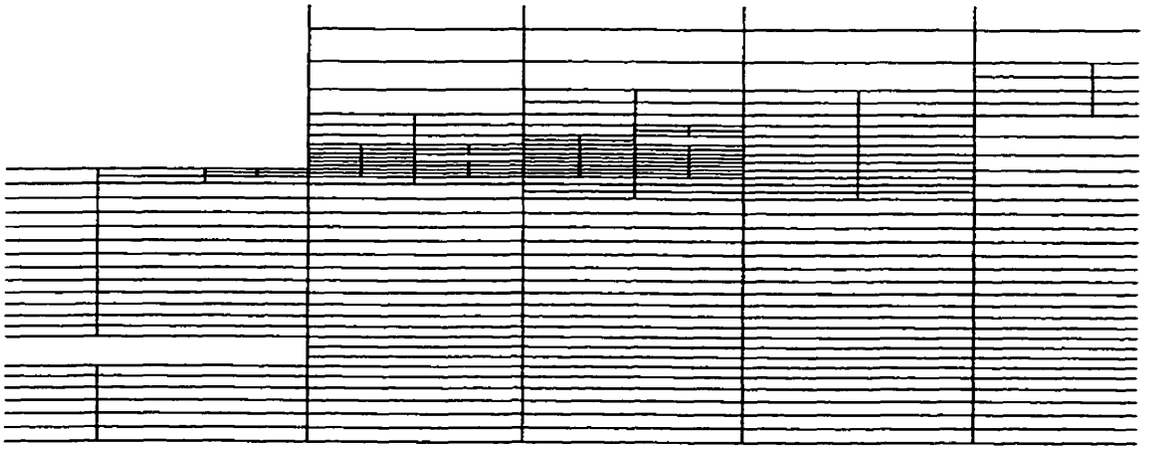

Figure 7.37 The detailed mesh

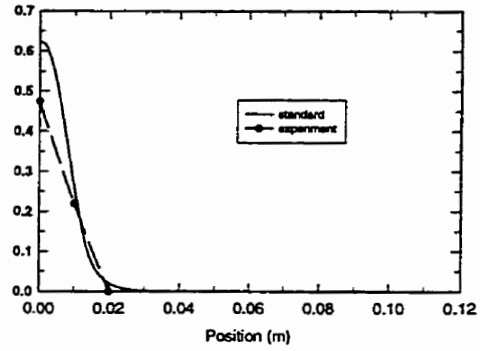

(9.5 cm)

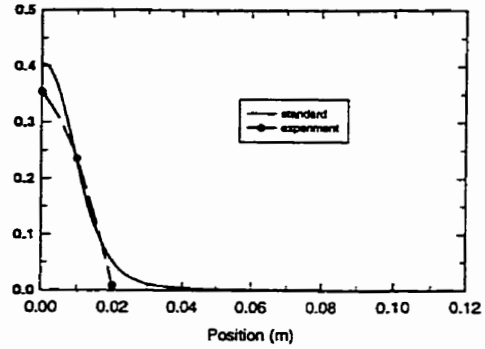

(17.5 cm)

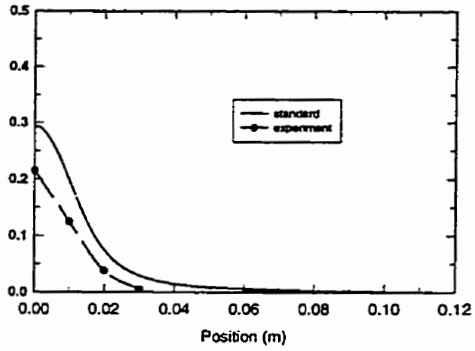

(24.6 cm)

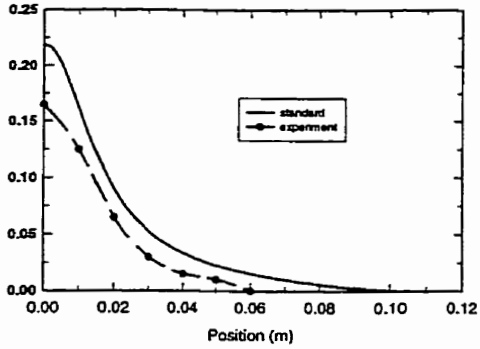

(32.7 cm)

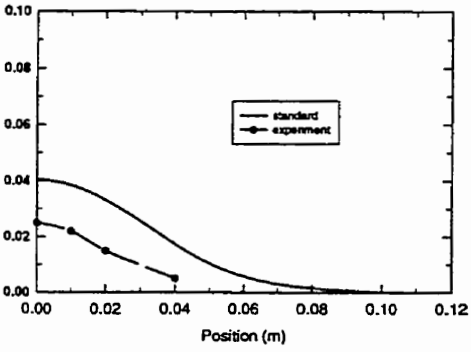

(47.6 cm)

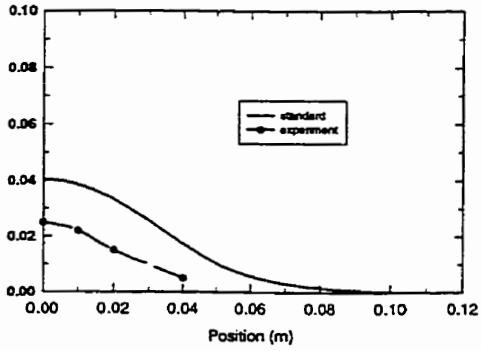

(63.2 cm)

Figure 7.38 Radial profiles CH_4 mole fraction profiles at several axial locations

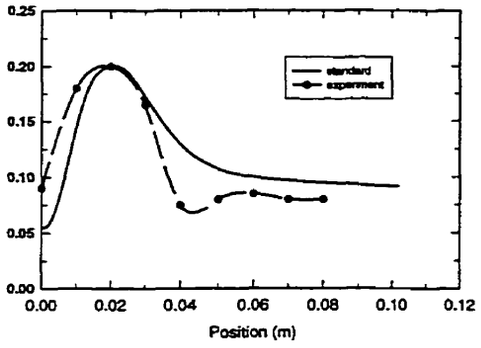

(9.5 cm)

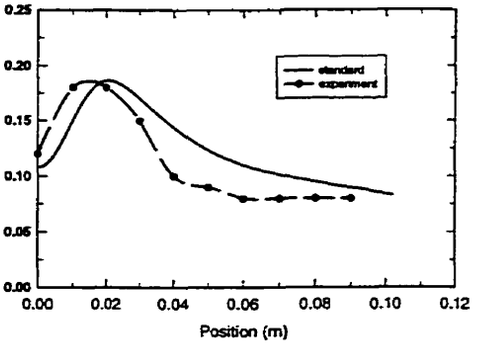

(17.5 cm)

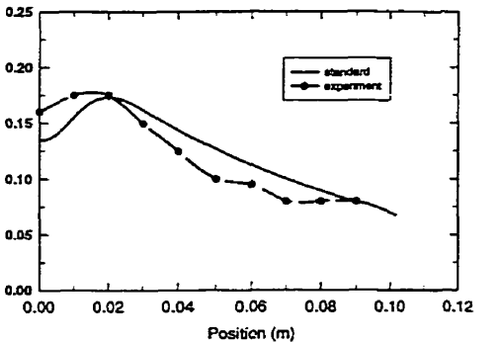

(24.6 cm)

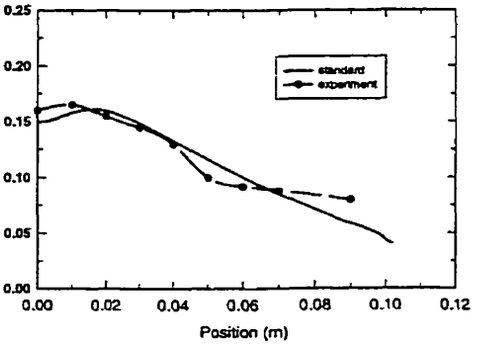

(32.7 cm)

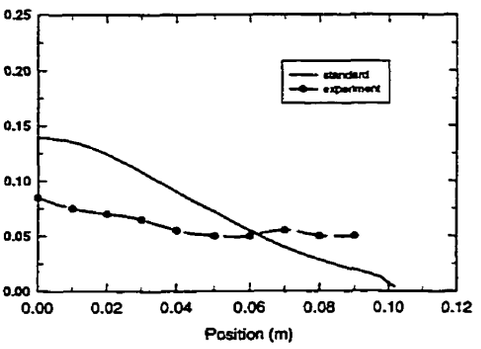

(47.6 cm)

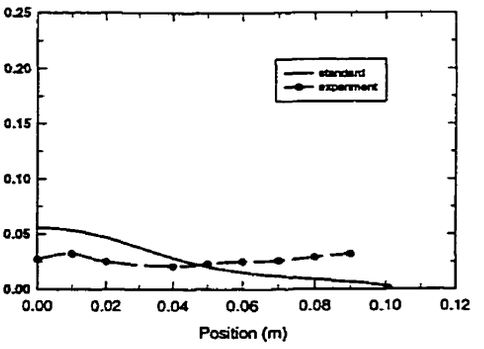

(63.2 cm)

Figure 7.39 Radial O_2 mole fraction profiles at several axial locations

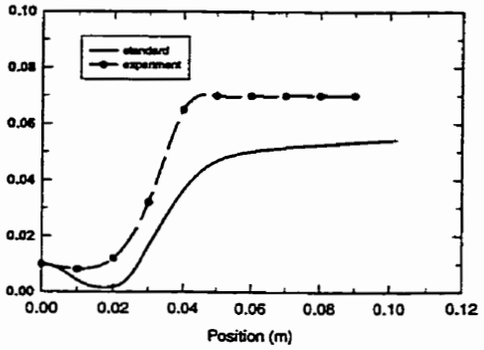

(9.5 cm)

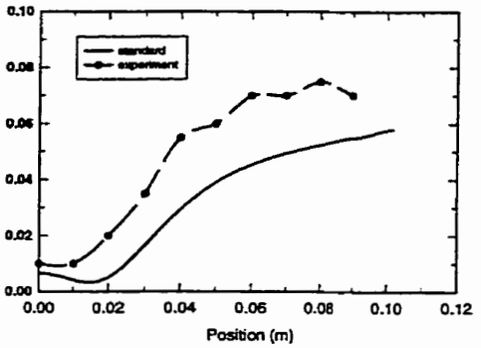

(17.5 cm)

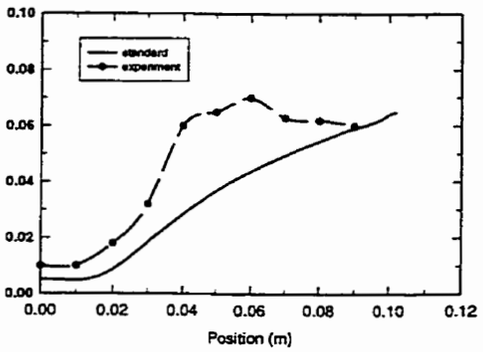

(24.6 cm)

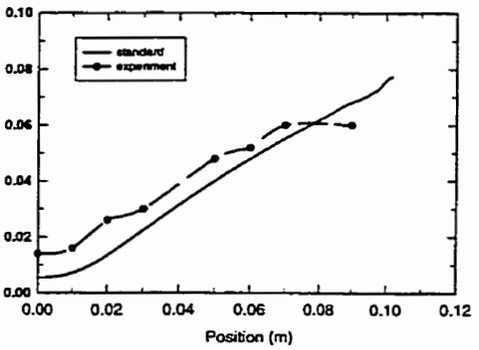

(32.7 cm)

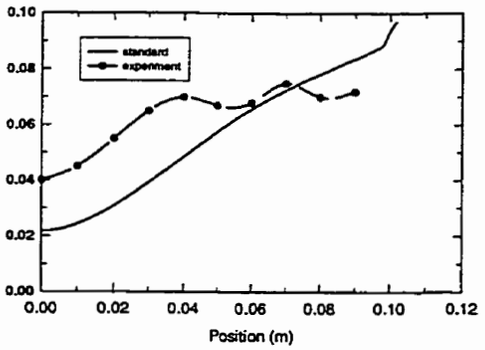

(47.6 cm)

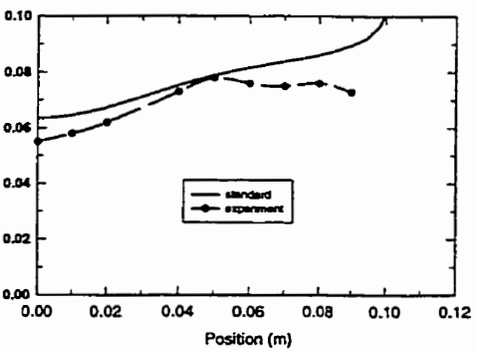

(63.2 cm)

Figure 7.40 Radial CO_2 mole fraction profiles at several axial locations

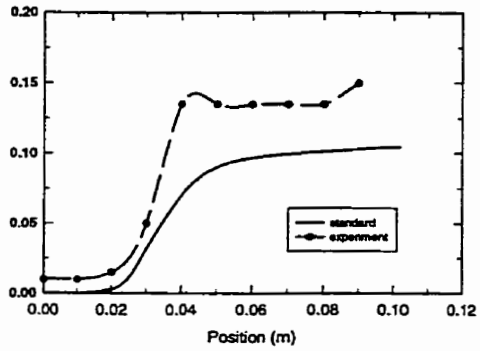

(9.5 cm)

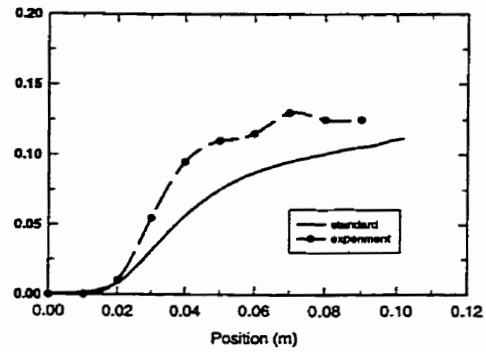

(17.5 cm)

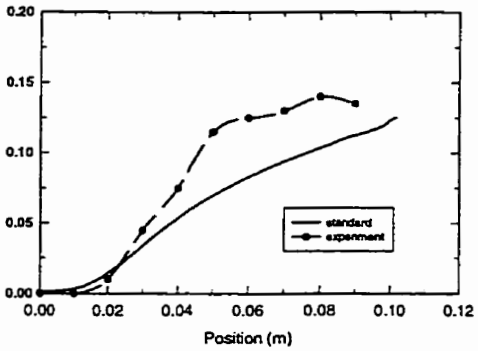

(24.6 cm)

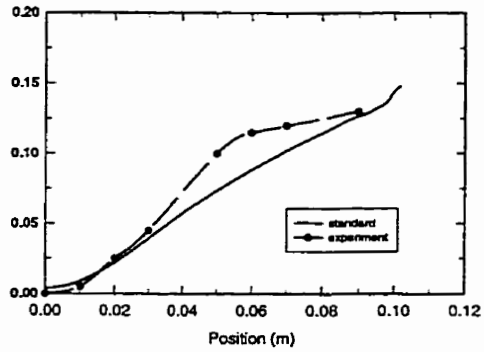

(32.7 cm)

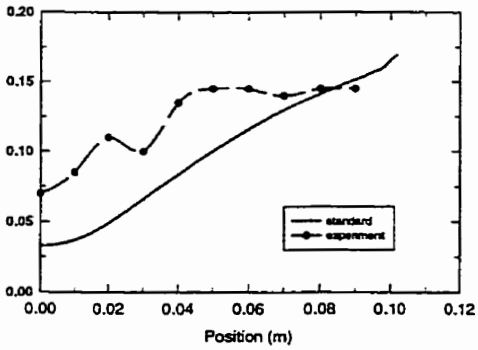

(47.6 cm)

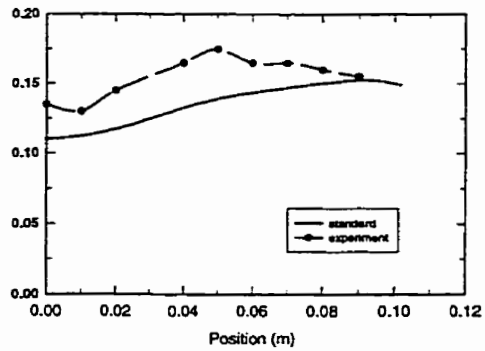

(63.2 cm)

Figure 7.41 Radial H_2O mole fraction profiles at several axial locations

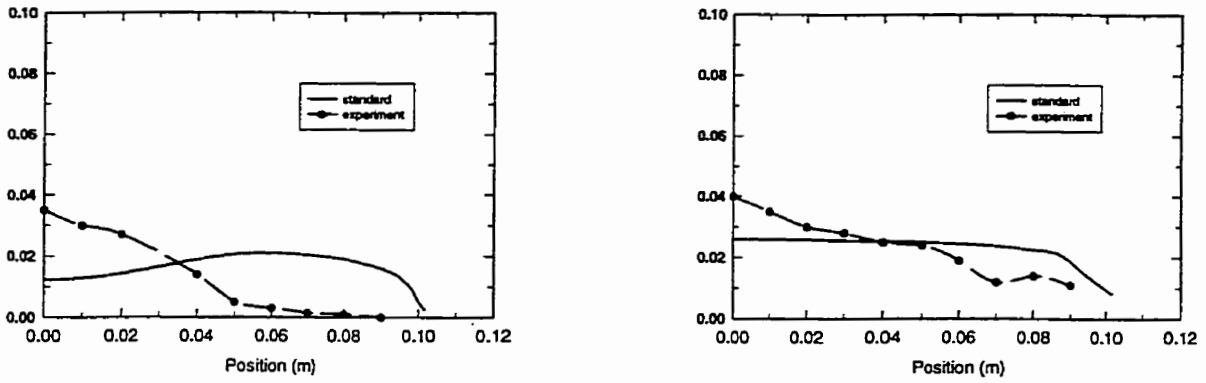

(63.2 cm) (78.5 cm)

Figure 7.42 Radial CO mole fraction profiles at several axial locations

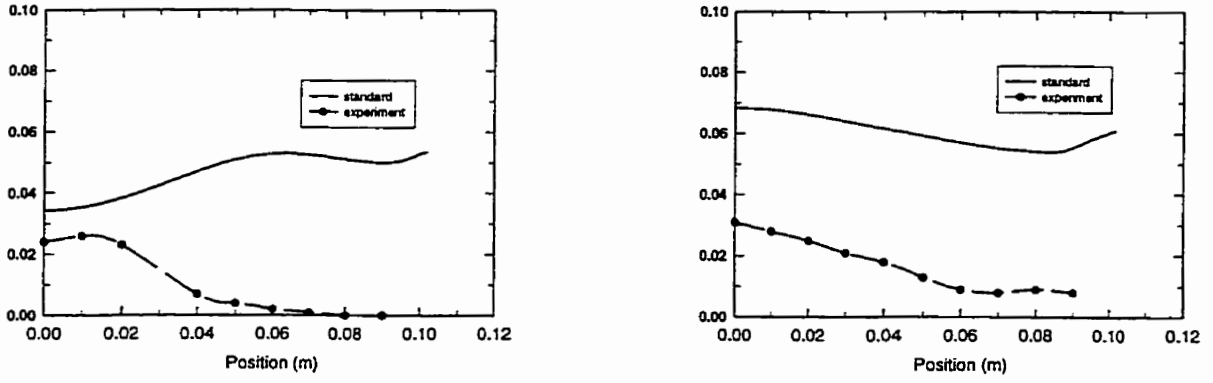

(63.2 cm) (78.5 cm)

Figure 7.43 Radial H_2 mole fraction profiles at several axial locations

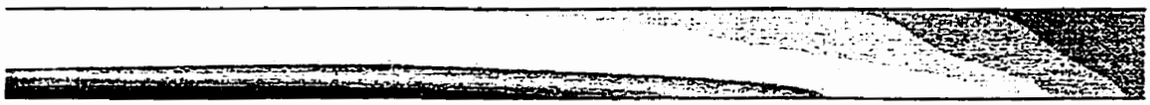

Figure 7.44 Temperature field

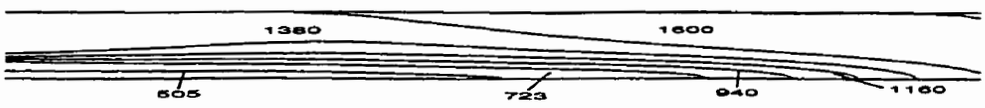

Figure 7.45 Temperature contours (local part)

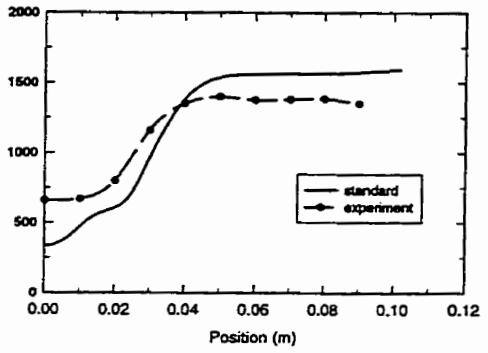

Figure 7.46 Temperature at 9.5 cm

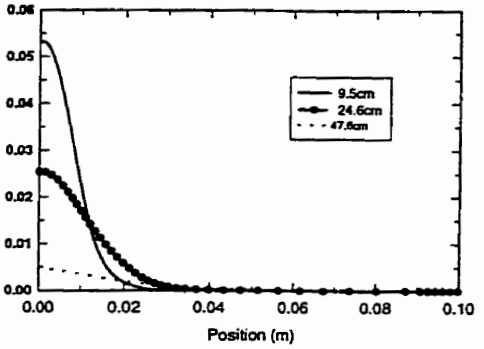

Figure 7.47 C_2H_6 Distribution

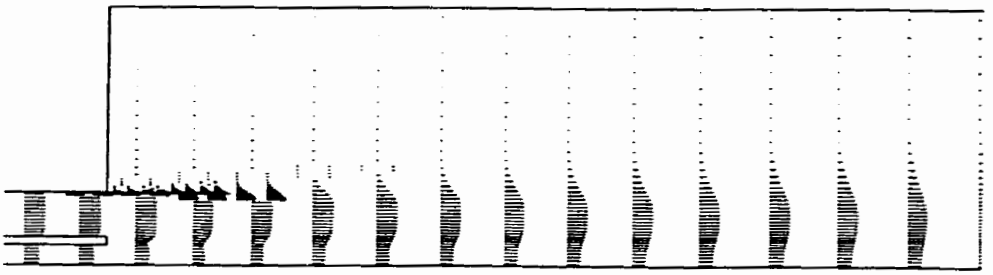

Figure 7.48 The velocity field

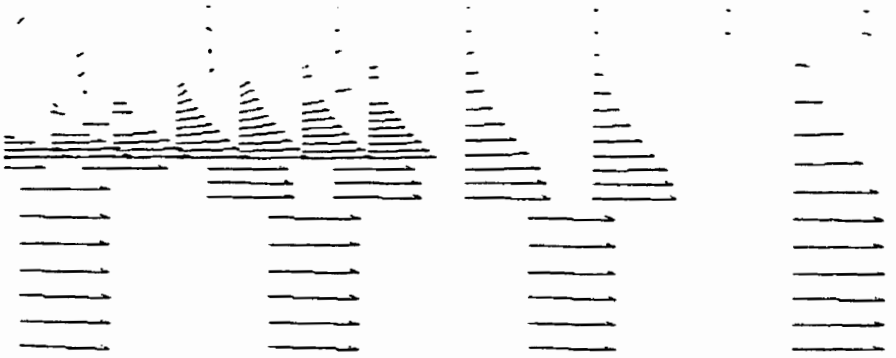

Figure 7.49 The detailed part of velocity field

7.4 The Effect of Turbulence Models

7.4.1 Problem Description

This section shows mainly the effect of the turbulence models. The Reynolds stress model and the large eddy simulation model are selected.

In Reynolds stress model, the pressure-strain term, ϕ_{ij} is modeled. The classical approach to modeling ϕ_{ij} uses the following decomposition:

$$\phi_{i,j} = \phi_{ij,1} + \phi_{ij,2} + \phi_{ij}^{w} \tag{5.53}$$

The slow pressure-strain term, $\phi_{ij,1}$, is modeled as

$$\phi_{ij,1} = -C_1 \rho \frac{\varepsilon}{k} \left[\overline{u_i u_j} - \frac{2}{3} \delta_{ij} k \right] \tag{7.18}$$

with $C_1 = 1.8$.

The rapid pressure-strain term, $\phi_{ij,2}$, is modeled as

$$\phi_{ij,2} = -C_2 \left[(P_{ij} + F_{ij} + G_{ij} - C_{ij}) - \frac{2}{3} \delta_{ij} (P + G - C) \right] \tag{7.19}$$

where $C_2 = 0.60$, P_{ij}, F_{ij}, G_{ij}, and C_{ij} are defined in Equation (4.50), $P = (1/2)P_{kk}$, $G = (1/2)G_{kk}$, and $C = (1/2)C_{kk}$.

The wall-reflection term, ϕ_{ij}^{w} is responsible for the redistribution of the normal stresses near the wall. It tends to dampen the normal stress perpendicular to the wall, while enhancing the stresses parallel to the wall. This term is modeled as

$$\begin{aligned} \phi_{ij}^{w} \equiv\ & C_1' \frac{\varepsilon}{k} \left(\overline{u_k u_m} n_k n_m \delta_{ij} - \frac{3}{2} \overline{u_i u_k} n_j n_k - \frac{3}{2} \overline{u_j u_k} n_i n_k \right) \frac{k^{3/2}}{C_l \varepsilon d} \\ +\ & C_2' \left(\phi_{km,2} n_k n_m \delta_{ij} - \frac{3}{2} \phi_{ik,2} n_j n_k - \frac{3}{2} \phi_{jk,2} n_i n_k \right) \frac{k^{3/2}}{C_l \varepsilon d} \end{aligned} \tag{7.20}$$

where $C_1' = 0.5, C_2' = 0.3$, n_k is the x_k component of the unit normal to the wall, d is the normal distance to the wall, and $C_l = C_m^{3/4}/\kappa$, $C_m = 0.09$ and $\kappa = 0.41$.

The Reynolds stresses at the wall-adjacent cells are computed from

$$\frac{\overline{u_{\tau\tau}'^2}}{k} = 1.098, \quad \frac{\overline{u_\eta'^2}}{k} = 0.247, \quad \frac{\overline{u_\lambda'^2}}{k} = 0.655, \quad -\frac{\overline{u_\tau' u_\lambda'}}{k} = 0.255$$

In LES model, the subgrid-scale turbulent viscosity is modeled by the Smagorinsky-Lilly(1966) model

$$\mu_t = \rho L_s^2 |\overline{S}| \tag{5.62}$$

where L_s is the mixing length for subgrid scales and $|\overline{S}| \equiv \sqrt{(2\overline{S}_{ij}\overline{S}_{ij})}$. L_s is computed using

$$L_s = min(\kappa d, C_s V^{1/3}) \tag{7.21}$$

where $\kappa = 0.42$, C_s is the Smagorinsky constant. d is the distance to the closest wall, and V is the volume of the computational cell.

Lilly derived a value of 0.23 for C_s from homogeneous isotropic turbulence in the inertial subrange. However, this value was found to cause excessive damping of large-scale fluctuations in the presence of mean shear or in transitional flows. C_s=0.1 has been found to yield the best results for a wide range of flows.

7.4.2 Results and Discussion

In all figures, "RS" serves as "Re Stress model" and "LES" is "large-eddy simulation". Then "standard" serves as $k-\varepsilon$ model. Figures 7.50-7.55 present computed results which include RS and $k-\varepsilon$ models and measured radial mole fractions of CH_4, CO_2, CO, O_2, H_2, H_2O. Figure 7.50 shows the computed and the measured CH_4 along the axial distance. For CO_2, the $k-\varepsilon$ model results are better than RS

model (Figure 7.51). Same results are shown for CO using both models in Figure 7.52. But for O_2, the RS model is quite higher than the test data. Figure 7.55 gives the distribution of the H_2O mole fraction, both model results are in good agreement with experimental data. The temperature distribution for both models is similar (Figure 7.56). From Figure 7.57, we deal with the large-eddy simulation results. Overall, the results are not satisfactory. Specially, the predicted radial profile for the CH_4 fraction is higher than the experimental and the standard calculated results (Figure 7.57). But the predicted CO_2 and CO mole fractions are very low in Figures 7.58 and 7.59, it is difficult to see the line for LES. In most locations, the O_2 is not in agreement with test data, specially at 63.2 cm, it is very high. A similar situation takes place for H_2O, at 63.2 cm the fraction of H_2O is low (Figure 7.61). The calculated temperature distribution is in Figure 7.63. The reason for the predicted error may be that in this example, the flow velocity is not fast enough in which the LES model is more suitable.

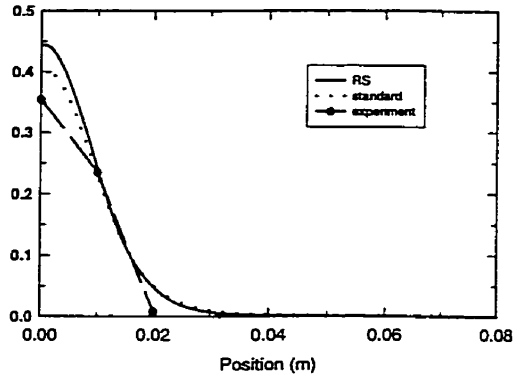

(17.5 cm)

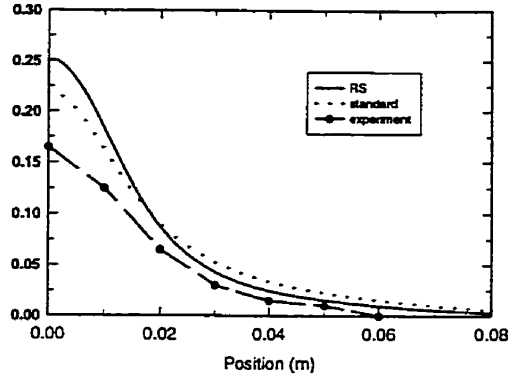

(32.7 cm)

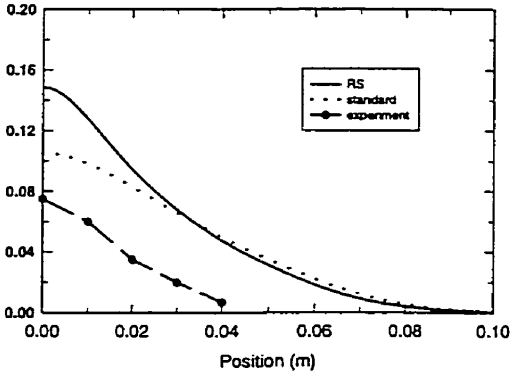

(47.6 cm)

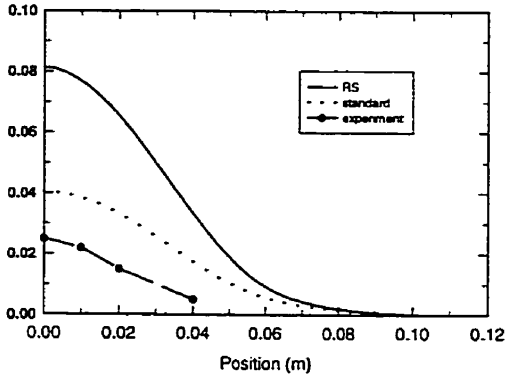

(63.2 cm)

Figure 7.50 Radial CH_4 mole fraction profiles at several axial locations

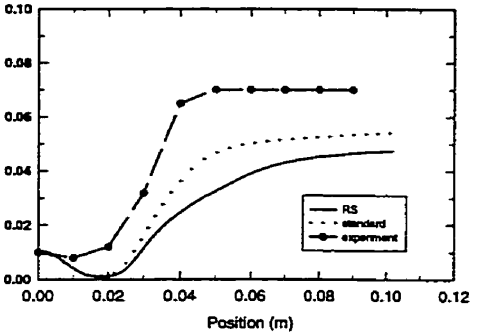

(9.5 cm)

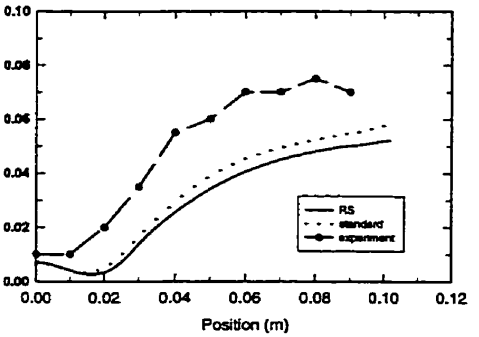

(17.5 cm)

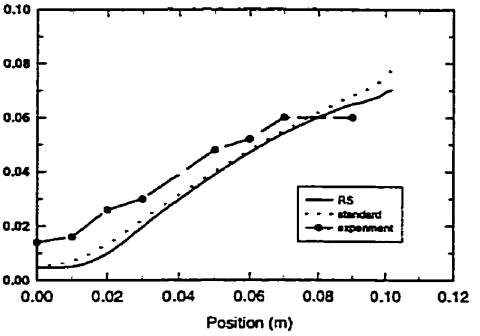

(32.7 cm)

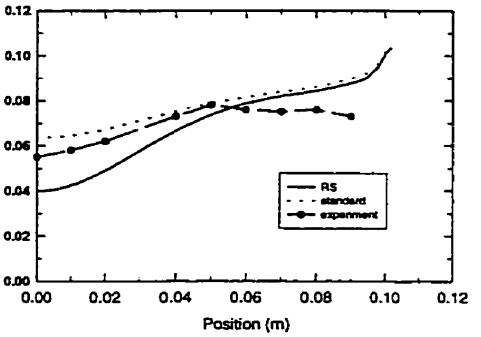

(63.2 cm)

Figure 7.51 Radial CO_2 mole fraction profiles at several axial locations

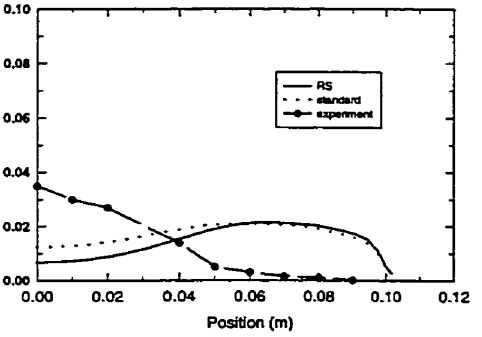

(63.2 cm)

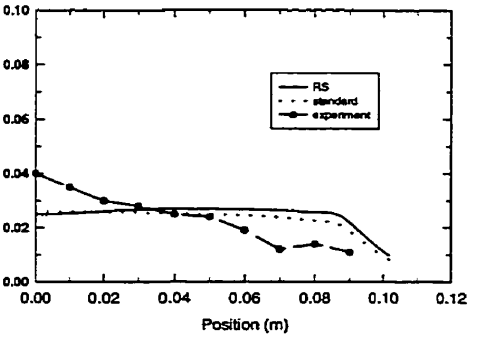

(78.5 cm)

Figure 7.52 Radial CO mole fraction profiles at several axial locations

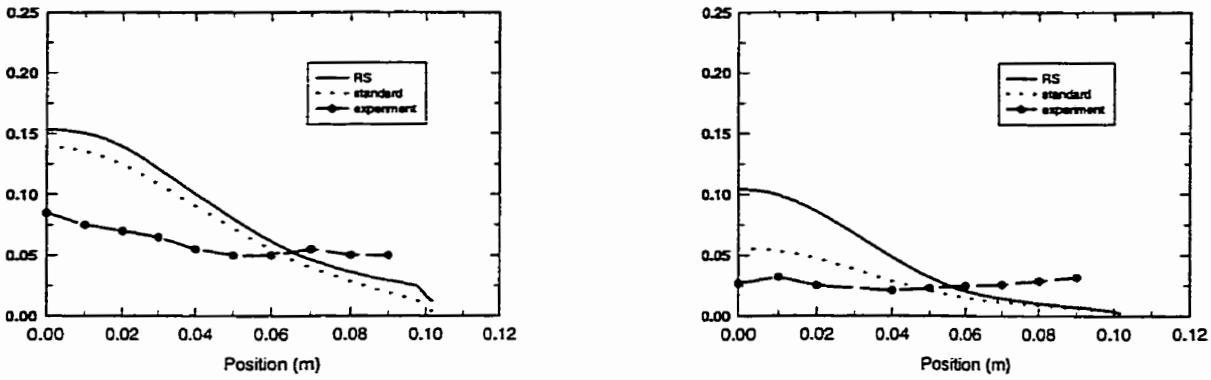

(47.6 cm) (63.2 cm)

Figure 7.53 Radial O_2 mole fraction profiles at several axial locations

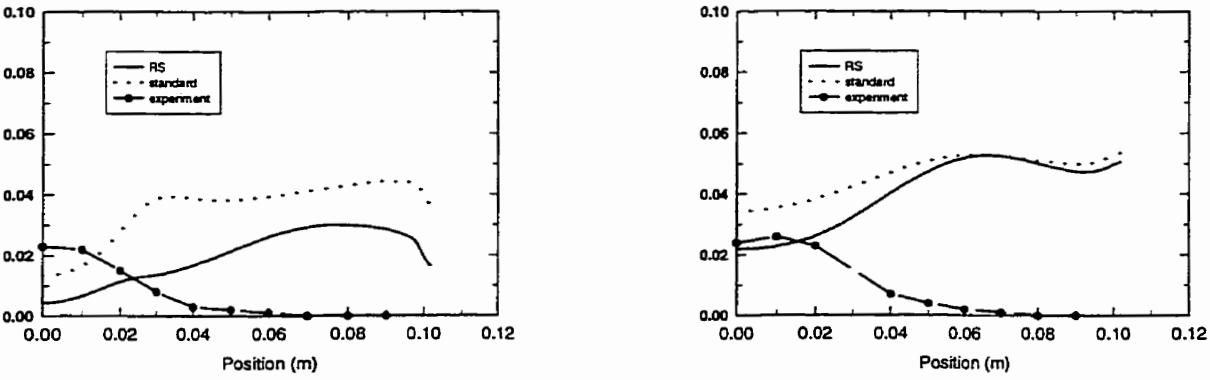

(47.6 cm) (63.2 cm)

Figure 7.54 Radial H_2 mole fraction profiles at several axial locations

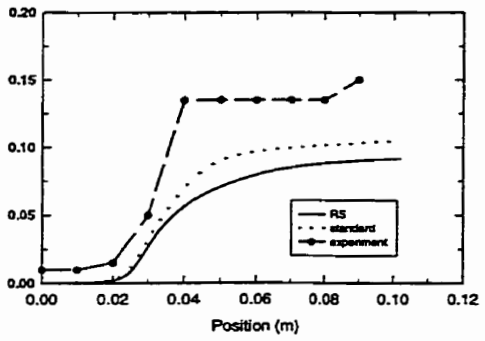

(9.5 cm)

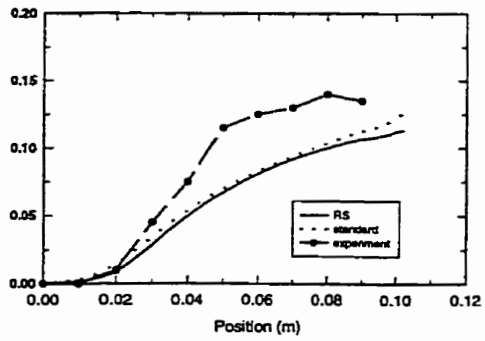

(24.6 cm)

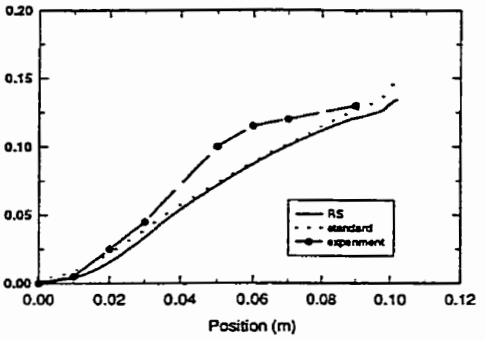

(32.7 cm)

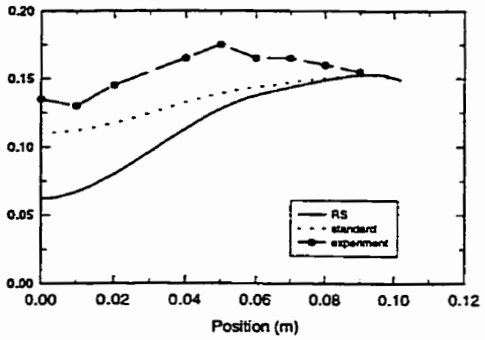

(63.2 cm)

Figure 7.55 Radial H_2O mole fraction profiles at several axial locations

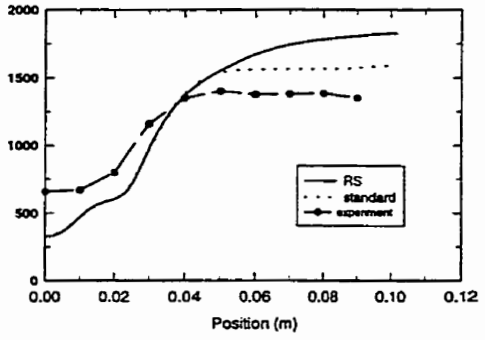

Figure 7.56 Radial temperature distribution at 9.5 cm

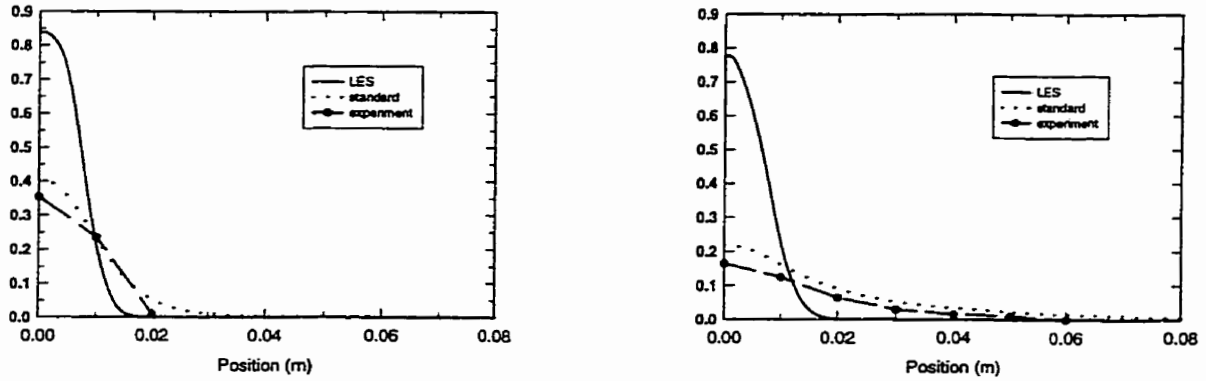

(17.5 cm) (32.7 cm)

Figure 7.57 Radial CH_4 mole fraction profiles at several axial locations

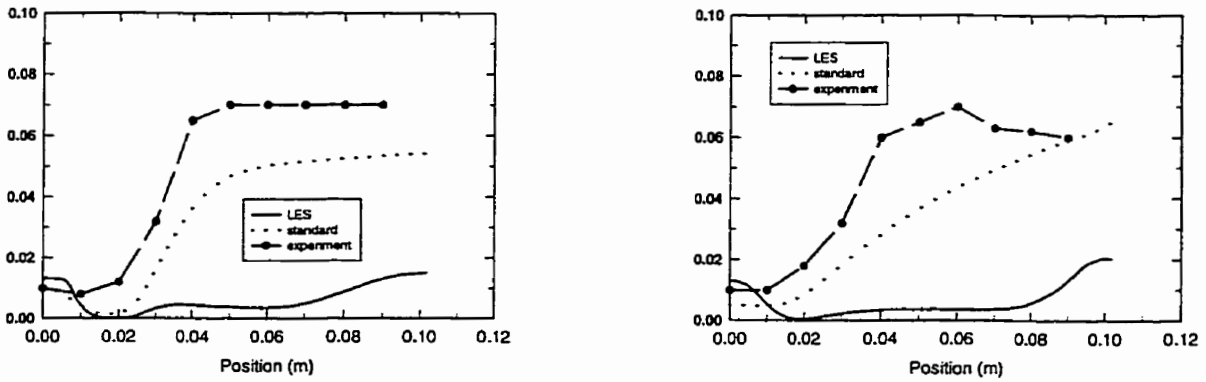

(9.5 cm) (24.6 cm)

Figure 7.58 Radial CO_2 mole fraction profiles at several axial locations

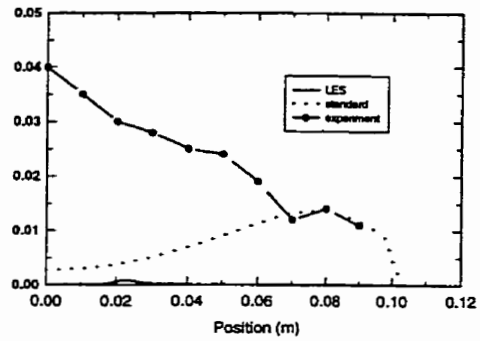

(47.6 cm)

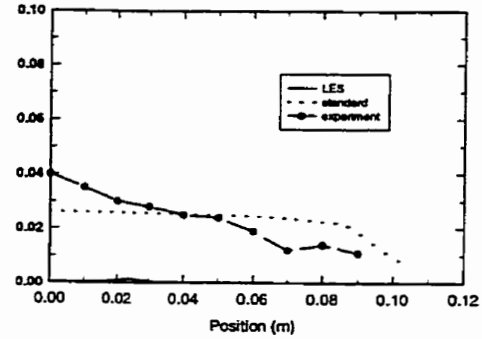

(78.5 cm)

Figure 7.59 Radial CO mole fraction profiles at several axial locations

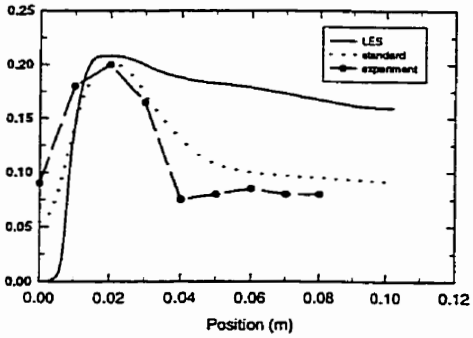

(9.5 cm)

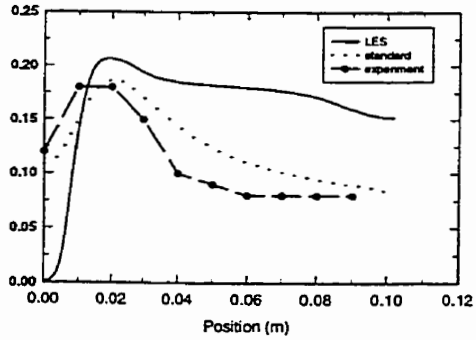

(17.5 cm)

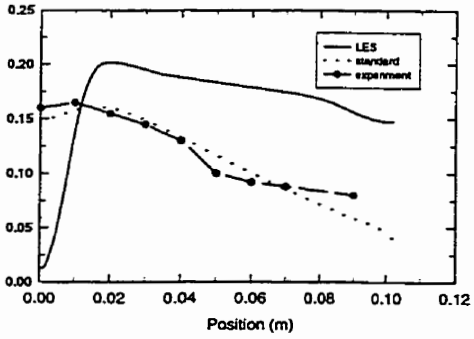

(32.7 cm)

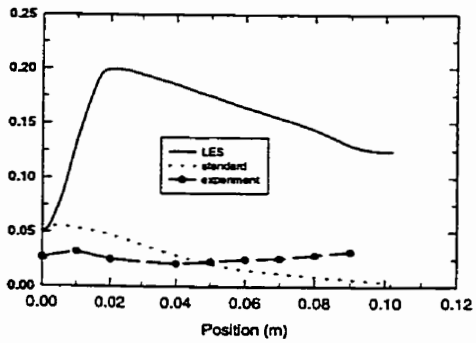

(63.2 cm)

Figure 7.60 Radial O_2 mole fraction profiles at several axial locations

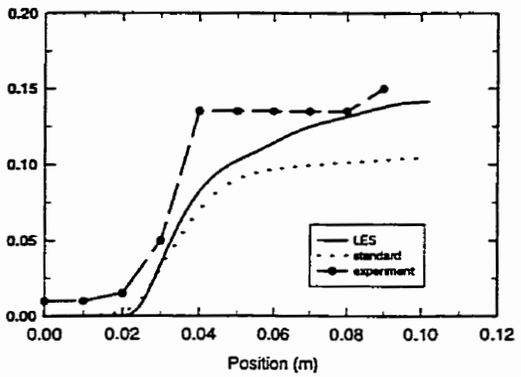

(9.5 cm)

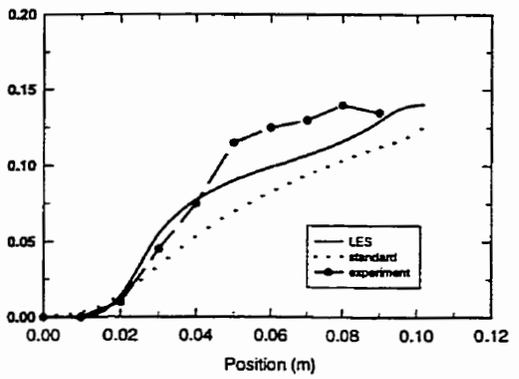

(24.6 cm)

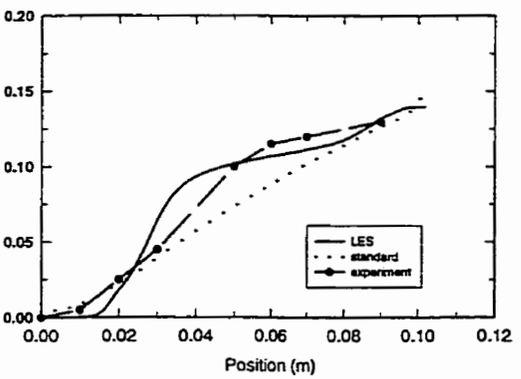

(32.7 cm)

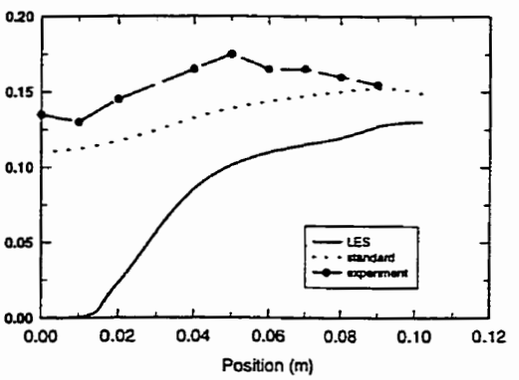

(63.2 cm)

Figure 7.61 Radial H_2O mole fraction profiles at several axial locations

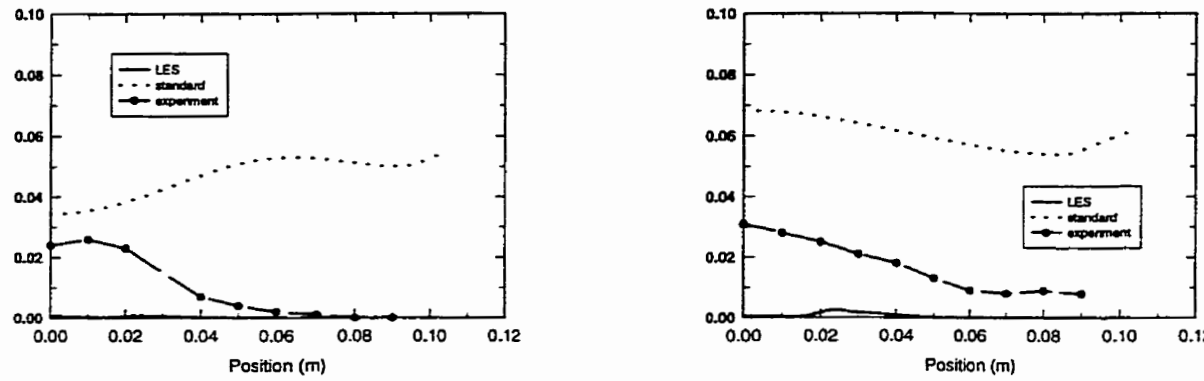

Figure 7.62 Radial H_2 mole fraction profiles at several axial locations

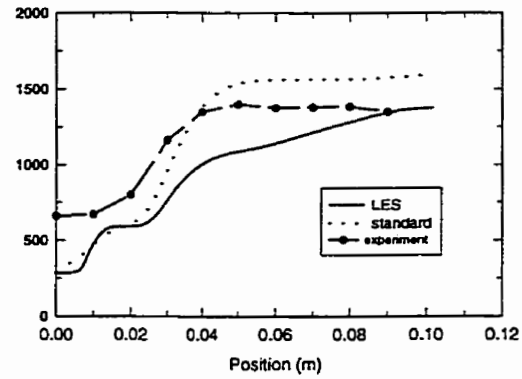

Figure 7.63 Radial temperature distribution at 9.5 cm

7.5 PDF Combustion

7.5.1 Problem Description

The power of the mixture fraction modeling approach is that through calculation of a single conserved scalar field, f, other important scalars of interest can be derived without solving individual transport equations to describe them. Given a description of the reacting system chemistry, and certain other restrictions on the system, the mixture fraction value at each point in the flow field can be used to compute the instantaneous values of individual species mole fractions, density and temperature. If, in addition, the reacting system is adiabatic, the instantaneous values of mole fractions, density, and temperature depend solely on the instantaneous mixture fraction, f:

$$\phi_i = \phi_i(f) \tag{7.22}$$

for a single fuel/oxidizer system.

Many reacting systems involve heat transfer to wall boundaries by convective and/or radiative heat transfer. In these systems, and in other systems as well, the local thermochemical state is no longer related only to f, but also to H^*. This is true because the system enthalpy impacts the chemical equilibrium calculation and the temperature of the reacted flow. Consequently, change in enthalpy due to heat loss must be considered when computing scalars from the mixture fraction. Thus, the scalar dependence becomes

$$\phi_i = \phi_i(f, H^*) \tag{7.23}$$

where H^* is the instantaneous enthalpy.

In such nonadiabatic systems, turbulent fluctuations should be accounted for by means of a joint PDF $\mathrm{p}(f, H^*)$. The computation of $\mathrm{p}(f, H^*)$ is not practical for

most engineering applications, however. The problem can be simplified significantly by assuming that the enthalpy fluctuations are independent of the enthalpy level. When this is assumed, we again have $p = p(f)$ and

$$\overline{\phi_i} = \int_0^1 \phi_i(f, \overline{H^*}) p(f) df \tag{7.24}$$

Determination of $\overline{f_i}$ in the nonadiabatic system thus requires solution of the modeled transport equation for time-averaged enthalpy:

$$\frac{\partial}{\partial t}(\rho \overline{H^*}) + \frac{\partial}{\partial x_i}(\rho u_i \overline{H^*}) = \frac{\partial}{\partial x_i}\left(\frac{k_t}{c_p}\frac{\partial \overline{H^*}}{\partial x_i}\right) + \tau_{ij}\frac{\partial u_i}{\partial x_k} + S_h \tag{7.25}$$

where S_h accounts for source terms due to radiation, heat transfer to wall boundaries, and heat exchange with the second phase.

In the presented work, β pdf shape is assumed for the probability distribution function. Chemical equilibrium is computed by means of an algorithm for Gibbs' free energy minimization. The adiabatic and nonadiabatic PDF models are used and both results are compared with experimental data.

7.5.2 Results and Discussion

In all figures, "pdfa" is "adiabatic-PDF" and "pdfn" is "nonadiabatic-PDF". Figures 7.64-7.69 show the predicted radial mole fractions of CH_4, CO_2, CO, O_2, H_2 and H_2O. There are disagreement with test results. From Figure 7.64 it is seen that the mole fraction of CH_4 is overpredicted. The one of CO_2 is underpredicted. The centerline predicted mole fraction of O_2 is zero. It is not satisfactory. The result of H_2O is closer to the experimental values (Figure 7.69) than other species. The nonadiabatic model is just a little better than adiabatic one. The radial mixture fraction distribution at four sections is presented in Figure 7.70. In both models, at all section, the mixture fraction is overpredicted. It is noted that the convergence of both models is very fast. For adiabatic it is less than 400 iterations (Figure

7.71) and for nonadiabatic it is about 4000 (Figure 7.72). In "standard model", the convergent times is over 10000 iterations. So, PDF model spends less CPU time than other models. The PDF model uses infinitely fast chemistry (with the chemical equilibrium assumption) therefore with no need to know complex reaction mechanisms. This is its main advantage. But most real chemical reactions are finite without equilibrium, so the results with PDF model may cause larger errors than with other models.

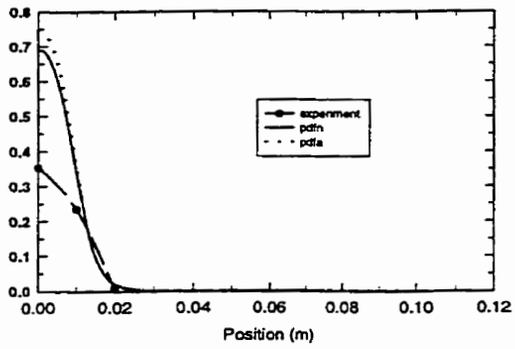

(17.5 cm)

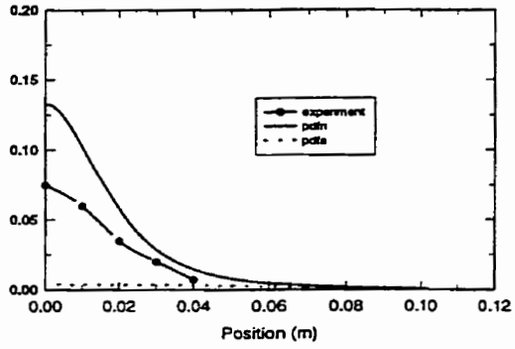

(47.6 cm)

Figure 7.64 Radial CH_4 mole fraction profiles at several axial locations

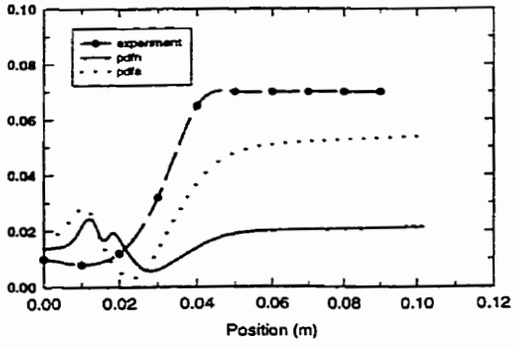

(9.5 cm)

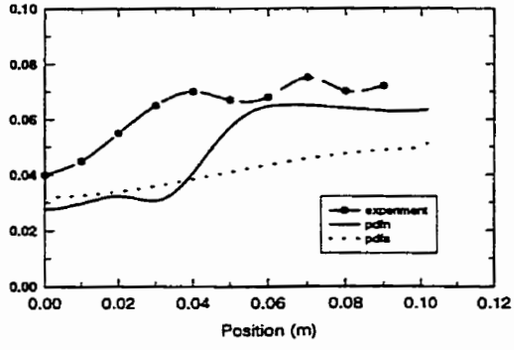

(47.6 cm)

Figure 7.65 Radial CO_2 mole fraction profiles at several axial locations

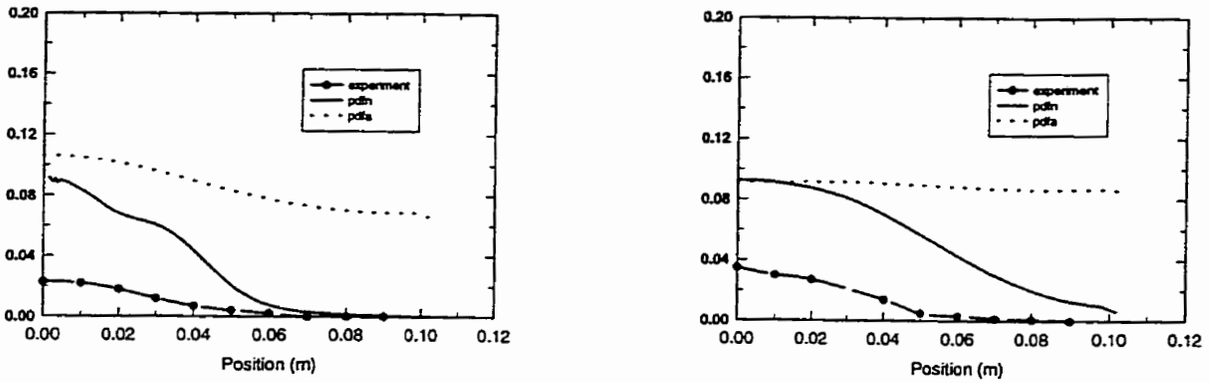

(47.6 cm) (63.2 cm)

Figure 7.66 Radial CO mole fraction profiles at several axial locations

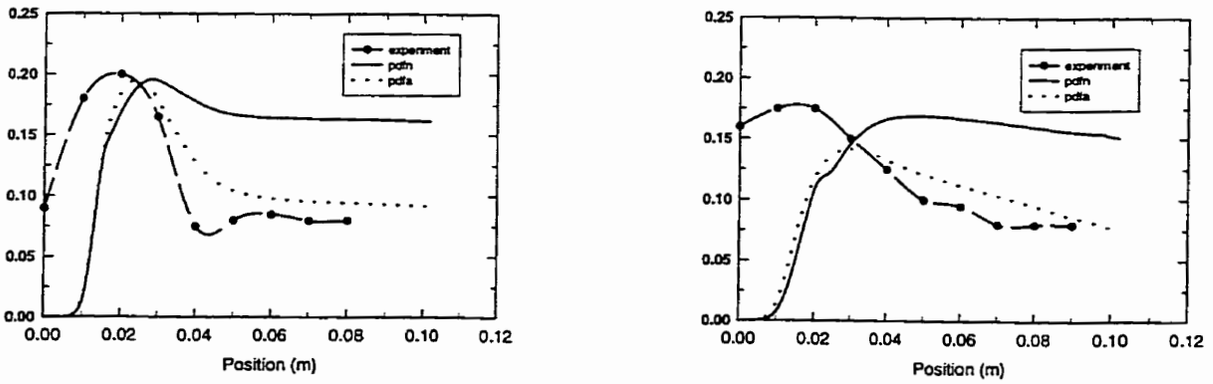

(9.5 cm) (24.6 cm)

Figure 7.67 Radial O_2 mole fraction profiles at several axial locations

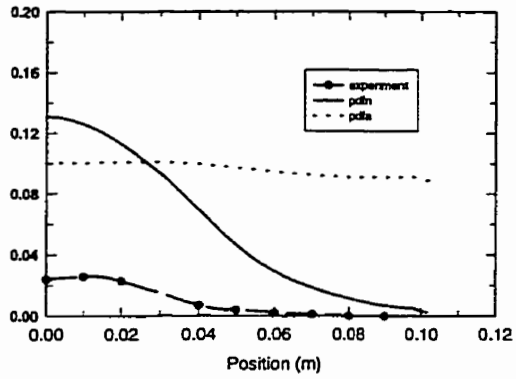

(63.2 cm)

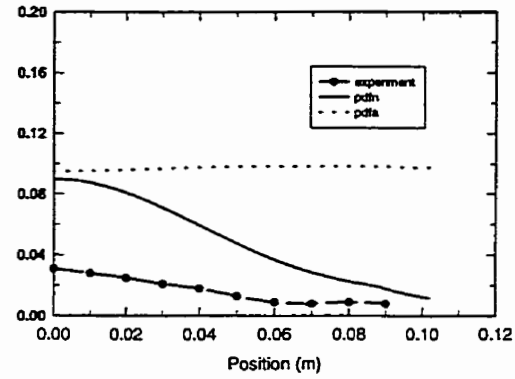

(78.5 cm)

Figure 7.68 Radial H_2 mole fraction profiles at several axial locations

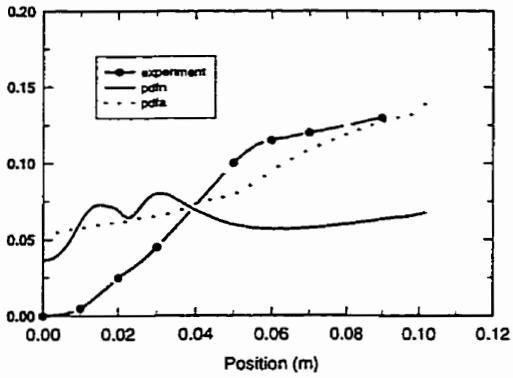

(32.7 cm)

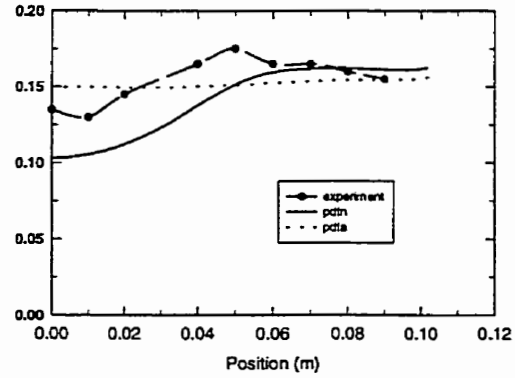

(63.2 cm)

Figure 7.69 Radial H_2O mole fraction profiles at several axial locations

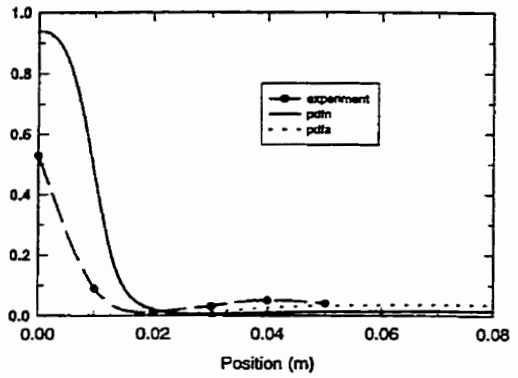

(9.5 cm)

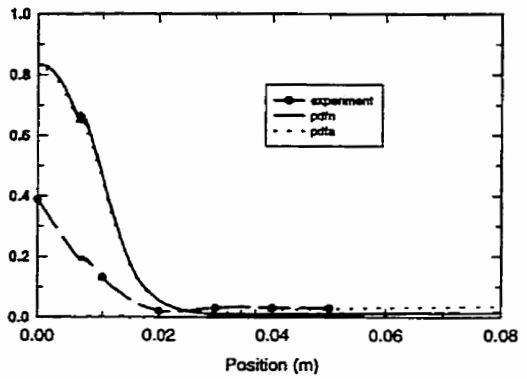

(17.5 cm)

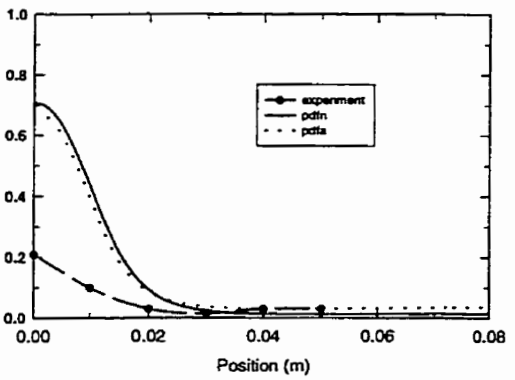

(24.6 cm)

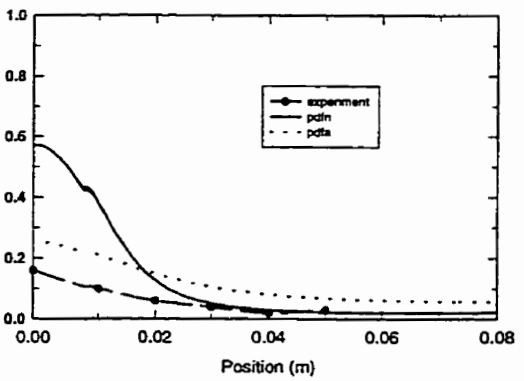

(32.7 cm)

Figure 7.70 The predicted radial distributions of mixture fraction at different stations based on PDF models

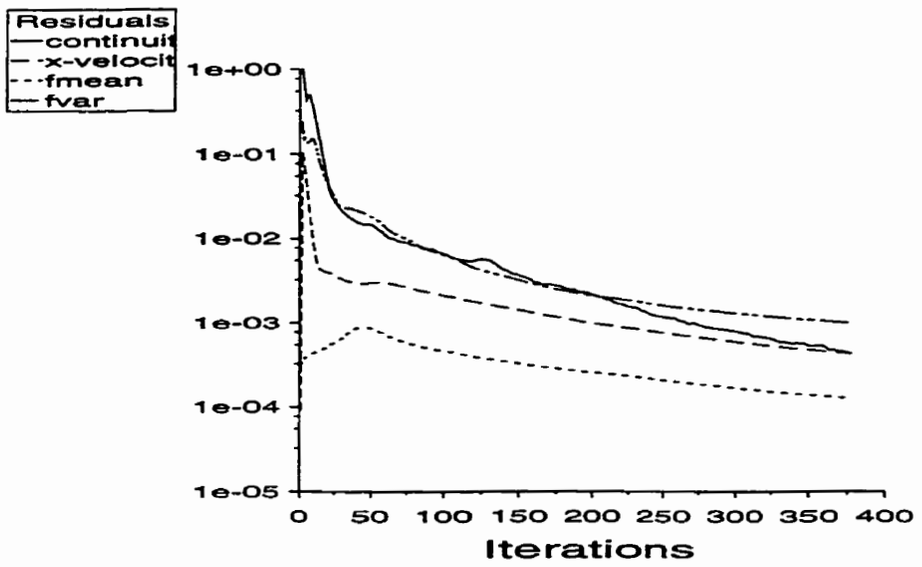

Figure 7.71 Convergence history of the adiabatic PDF

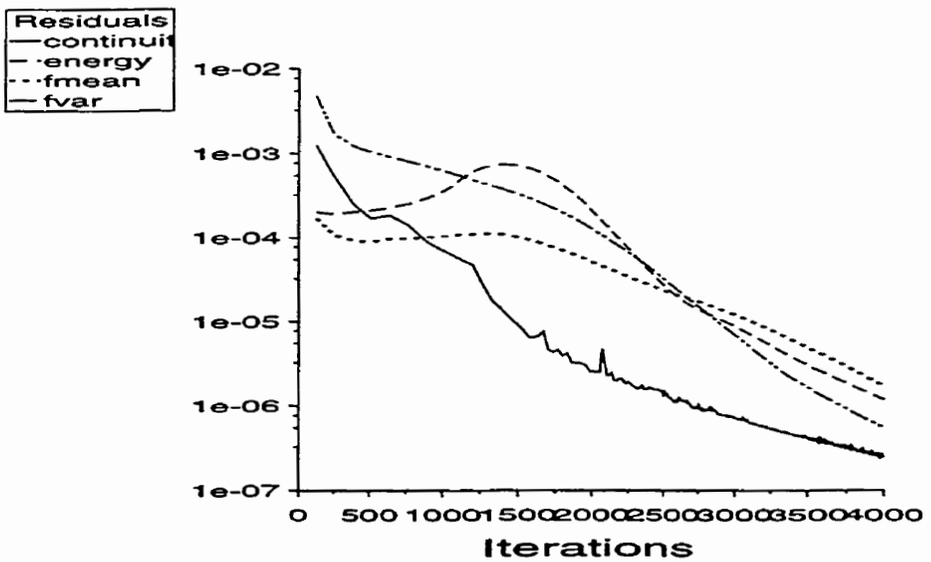

Figure 7.72 Convergence history of the nonadiabatic PDF

7.6 Mixing Coefficient

7.6.1 Problem Description

In Section 7.3, we introduced "Standard scheme" where "Eddy Break-Up" model is used and the coefficients A and B equal to 4 and 0.5 respectively that Magnussen and Hjertager (1977) suggested initially. In general, mixing play a more important role than chemical reaction in turbulent flow. It is worth to research the effect on chemical species and temperature with different values of the coefficients. In the standard scheme, the calculated CO fraction is higher than the experimental one and the CO_2 fraction is lower. So, for reaction equation (7.12),

$$CO + H_2O \rightarrow CO_2 + H_2$$

we use different A and B values, double or half of normal value. The detailed values are seen in Table 7.6.

Schemes No.	Changed	A	B
1	normal	4	0.5
2	$A\uparrow$	8	0.5
3	$B\uparrow$	4	1
4	$A\uparrow B\uparrow$	8	1
5	$A\downarrow$	2	0.5
6	$B\downarrow$	4	0.25
7	$A\downarrow B\downarrow$	2	0.25
8	$A\uparrow B\downarrow$	8	0.25
9	$A\downarrow B\uparrow$	2	1

Table 7.6 The coefficients for different schemes

7.6.2 Discussion

The calculated results are shown in Tables 7.7-7.14. It is seen that the distributions of CH_4 are not changed with the change of coefficients. The different schemes provide the satisfactory prediction for O_2 and CO_2. For H_2O and CO, increasing A and B is better than decreasing A and B. But the whole field maximum temperature is higher as increasing A and B. In general, the various effects of changing coefficients A and B must be considered, current values of A and B are acceptable.

unit: mole fraction

x (cm)	test	1	2	3	4	5	6	7	8	9
9.5	50.	63.	63.	63.	63.	63.	63.	63.	63.	63.
24.6	17.5	30.	30.	30.	30.	30.	30.	30.	30.	30.
47.6	8.	11.5	11.	11.	11.	11.	11.	11.	11.	11.5
78.5	1.	1.	0	0	0	0	0	0	0	0

Table 7.7 The maximum CH_4 percentage at different locations with different schemes

unit: mole fraction

x (cm)	test	1	2	3	4	5	6	7	8	9
9.5	20.	20.	20.	20.	20.	20.	20.	20.	20.	20.
24.6	18.	17.	17.5	17.5	17.	17.	17.	17.5	17.5	17.5
47.6	8.	13.5	14.	13.5	14.	13.	13.5	13.	14.	13.
78.5	1.	1.	1.	1.	1.	0.5	0.5	0.5	0.5	0.5

Table 7.8 The maximum O_2 percentage at different locations with different schemes

unit: mole fraction

x (cm)	test	1	2	3	4	5	6	7	8	9
9.5	6.	5.	4.5	5.5	4.5	5.5	5.5	5.5	4.5	5.5
24.6	6.5	6.5	5.	7.	5.5	6.8	7.	6.5	5.5	7.
47.6	7.	10.	10.	10.	10.5	10.	10.	10.	10.5	10.
78.5	8.	10.	11.	10.5	11.	10.	10.5	9.5	11.	9.5

Table 7.9 The maximum CO_2 percentage at different locations with different schemes

unit: mole fraction

x (cm)	test	1	2	3	4	5	6	7	8	9
9.5	13.5	13.	10.	12.	10.	12.	12.	12.	11.	12.
24.6	14.	15.	11.	13.	12.	14.	14.	13.5	12.	14.
47.6	14.	17.	17.	18.	17.	18.	18.	18.	17.	18.
78.5	16.5	14.	16.	16.5	16.	20.	20.	20.5	18.	18.5

Table 7.10 The maximum H_2O percentage at different locations with different schemes

unit: mole fraction

x (cm)	test	1	2	3	4	5	6	7	8	9
9.5	0	0	0	0	0	0	0	0	0	0
24.6	0	0.15	0	0.2	0	0.25	0.15	0.25	0	0.25
47.6	2.	1.6	0.7	1.6	0.6	2.4	1.6	3.5	0.6	2.4
78.5	4.	3.	2.1	3.3	1.8	8.5	8.5	10.	5.2	6.5

Table 7.11 The maximum CO percentage at different locations with different schemes

unit: mole fraction

x (cm)	test	1	2	3	4	5	6	7	8	9
9.5	0	0	0	0	0	0	0	0	0	0
24.6	0	0.5	0	0.5	0	0.5	0.5	0.5	0.2	0.5
47.6	2.	4.	4.5	4.	4.5	3.5	3.8	3.6	4.	3.6

Table 7.12 The maximum H_2 percentage at different locations with different schemes

test	1	2	3	4	5	6	7	8	9
-	2037	2314	2256	2327	2044	2060	2027	2045	2038

Table 7.13 The maximum temperature value for the whole field, K

Scheme	1	2	3	4	5	6	7	8	9
T_{max}	-	0	0	0	-10	-20	-20	-10	-15

Table 7.14 The maximum temperature at 9.5 cm comparison with scheme 1, K

7.7 User-Defined Reaction Rate

7.7.1 Problem Description

The geometry and physical conditions are the same as in Section 7.3. A new improved reaction rate equation in Chapter 6 is used

$$\bar{\dot{w}}_f = -0.0117\bar{\rho}Y_B\frac{\varepsilon}{k} \tag{6.74}$$

An extension to multi-step and reversible reactions is done here. There is only one reactant in Equation (7.15), where the fuel and the oxidant are not distinguished. So, the O_2 species is added with its stoichiometric coefficient equal to zero.

A user-defined function is adopted which calculates the Arrhenius reaction rate (Equation (6.17)), the eddy-dissipation-model reaction rates (Equations (6.24) and (6.25)) and Equation (6.74). It is named the "FEU Scheme"(finite-rate + eddy-break-up + used-defined-function). The slowest rate is used as the reaction rate and the contributions to the source terms in the species conservation and energy equations are calculated from this reaction rate. The UDF file is seen in Appendix B.

In order to efficiently reduce the numerical error in the digital solution, we use grid refinement. Assuming the greatest error occurs in high-gradient regions, the readily available physical features of the evolving flow field may be used to drive the grid adaptation process. In practice, the convergence criterion for energy is the least. In other word, the energy convergence controls the whole calculation. So, "Total Energy" is chosen as the gradient adaptation function. The initial grid, shown in Figure 7.73, is coarse. Several adaptations are made after iterations 750, 1500, 3000 and 4000 iterations. The final grid is shown in Figure 7.74. The detailed grid sizes are seen in Table 7.15. The solution is converged after 7104 iterations.

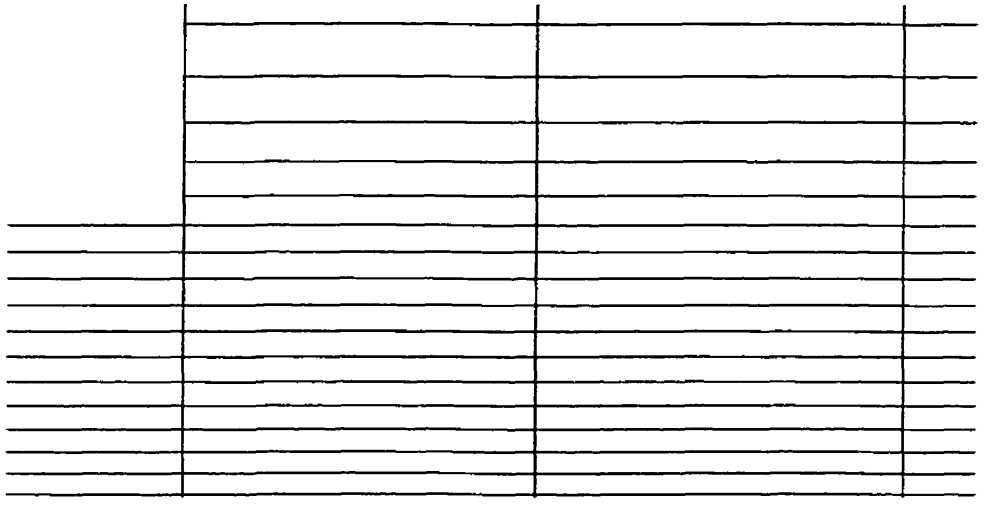

Figure 7.73 The initial grid

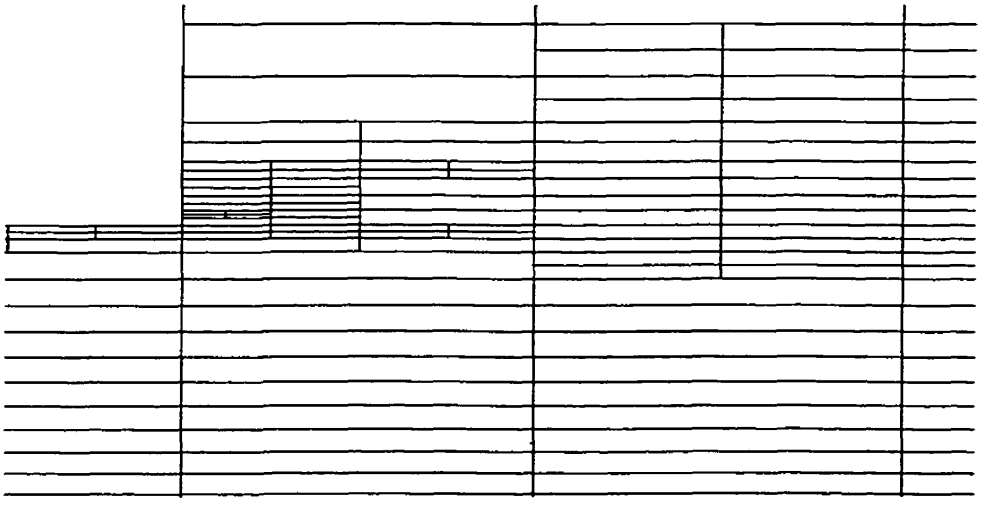

Figure 7.74 The final grid

	original	750 iter.	1500 iter.	3000 iter.	4000 iter.
cells	2888	3932	4745	5138	5354
faces	5896	8158	9927	10799	11271
nodes	3009	4227	5183	5662	5918

Table 7.15 The change of grid sizes

7.7.2 Results

The main calculation results are shown in Figures 7.75-7.82. Comparison with the "standard" from Section 7.3, Radial composition profiles for CH_4, CO_2, CO and H_2 are nearly identical. For CH_4, at axial locations of 9.5 cm, 17.5 cm, 24.6 cm, 32.7 cm, the distributions correspond with the "standard", just at 63.2 cm there is a slight difference (Figure 7.75). It is important that the calculated O_2 and H_2O compositions are closer to experimental results than the Standard scheme. From figure 7.76, it is found that on the centerline the predicted O_2 species by FEU at 63.2 cm is very closed to the experimental data. In the new model (Figure 7.78), at 9.5 cm, the H_2O percentage is 0 on the centerline, then increases gradually along radial direction to 12.6% near the wall, but it is just 10.4% in the standard, and is lower than the experimental value of 15%. Similarly, at 17.5 cm, near the wall the maximum H_2O percentage increases from 11.2% in the standard to 13.4%, closes to the experimental results 13%. At 24.6 cm, the standard percentage is lower than 4%, FEU increases 2%, but still lower than the test results about 2%. For CO_2 (Figure 7.77), CO (Figure 7.79) and H_2 (Figure 7.80), it can be seen that the results of the FEU method are almost the same as that of the "standard". Figures 7.81 and 7.82 present the temperature distribution. The calculated temperature is slightly low on centerline and slight high near the wall. By comparison with the experimental data, we have shown that the results of O_2 and H_2O with FEU model are better than that with "standard" method, for CH_4, CO_2, CO and H_2, the results of both methods are the same and close to the experimental values.

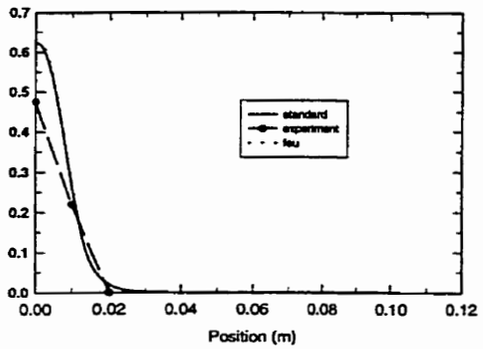

(9.5 cm)

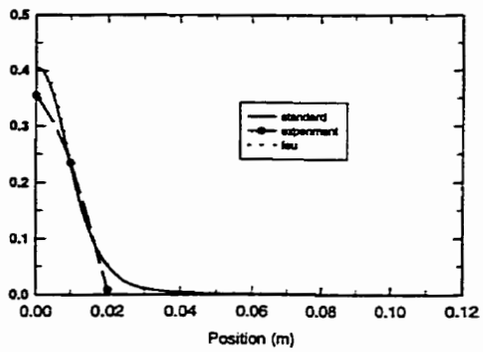

(17.5 cm)

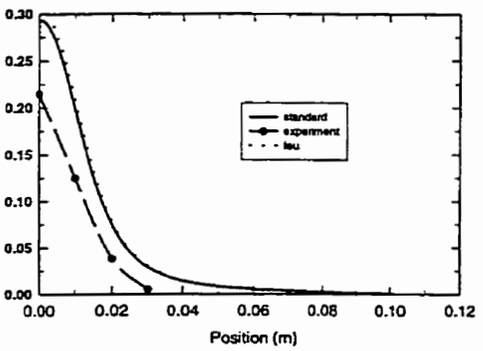

(24.6 cm)

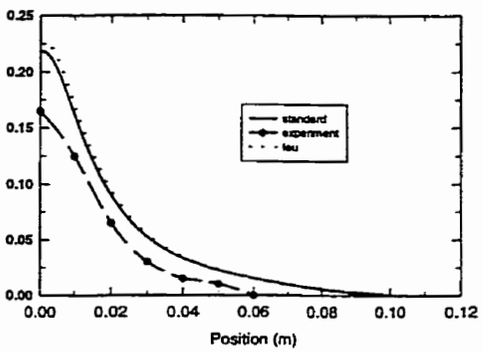

(32.7 cm)

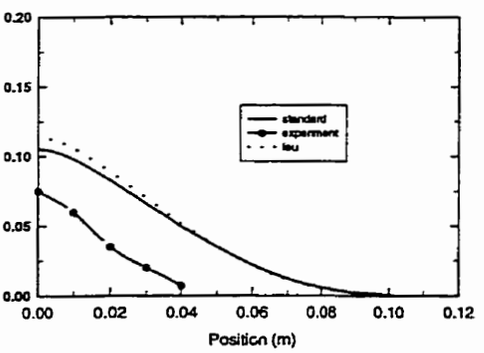

(47.6 cm)

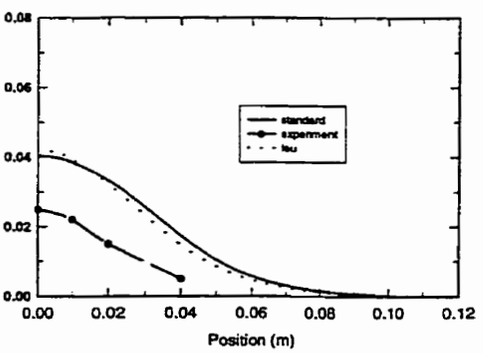

(63.2 cm)

Figure 7.75 Radial profiles CH_4 mole percent profiles at several axial locations

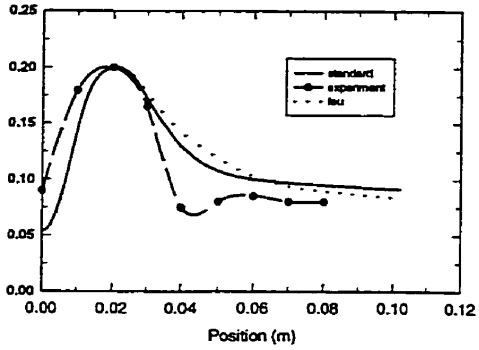

(9.5 cm)

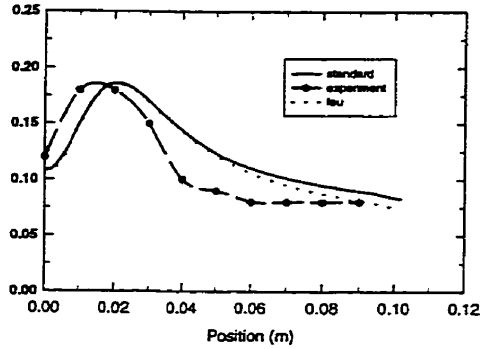

(17.5 cm)

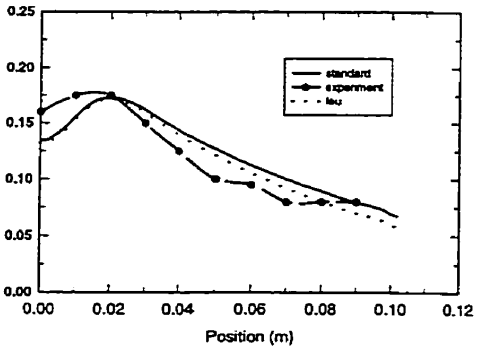

(24.6 cm)

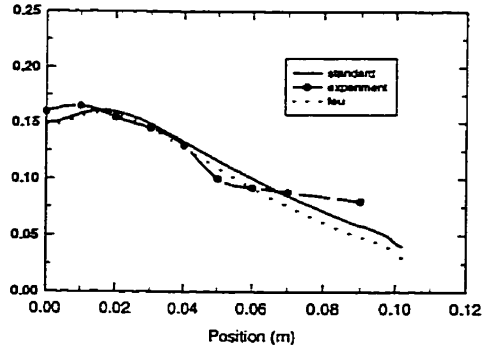

(32.7 cm)

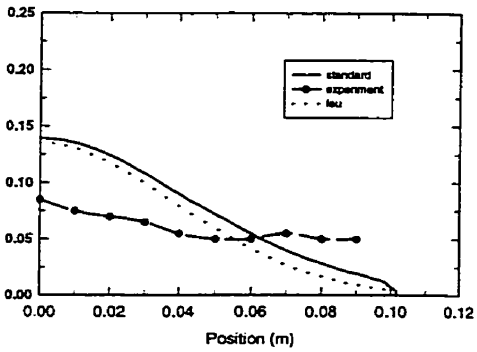

(47.6 cm)

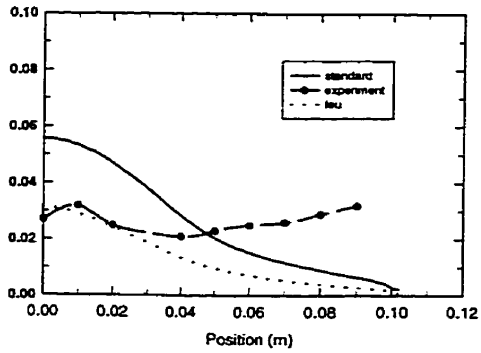

(63.2 cm)

Figure 7.76 Radial O_2 mole percent profiles at several axial locations

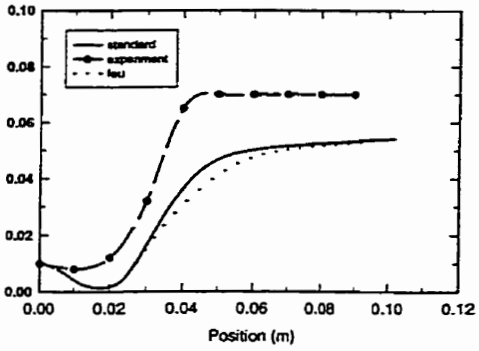

(9.5 cm)

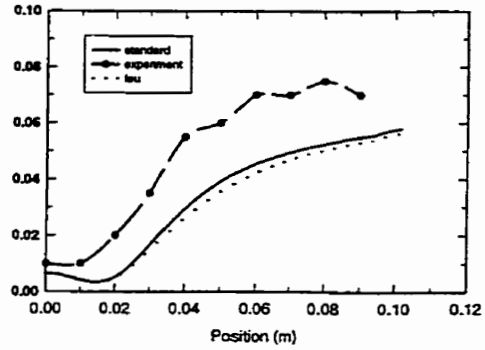

(17.5 cm)

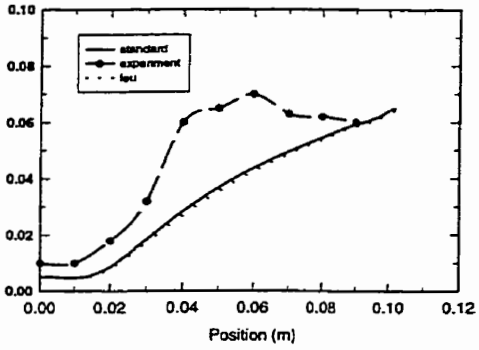

(24.6 cm)

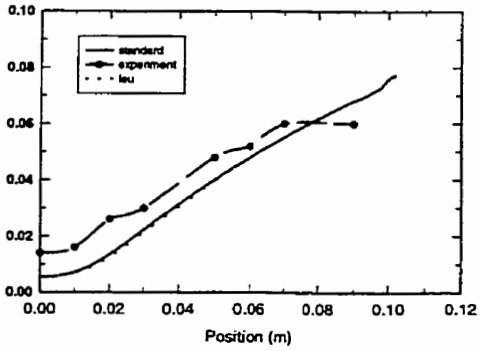

(32.7 cm)

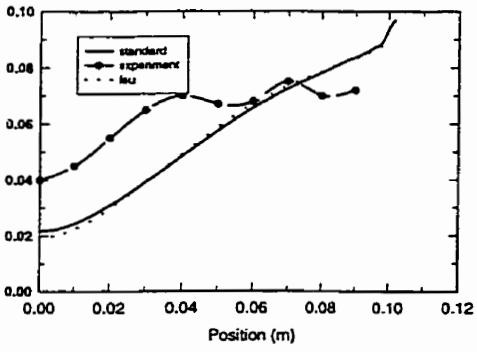

(47.6 cm)

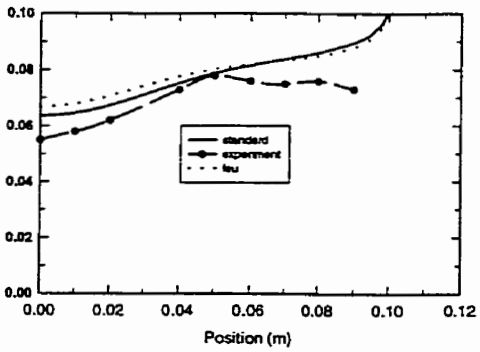

(63.2 cm)

Figure 7.77 Radial CO_2 mole percent profiles at several axial locations

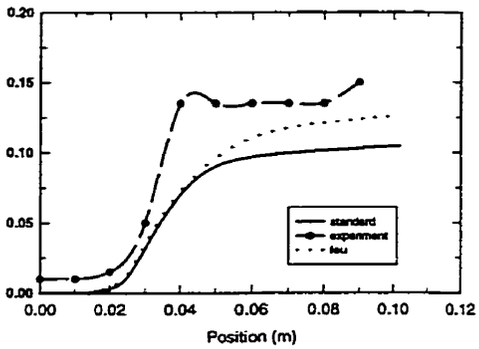

(9.5 cm)

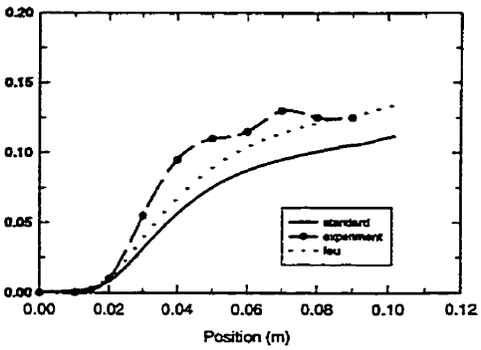

(17.5 cm)

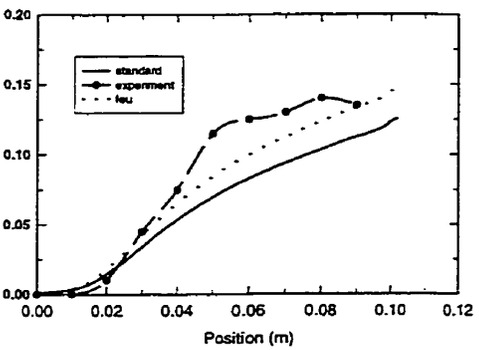

(24.6 cm)

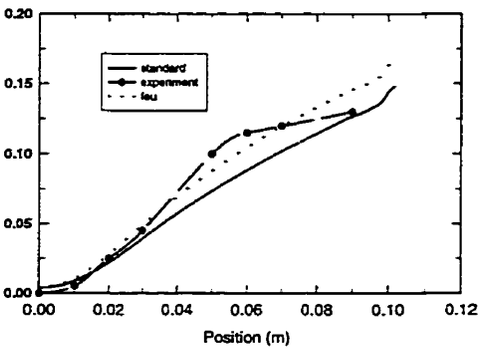

(32.7 cm)

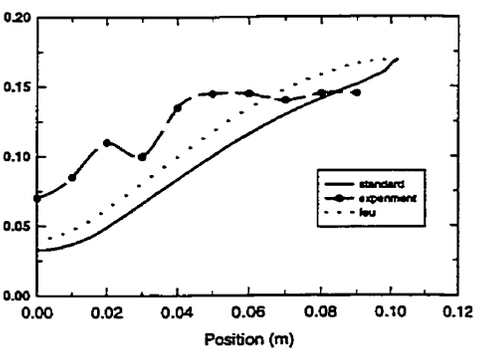

(47.6 cm)

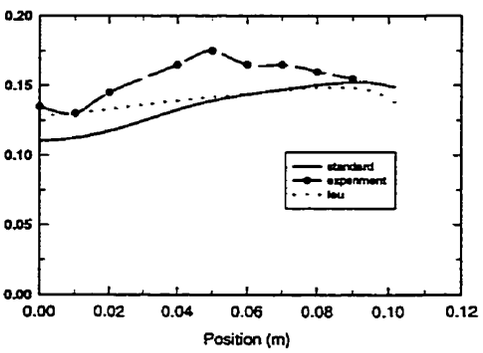

(63.2 cm)

Figure 7.78 Radial H_2O mole percent profiles at several axial locations

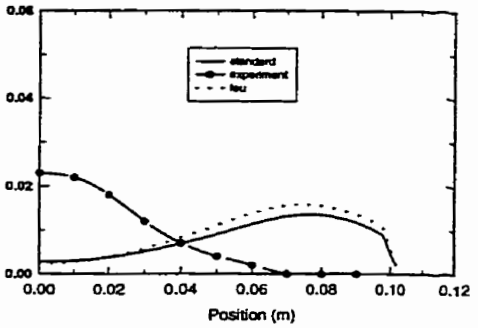

(47.6 cm)

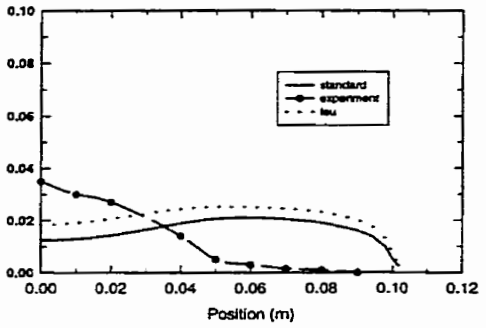

(63.2 cm)

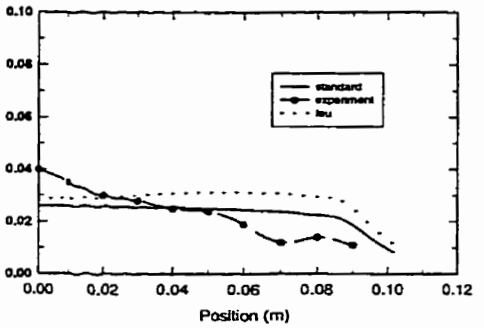

(78.5 cm)

Figure 7.79 Radial CO mole percent profiles at several axial locations

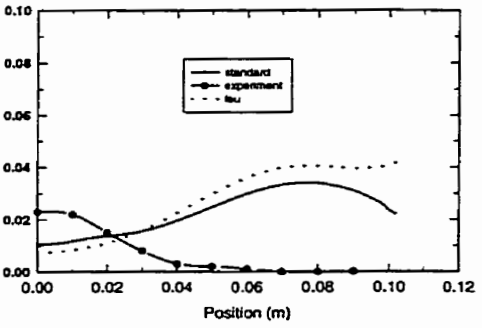

(47.6 cm)

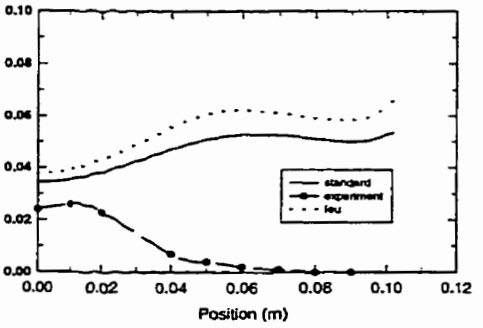

(63.2 cm)

Figure 7.80 Radial H_2 mole percent profiles at several axial locations

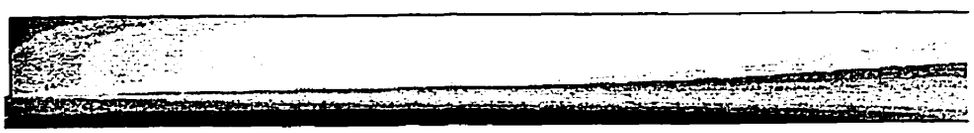

Figure 7.81 Temperature field

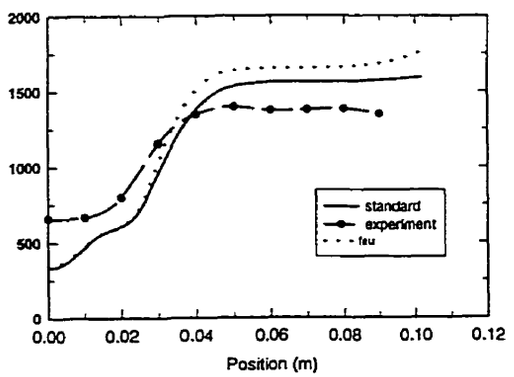

Figure 7.82 Temperature at 9.5 cm

Conclusions

Various physical and chemical models have been used for the numerical simulation of laminar and turbulent reacting flows in this thesis. The following conclusions were obtained:

1. In the multi-step model, the presence of CO and H_2 lowers the total heat release and the adiabatic flame temperature is below the values predicted by the one-step method. The results are much closer to the real situation. With engineering consideration for calculation time (or cost) and accuracy, it is recommended to adopt the six-step model.

2. An unstructured mesh can often be created with far fewer cells than the structured mesh consisting of quadrilateral elements under similar accuracy.

3. For simulation of turbulent combustion, using the "standard" scheme turbulence closure models can provide quite good results. But there is quite an error with chemical species composition. It is to point out that relaxation factors play an important role in the convergence process. In general, under-relaxation factors are chosen by experience, there are different optimum values with different cases.

4. The Reynolds stress model is slightly better than the $k-\varepsilon$ model. In brief, both model results are in good agreement with experimental data. In our examples, the large-eddy simulation results are not satisfactory.

5. The probability density function (including adiabatic and nonadiabatic PDF) models spend less CPU time than other models. The convergence is very fast. This is its main advantage. Comparison with experimental results, the mixture fraction is overpredicted. When the reaction is not with chemical equilibrium, the predicted species radial mole fractions are more likely in disagreement with test results.

6. In general, mixing plays a more important role than chemical reaction in turbulent flow. The change in the coefficients for the EBU model affects mainly the CO and H_2O distributions. Increasing coefficients A and B is better than decreasing A and B.

7. By combination of finite-rate reaction and PDF, the coefficient of EBU model could be expressed as a function of mixture fraction and standard deviation. The "FEU" Scheme is successfully applied to the prediction of turbulent reaction combustion. The calculated chemical species mole fraction distributions are better than that of "standard" method and close to the experimental values.

8. By using solution-adaptive refinement, the features of the flow field are better resolved. When adaptation is used properly, the resulting mesh is optimal for the flow solution. Computational resources can be utilized effectively.

9. Furture research work will be concerned with: (a) using complete Bigler's model and making comparison with simplified model; (b)calculating more examples and validating the new model; (c) consideration of radiation effect; (d) adoption of more reasonable multi-step chemical reaction equations.

Bibliography

Abdalla A.Y. Bradlay D., Chin S.B. and Lam C., "Comparisons of Experimental and Computed Length Scales and Velocities in Turbulent Combustion", Dynamics of Flames and Reactive Systems; Progress in Astronautics and Aeronautics, Vol. 95, pp. 356-366, 1984.

Adjerid S. and flaherty J.E., "Second-Order Finite-Element Approximations and A Posteriori Error Estimation for Two-Dimensional Parabolic Problems", Numer. Math. Vol.53, pp.183-198, 1988.

Baldwin B.S. and Lomax H., "Thin Layer Approximations and Algebraic Model for Separated Turbulent Flows," AIAA Paper 78-287, 1978.

Bejan A., "Heat Transfer", John Wiley & Sons, Inc., ISBN 0-471-50290-1, 1993.

Bialecki R., "Applying the Boundary Element Technique to the Solution of Heat Radiation Problems in Cavities Filled by a Nongray Emitting-Absorbing Medium", J. of Numerical Heat Transfer, Part A, Vol. 20, pp.41-64, 1991.

Bilger R.W., "The Structure of Diffusion Flames", J. of Combustion Science and Technology, Vol.13, pp.155-170, 1976.

Bilger R.W., "Turbulent Flows with Nonpremixed Reactants", Turbulent Reacting

Flows, Springer-Verlag, pp.65-113, 1980.

Birkhoff G., "Numerical Fluid Dynamics", SIAM Review, Vol. 25, 1982.

Biswas D. et al., "Three-Dimensional Computation of Gas Turbine Combustors and the Validation Studies of Turbulence and Combustion Models", ASME Paper 97-GT-362, 1997.

Brizuela E.A. and Bilger R.W., "Brief Communication on the Eddy Break-Up Coefficient", J. of Combustion and Flame, Vol.104, pp.208-212, 1996.

Burns P.J., Loehrke R.I., Dolaghan J.S. and Maltby J.D., "Photon Tracing in Axisymmetric Enclosures", HTD-Vol. 203, Developments in Radiative Heat, ASME paper, pp.93-100, 1992.

Cebeci T. and Smith A. M. O., "Analysis of Turbulent Boundary Layers," Academic, New York, 1974.

Chiu E.H., "Modelling of Radiative Heat Transfer in Participating Media by the Finite Volume Method", Ph.D Thesis, University of Waterloo, Dept. of Mech. Eng., Waterloo, Ontario, Canada, 1990.

Choudhury D., "Introduction to the Renormalization Group Method and Turbulence Modeling", Fluent Inc. Technical Memorandum TM-107, 1993.

Chung T.J., "Numerical Modeling in Combustion", Taylor & Francis, ISBN 0-89116-822-2, 1993.

Dacles-Mariani J., Zilliac,G. G., Chow J. S., and Bradshaw P., "Numerical/Experimental Study of a Wingtip Vortex in the Near Field", AIAA Journal, Vol.33, No.9, pp.1561-1568, 1995.

De Champlain A. et. al., "Smoke Number Prediction in Gas Turbine Exhaust", ASME paper 93-GT-168, 1993.

Doherty P. and Fairweather M., "Predictions of Radiative Transfer from Nonhomogeneous Combustion Products Using the Discrete Transfer Method", J. of Combustion and Flame, Vol. 71, pp.79-87, 1988.

Duterque J.B. et al., "Study of Quasi-Global Schemes for Hydrocarbon Combustion", J. of Combustion Science and Technology, Vol.26, pp.1-15, 1981.

Edwards D.K., "Molecular Gas Band Radiation", Advances in Heat transfer, Academic Press, New York, Vol.12, pp.115-193, 1976.

Elkaim D., Reggio M. and Camarero R., "Control Volume Finite-Element Solution of a Confined Turbulent Diffusion Flame", J. of Numerical Heat Transfer, Part A, Vol.23, pp. 259-279, 1993.

Erlebacher G. and Hussaini M.Y., "Stability and Transition in Supersonic Boundary Layers," AIAA Paper 87-1416, 1987.

Espino R.L., "Problem Solving by Computer Simulation", Chemical Engineering Progress, Vol.83, pp.20-24, 1987.

Fabris G., Harsha P.T. and Edelman R.B., "Multiple-Scale Turbulence Modeling of Boundary Layer Flows for Scramjet Applications," NASA CR-3433, 1981.

Faires V.M. and Simmang C.M., "Thermodynamics", ISBN 0-02-335530-1, 1970

Fiveland W.A. and Jessee J.P., "A Finite Element Formulation of the Discrete-Ordinates Methods for Multidimensional Geometries", HTD-Vol. 244, Radiative Heat Transfer: Theory and Applications, pp.41-48, 1993.

Fluent Incorporated, "Fluent 5 User's Guide", 1998.

Frenklach M. and Warnatz J., "Detailed Modeling of PAH Profiles in a Sooting Low-Pressure Acetylene Flame", J. of Combustion Science and Technology, Vol.51, pp.265-283, 1987.

Frenklach M., Wang H. and Rabinowitz M.J., "Optimization and Analysis of Large Chemical Kinetic Mechanisms Using the Solution Mapping Method–Combustion of Methane", Progress in Energy and Combustion Science, Vol.18, pp. 47-73, 1992.

Gibson M. M. and Launder B. E., "Ground Effects on Pressure Fluctuations in the Atmospheric Boundary Layer", J. of Fluid Mechanics, Vol.86, pp.491-511, 1978.

Givi P., Ramos J.I. and Sirignano W.A., "Turbulent reacting concentric jets: comparison between pdf and moment calculations", Dynamics of Flames and reactive Systems; Progress in Astronautics and Aeronautics, Vol. 95, pp. 384-418, 1984.

Givi P. et al., "Flame Extinction in a Temporally developing Mixing Layer", 21st Symposium on Combustion, pp.1251-1261, 1988.

Glassner A.S., "An Introduction to Ray Tracing", Academic Press, New York, 1989.

Gökalp I., Zarrad N., Dumas G.M.L. and Ben Aïm R.I., "Flow rate and equivalence ratio influences on the thermal field of a turbulent cool flame", Dynamics of Flames and reactive Systems; Progress in Astronautics and Aeronautics, Vol. 95, pp. 367-383, 1984.

Gorner K. and Dizet U., "Calculations of Radiative Exchange by the Monte-Carlo d. Theory and Applications to Industrial Combustion Systems", International Chemical Engineering, Vol. 33, No. 2, pp.165-177, 1993.

Gosman A.D. and Lockwood F.C., "Incorporation of a Flux Model for Radiation

into a Finite-Difference Procedure for Furnace Calculation", 14th Symposium on Combustion, pp.661-671, 1973.

Hanjalic K., Launder B.E. and Schiestel R., "Multiple-Time Scale Concepts in Turbulent Transport Modeling," Second Symposium on Turbulent Shear Flows, pp.10.31-36, 1979.

Hanjalic K. and Launder B.E., "Sensitizing the Dissipation Equation to Irrotational Strains," J. of Fluids Engineering, Trans. ASME, Vol.102, pp.34-80, 1980.

Harlow F.H. and Amsden A.A., "Fluid Dynamics, A LASL Monograph", Los Alamos Scientific Lab., Rept. LA4700, 1971.

Hautman D.J. et al., "A Multiple-step Overall Kinetic Mechanism for the Oxidation of Hydrocarbons", J. of Combustion Science and Technology, pp.219-235, 1985.

Hoffmann K.A. and Chiang S.T., "Computational Fluid Dynamics for Engineers", ISBN 0-9623731-7-6, 1993.

Hoffmann S. et al., "Results of Experiments and Models for Predicting Stability Limits of Turbulent Swirling Flames", J. of Engineering for Gas Turbines and Power, Vol. 120, pp.311-316, 1998.

Hottel H.C. and Cohen E.S., "Radiant Heat Exchange in a Gas Filled Enclosure: Allowance for Non-Uniformity of Gas Temperature", AICHE J., Vol. 4, No.1, pp.3-14, 1958.

Hottel H.C. and Sarofim A., "Radiative Transfer", McGraw-Hill, 1967.

Howell J.R., "Application of Monte Carlo to Heat Transfer Problems", Advances in Heat Transfer, Vol.5, pp.1-54, Academic Press, New York, 1968.

Howell J.R., "Thermal Radiation in Participating Media: the Past, the Present, Some Possible Futures", J. of Heat Transfer, Vol. 110, pp.1220-1226, 1988.

Hyer P., Stocker D. and Clark I.O., "Gravitational Effects on Laminar Diffusion Flames", Creare.X Users' Group Meeting Proceedings, pp.345-372, 1991.

Janicka J. and Kollmann W., "A Prediction Model for Turbulent Diffusion Flames Including NO Formation", AGARD Proc. No.275, 1980.

Jones W.P. and Launder B.E., "The Prediction of Laminarization with a Two-Equation Model of Turbulence," J. of Heat and Mass Transfer, Vol. 15, pp.301-308, 1972.

Jones W.P., "Models for Turbulent Flows with Variable Density and Combustion, In Prediction Methods for Turbulent Flows", Hemisphere Publishing Co., 1980.

Jou W.H. and Riley J.J., "Progress in Direct Numerical Simulation of Turbulent Reacting Flows", AIAA J. Vol.27, pp.1543-1557, 1989.

Karki K.C. and Patankar S.V., "Calculation Procedure for Viscous Incompressible Flows in Complex Geometries", J. of Numerical Heat Transfer, Vol. 14, pp.293-307, 1988.

Karniadakis G.E., "Spectral Element-Fourier Methods for Incompressible Turbulent Flows", Computer Methods in Appl. Mech. and Eng., Vol.80, pp.367-380, 1990.

Keller J.O. and Westbrook C.K., "Response of a Pulse Combustor to Changes in Fuel Composition", Twenty-First Symposium on Combustion, The Combustion institute, Pittsburgh, PA, pp.547-555, 1988.

Kent J.H. and Bilger R.W., "The Prediction of Turbulent Diffusion Flame Fields and Nitric Oxide Formation", 16th Symposium on Combustion, pp. 1643-1656,

1977.

Khalil E.E. "Modelling of Furnaces and Combustors", Abacus Press, Turnbridge Wells, 1982.

Kidin N. and Librovich, "On Sound Sources in Turbulent Combustion", Dynamics of Flames and reactive Systems; Progress in Astronautics and Aeronautics, Vol. 95, pp. 343-355, 1984.

Kim S.E. and Choudhury D., "A Near-Wall Treatment Using Wall Functions Sensitized to Pressure Gradient", In ASME FED Vol. 217, Separated and Complex Flows, ASME, 1995.

Kretschmer D. and Odgers J., "Modelling of Gas Turbine Combustors - A Convenient Reaction Rate Equation", Trans. ASME, J. Eng. Pow., 1972.

Kretschmer D. and Odgers J., "The Effects of Hydrocarbon Fuels upon Exhaust Pollutants in Gas Turbine Combustors", 34th ASME International Gas Turbine & Aeroengine Congress & Exhibition, Toronto, 1989.

Ku A.C., Doria M.L. and Lloyd J.R., "Numerical Modeling of Unsteady Buoyant Flows Generated by Fire in a Corridor", Thirteenth Symposium on Combustion, pp.1373-1379, 1977.

Kuo K. K., "Principles of Combustion", John Wiley & Sons, Inc., Toronto, 1986.

Larsen M.E. and Howell J.R., "The Exchange Factor Method: An Alternative Basis for Zonal Analysis of Radiating Enclosures", J. of Heat Transfer, Vol. 107, pp.936-942, 1985.

Launder B. E. and Spalding D. B., Lectures in Mathematical Models of Turbulence, Academic Press, London, England, 1972.

Launder B. E. and Spalding D. B., "The Numerical Computation of Turbulent Flows", Computer Methods in Applied Mechanics and Engineering, Vol.3, pp.269-289, 1974.

Launder B. E., Reece G. J. and Rodi W., "Progress in the Development of a Reynolds-Stress Turbulence Closure", J. of Fluid Mechanics, Vol. 68, No.3, pp.537-566, April 1975.

Lewis M.H. and Smoot L.D., "Turbulent Gaseous Combustion Part I: Theory and Local Species Concentration Measurements", J. of Combustion and Flame, Vol.42, pp.183-196, 1981.

Lien F. S. and Leschziner M. A., "Assessment of Turbulent Transport Models Including Non-Linear RNG Eddy-Viscosity Formulation and Second-Moment Closure", J. of Computers and Fluids, Vol.23, No.8, pp.983-1004, 1994.

Lilly D. K., "On the Application of the Eddy Viscosity Concept in the Inertial Subrange of Turbulence", NCAR Manuscript 123, 1966.

Lily D.K., "Numerical Simulation Studies of Two-Dimensional Turbulence: Part 1. Models of Statistically Steady Turbulence", Geophys. Fluid Dynamics, Vol.228, pp.321-342, 1972.

Lockwood F.C. and Naguib A.S., "The Prediction of the Fluctuations in the Properties of Free, Round-Jet, Turbulent, Diffusion Flame", J. of Combustion and Flame, Vol.24, pp. 109-124. 1975.

Longwell J.P. and Weiss M.A., "High Temperature Reaction Rates in Hydrocarbon Combustion", I & EC, 47, 1956.

Magnussen B. F. and Hjertager B. H., "On Mathematical Models of Turbulent Com-

bustion with Special Emphasis on Soot Formation and Combustion", 16th Symposium on Combustion. The Combustion Institute, 1976.

McKenty F., Meng F.L., and Camarero R., "Comparative Study of Four Combustion Models for the Simulation of Turbulent Methane-Air Flames Using the Control Volume Finite Element Method", ASME, The 1993 international Joint Power Generation Conference & Exposition, Kansas City, 1993.

Mellor A.M., "Current Kinetic Modelling Techniques for Continuous Flow Combustors", Plenum Press, 1972.

Meneveau C. and Katz J., "Scale-Invariance and Turbulence Models for Large-Eddy Simulation", Annu. Rev. Fluid Mech. 2000. Vol.32, pp.1-32, 2000.

Meng F.L., "A Staggered Control Volume Finite Element Method for Turbulent Reaction Flows Coupled with Radiation", Doctoral thesis, University of Montreal, 1994.

Meng F.L., Mckenty F., Elkaim D. and Camarero R., "Predicting Radiative Heat Transfer in Two-Dimensional Rectangular and Axisymmetric Enclosures Using the Discrete Transfer Method", Advanced Computational Methods in Heat transfer, Vol. 1: Conduction, Radiation and Phase Change, pp.161-180, 1992.

Misra A. and Pullin D.I., "A Vortex-Based Subgrid Stress Model for Large-Eddy Simulation", Physics of Fluids, Vol.9, pp.2443-2454, 1997.

Mitchell R.E., Sarofim A.F. and Clomburg L.A., "Experimental and Numerical Investigation of Confined Laminar Diffusion Flames", J. of Combustion and Flame, Vol. 37, pp.227-244, 1980.

Mongia H. C., "A Status Report on Gas Turbine Combustion Modeling", AGARD

CP 422, pp.26.1-14, 1988.

Mongia H.C., Reynolds R. S. and Srinivasan R., "Multidimensional Gas Turbine Combustion Modeling: Applications and Limitations", AIAA Journal, Vol.24, No.6, 1986.

Munson B.R., Young D.F. and Okishi T.H., "Fundamentals of Fluid Mechanics", Wiley, 1998.

Naraghi M.H.N. and Chung B.T.F. and Litkouhi B., "A Continuous Exchange Factor Method for Radiative Exchange in Enclosures with Participating Media", J. of Heat Transfer, Vol. 110, pp.456-462, 1988.

Nikjooy M., So R.M.C. and Peck R.E., "Modeling of Jet- and Swirl-Stabilized Reacting Flows in Axisymmetric Combustors", J. of Combustion Science and Technology, Vol.58, pp. 135-153, 1988.

Oran E.S. and Boris J.P., "Numerical Solution of reactive Flow", Elsevier, New York, 1987.

Oran E.S. and Boris J.P., "Numerical Approaches to Combustion Modeling", AIAA Inc. ISBN 1-563347-004-7, 1991.

Odgers J., "Current Theories of Combustion within Gas Turbine Chambers", Invited Paper to the Fifteenth Symposium on Combustion, Tokyo, Pending Publication, 1974.

Patankar S.V., "Numerical Heat Transfer and Fluid Flow", Hemisphere Publishing Co., 1980.

Patankar S.V. and Spalding D.B., "A Calculation Procedure for Heat, Mass, and Momentum Transfer in 3-D Parabolic Flow", J. of Heat and Mass Transfer, Vol.15,

pp.1987-1995, 1972.

Patel V.C., "Turbulence Models for Near-wall and Low Reynolds-Number Flows", J. of AIAA, Vol.23, pp.1308-1319, 1985.

Patterson G.S. and Orszag S.A., "Spectral Calculation of Isotropic Turbulence: Efficient Removal of Aliasing Interaction", J. of Physics of Fluids, Vol.14, pp.2538-2541, 1971.

Peters N. and Williams F.A., "The Systematic Structure of Methane Flames, Part I: Stoichiometric Flames", Springer Series in Chemical Physics, Vol.47, pp.310-317, 1987.

Peters N., 1988, "Systematic Reduction of Flame Kinetics: Principles and Details", Dynamics of Reactive Systems, Part I, Vol.113, pp.67-86, 1988.

Peyret R. and Taylor T.D., "Computational Methods for Fluid Flow", Springer-Verlag, 1983.

Poinsot T., Candel S. and Trouve A., "Direct Numerical Simulation of Premixed Turbulent Combustion", Progress in Energy and Combustion Science, Vol.12, pp.531-576, 1996.

Raithby G.D. and Chui E.H., "A Finite-Volume Method for Predicting a Radiant Heat Transfer in Enclosures with Participating Media", J. of Heat Transfer, Vol. 112, pp.415-423, 1990.

Richtmyer R.D. and Morton K.W., "Difference Methods for Initial Value Problems", Interscience, New York, 1967.

Rizk N.K. and Mongia H.C., "Three-Dimensional Gas Turbine Combustor Emissions Modeling", ASME paper 92-GT-129, 1992.

Rizk N.K. and Mongia H.C., "A Semi-Analytical Emission Model for Diffusion Flame, Rich/Lean and Premixed Lean Combustors", ASME J. of Engineering for Gas Turbines and Power, Vol.117, pp.290-301, 1995.

Roache P.J., "Computational Fluid Dynamics", Hermosa, Albuquerque, 1976.

Rodi W., "The Prediction of Free Turbulent Boundary Layers by Use of Two-Equation Model of Turbulence", Ph.D. Thesis, University of London, 1972.

Saltiel C.J. and Naraghi M.H.N., "An Exchange Factor Method for Analysis of Radiative Heat Transfer in Nonhomogeneous Media", HTD-Vol. 160, Fundamentals of Radiation Heat Transfer, pp.55-68, 1991.

Schumann U., "Subgrid Scale Model for Finite Difference Simulations of Turbulent Flows in Plane Channels and Annuli", J. of computational Physics, Vol.18, pp.376-404, 1975.

Shah N.G., "New Method of Computation of Radiant Heat Transfer in Combustion Chambers", Ph.D. Thesis, Imperial College, University of London, England, 1979.

Shyy W. and Vu T.C., "On the Adoption of Velocity Variable and Grid System for Fluid Flow Computation in Curvilinear Coordinates", J. of computational Physics, Vol. 92, pp. 82-105, 1991.

Sindir M.M., "Numerical Study of Turbulent Flows in Backward-Facing Step Geometries; Comparison of Four Models of Turbulence", Ph.D. Thesis, Univ. of California, 1982.

Sivathanu Y. R. and Faeth G. M., "Generalized State Relationships for Scalar Properties in Non-Premixed Hydrocarbon/Air Flames" J. of Combustion and Flame, Vol. 82, pp.211-230, 1990.

Sloan D.G. and Sturgess G.J., "Modeling of Local Extinction in Turbulent Flames", ASME J. of Engineering for Gas Turbines and Power, Vol.118, pp.292-307, 1996.

Smagorinsky J., "General Circulation Experiments with the Primitive Equations, I. The Basic Experiment", Month. Wea. Rev., Vol.91, pp.99-164, 1963.

Smith P.J. and Smoot L.D., "Turbulent Gaseous Combustion, Part II: Theory and Evaluation for Local Properties", J. of Combustion and Flame, Vol.42, pp.277-285, 1981.

Smooke M.D., Mitchel R.E. and Keyes D.E., "Numerical Solution of Two-Dimensional Axisymmetric Laminar Diffusion Flames", J. of Combustion Science and Technology, Vol.67, pp.85-122, 1989.

Spalding D.B., "Mixing and Chemical Reaction in Steady, Confined Turbulent Flame", 13th Symposium on Combustion, 1970.

Spalding D.B., "Development of the Eddy-Break up Model of Turbulent Combustion", 16th Symposium on Combustion, 1976.

Spalart P. and Allmaras S., "A One-Equation Turbulence Model for Aerodynamic Flows", Technical Report AIAA-92-0439, American Institute of Aeronautics and Astronautics, 1992.

Speigel M.R., "Probability and Statistics", Schaum's Outline Series in Mathematics, pp. 116-117, McGraw-Hill, New York, 1975.

Speziale C.C., Erlebacher G., Zang T.A. and Hussaini M.Y., "On the Subgrid-Scale Modeling of Compressible Turbulence," NASA CR-178420, 1987.

Sturgess G.J., et al., "Lean Blowout in a Research Combustor at Simulated Low pressures", ASME J. of Engineering for Gas Turbines and Power, Vol.108, pp.773-

781, 1996.

Taki S. and Fujiwara T., "Numerical Simulation of Triple Shock Behavior of Gaseous Detonation", Eighteenth Symposium on Combustion, pp.1671-1681, 1981.

Tan Z.Q., "Radiative Heat Transfer in Multi-Dimensional Emitting, Absorbing, and Anisotropic Scattering Media: Mathematical Formulation and Numerical Method", J. of Heat Transfer, Vol. 111, pp.141-147, 1989.

Tennekes H. and J.L. Lumley, "A First Course in Turbulence", Cambridge, MIT Press, 1972.

Torrance K.E., "Comparison of Finite-Difference Computations of Natural Convection", NBS Journal of Research, Vol.72B, No.4, pp.281, 1968.

Torrance K.E. and Rockett J.A., "Numerical Study of Natural Convection in an Enclosure with Localized Heating from Below", J. of Fluid Mechanics, Vol.36, pp.33, 1969.

Vervisch L. and Poinsot T., "Direct Numerical Simulation of Non-Premixed Turbulent Flames", Annu. Rev. Fluid Mech., Vol. 30, pp.655-691, 1998.

Viskanta R. and Menguc, "Radiation Transfer in Combustion Systems", Progress in Energy and Combustion Science, Vol. 13, No.2, pp.97-160, 1987.

Wang Hai and Frenklach M., "A Detailed Kinetic Modeling Study of Aromatics Formation in Laminar Premixed Acetylene and Ethylene Flames", J. of Combustion and Flame, Vol.112, No.1-2, pp.173-221, 1997.

Warnatz J., "Chemistry of high Temperature Combustion of Alkanes up to Octane", Twentieth Symposium on Combustion, Pittsburgh, PA, pp.845-856, 1985.

Wei J. and Prater C.D., "The Structure and Analysis of Complex Reaction Systems", Advances in Catalysis, Vol.13, pp.203-392, 1962.

Westbrook C.K. and Dryer F.L., "Simplified Reaction Mechanisms for the Oxidation of Hydrocarbon Fuels in Flames", J. of Combustion Science and Technology, Vol.27, pp.31-43, 1981.

Westbrook C.K. and Pitz W.J. "A Comprehensive Chemical Kinetic Reaction Mechanism for Oxidation and Pyrolysis of Propane and Propene", J. of Combustion Science and Technology, Vol.37, pp.117-152, 1984.

Williams F.A., "Combustion Theory" , Menlo Park, Benjamin/Cummimgs Publishing Co., 1985.

Yakhot A., Orszag S. A., Yakhot V. and Israeli M., "Renormalization Group Formulation of Large-Eddy Simulation", J. of Scientific Computing, Vol.4, pp.139-158, 1989.

Yetter R.A. et al., "Complications of One-Step Kinetics for Moist CO Oxidation", Twenty-first Symposium on Combustion, pp.749-760, 1988.

Yuen W.W., Ma A.K. and Takara E.E., "Evaluation of Radiative Heat Transfer Using the Generalized Zonal Method and the Absorption Mean Beam Length Concept", HTD-Vol. 203, Developments in Radiative Heat transfer, pp.265-273, 1992.

Zang T.A., Krist S.E. and Hussaini M.Y., "Resolution Requirements for Numerical Simulations of Transition", ICASE Report, 89-9, Hampton, NASA Langley Research Center, 1989.

Appendix A Classification of Partial Differential Equations

Most of the governing equations of fluid mechanics, combustion and heat transfer are expressed as second-order partial differential equations (PDEs) and the solution procedure of PDEs depends on the type of the equation. Therefore it is important to study various classifications of PDEs.

To classify the second-order PDE, consider the following equation

$$A\frac{\partial^2\phi}{\partial x^2} + B\frac{\partial^2\phi}{\partial x\partial y} + C\frac{\partial^2\phi}{\partial y^2} + D\frac{\partial\phi}{\partial x} + E\frac{\partial\phi}{\partial y} + F\phi + G = 0 \qquad \text{(A.1)}$$

Where, in general, the coefficients A, B, C, D, E, F and G are functions of the independent variables x and y and of the dependent variable ϕ. Assume that $\phi = \phi(x, y)$ is a solution of the differential equation. This solution describes a surface in space, on which space curves may be drawn. These curves patch various solutions of the differential equation and are known as the characteristic curves.

The second-order PDE previously expressed as Equation (A.1) is classified according to the sign of the expression $(B^2 - 4AC)$. It will be

elliptic, if $(B^2 - 4AC) < 0$ (A.2)

parabolic, if $(B^2 - 4AC) = 0$ (A.3)

hyperbolic, if $(B^2 - 4AC) > 0$ (A.4)

Note that the classification depends only on the coefficients of the highest order derivatives.

Appendix B The UDF file

```
#include "udf.h"

DEFINE_VR_RATE(n6_rate, c, t, r, wk, yk, rate, rr_t)
{

  real minR = 1.e+20, numerator = 0., denom = 0.;
  real AA=4.0;
  real ccon=0.0117;
  real ci, r1, r2;
  real r3, ci0, yb, cr, yw1, yw2,r0;
  int  i;
  float prod, conc;

% to calculate standard EBU rate r1 %
  {
  for(i=0;i<r->n_reactants;++i)
    if (r->stoich_reactant[i] != 0.)
      {
        ci = C_R(c,t)*yk[r->reactant[i]]/wk[r->reactant[i]];
        SETMIN(minR, ci/r->stoich_reactant[i]);
      }
```

```
  for(i=0;i<r->n_products;++i)
    {
      ci = C_R(c,t)*yk[r->product[i]]/wk[r->product[i] ];
      numerator += ci*wk[r->product[i]];
      denom += r->stoich_product[i]*wk[r->product[i]];
    }

  r1 = r->Amix * C_D(c,t)/C_K(c,t) * MIN(minR, r->Bmix *numerator/denom);
  }

% to calculate finite vhemical reaction rate r2 %
  {
      prod = 1.;
      for(i=0; i<r->n_reactants; i++)
        {
          conc =  C_R(c,t)*yk[r->reactant[i]]/wk[r->reactant[i]];
          prod *= pow(conc,r->exp_reactant[i]);
        }

      r2 = r->A * exp(- r->E/(UNIVERSAL_GAS_CONSTANT*C_T(c,t)) ) *
              pow(C_T(c,t), r->b) * prod;
  }

% to calculate user-defined rate r3 %
  {
   cr = r->stoich_reactant[1]*wk[r->reactant[1]];
   cr = cr/(r->stoich_reactant[0]*wk[r->reactant[0]]);
%  cr: the air:fuel ratio %
   yw1 = yk[r->reactant[0]]/wk[r->reactant[0]];
   yw2 = yk[r->reactant[1]]/wk[r->reactant[1]];
```

```
    yb = yw1+yw2/cr;              % to calculate constant Yb %

   r3 = ccon * yb*C_R(c,t)*C_D(c,t)/C_K(c,t);
   }

% to choose the slowest rate as the reaction rate %
   r0 = MIN(r1,r2);
   *rr_t = MIN(r0,r3);

}
```